# CENP-F Loss of Function Studies: A Case for Microtubule Dysfunction in Cardiac Disease

**By**

**Annabelle E. Manalo**

**Dissertation**

**Submitted to the Faculty of the**

**Graduate School of Vanderbilt University**

**in partial fulfillment of the requirements**

**for the degree of**

**DOCTOR OF PHILOSOPHY**

**In**

**Cell and Developmental Biology**

**May 11, 2018**

**Nashville, Tennessee**

**Approved:**

**H. Scott Baldwin, M.D., Ph.D.**
**David Bader, Ph.D.**
**Javid Moslehi, M.D.**
**Dylan Burnette, Ph.D.**
**Ryoma Ohi, Ph.D.**

**To my three children, Aaliyah, Braylon, and Macario,**

**who will obtain whatever they reach for.**

## ACKNOWLEDGEMENTS

The following work would not be possible without the financial support of the (insert grant) and Vanderbilt University Cardiology Department. I am especially indebted to Dr. David Bader, my principal investigator and associate professor in the Cell and Developmental Biology Department, who has been supportive of my educational goals and worked patiently to provide me with flexibility to think innovatively and worked diligently to push me to have better organization.

I am grateful for the caliber of individuals who I have had the pleasure to work with during all of the projects I was involved in, especially the studies mentioned here. Each of the members of my Dissertation Committee have provided me with outstanding professional guidance in scientific research that I will carry with me in my personal life forever. I would especially like to thank Dr. Dylan Burnette who is a member of my committee. As a scientific mentor, Dylan has spent countless hours working through data with me and never hesitates to provide extremely helpful insight. I also feel motivated after the conversations that Dr. Burnette and I share. He has given me tools on not only how to be a good scientist but most of all, a good person. I have to thank my colleague and good friend, Dr. Johnathan Fleming. He was the first person I met at Vanderbilt and he has guided me and assisted me in so many different ways.

Nobody has motivated me in the pursuit of this project more than the members of my family. First and foremost, I give God all the glory. My faith constantly has me climbing in a positive direction and I am blessed beyond my knowledge. I am humbled. I would like to thank my parents and brother Russell in Canada; whose love and support are always with me in all goals that I pursue throughout life. I've sacrificed quality time to be away from them and their understanding has kept me focused and motivated. Most importantly, I'd like to thank my fiancé Roy Morgan and amazing children, especially Roy Morgan Jr., Aaliyah, BJ, and Macario for the type of love and support that cannot be described in words. Gramps has been an inspiration that has fueled me to the finish line and my children have given me a reason to never give up. This embodiment of work would not have been possible without the support system mentioned here.

# TABLE OF CONTENTS

# LIST OF TABLES

**Table** **Page**

## LIST OF FIGURES

**Figure** **Page**

# CHAPTER 1

## INTRODUCTION TO CENP-F LOSS OF FUNCTION STUDIES: A CASE FOR MICROTUBULE DYSFUNCTION IN CARDIAC DISEASE

The process of cellular development is an intricate ordered process critical for life. Even a very minor discrepancy in the patterning or cell division can result in abnormalities in organ development. Furthermore, the patterned developmental process depends on the differentiation of tissue specific cell types. Understanding the role of how these different cell types interact is critical to proper organogenesis. In the heart, cardiogenesis is achieved by the regulation of several stages associated with proper assembly of the cardiac myocyte population. Once the key components of the heart are in place, understanding the functionality at the cellular level is essential. Cardiomyocytes, cardiac myocytes, or myocardiocytes, represent the work horse of the heart and are very abundant. Cardiac myocytes begin assembly during the early developmental stages of the heart, then progress to a highly ordered structure. While reviewing cardiac structure and development, I will highlight the important implications of the microtubule network on development of the structure and physiology of the adult cardiac system.

My thesis research will emphasize how critical a protein can be to the proper organ development and stress the need to better understand the different processes that govern cardiac cell types functionality. The specific focus, however, will center on laboratory outcomes on how a disruption in the cardiac microtubule network can result in cardiac dysfunction and disease. First, a brief examination of microtubule development juxtaposed to the development of the contractile components within a cardiomyocyte versus in other cell types will be provided. Secondly, a thorough evaluation of the specific cell biological implications of the loss of centromere protein F (CENP-F) in cardiac myocytes will be evaluated. Through understanding the impact of CENP-F disruption on cardiac infrastructure, there becomes a need to grasp the role of microtubules in the heart, a field that is almost currently inexistent. Ultimately, these studies lay the groundwork for a vital role of microtubules in genesis and potential progression of heart disease.

In addition to the cardiomyocyte specific studies, data detailing the developmental processes of the mesothelium during embryogenesis is in Chapter 5 of this dissertation. In the heart, the mesothelium is initiated by an extrinsic population of cells, and prior to this study, it has been the accepted model in mesotheliogenesis. Our findings, however, show that several other developing organs acquire a mesothelium through an intrinsic source. This study is of great significance, as it reiterates that it is necessary to study the specific tissue and relating cell types of the organ of interest.

**Cardiomyocyte Development and Function**

The four-chambered heart of the vertebrate is generally comprised of four main cell types; cardiac fibroblasts, myocytes, endothelial cells, and vascular smooth muscle cells (Banerjee et al., 2007). Together, all cells are responsible for the chemical, physiological, and structural properties of a functioning heart (Table 1.1).

Although comprised of mainly four different cell types, only 20% of the cardiac cell population includes cardiac fibroblasts, 60% are endothelial cells, and a majority of the heart mass can be attributed to cardiac myocytes (Xin et al., 2013; Pinto, 2016). Cardiac fibroblasts resemble the classic fibroblast in appearance and are important for maintaining proper structure and function of the heart (Pfaltzgraff et al., 2016). The cardiac myocytes are rod-shaped cells that differentiate from myoblasts which originate from lateral splanchnic mesoderm (Brooks et al., 1998; Kruithof et al., 2003).

For comparative purposes, this thesis includes data on the cardiac fibroblast, however, the bulk of single cell examination will be on the cardiomyocyte population. During mouse embryogenesis, myocardial cells arise from cardiogenic progenitor cells that form two groups of cells on either side of the midline. The primary heart field forms a cardiac crescent and by E8, giving rise to a beating tubular heart. Here, the endocardium and myocardium layers are separated by the cardiac jelly (Moorman et al., 2003; Savolainen et al., 2009). Cardiomyocytes continue to proliferate until birth and during this time, the rate of contraction increases rapidly (Ishiwata et al., 2003). Cardiomyocytes continue to grow by hypertrophy into a terminally differentiated cell until post-natal day 30 (Xin et al., 2013; Ahuja et al., 2013; Brooks et al., 1998)(Table 1.2).

The resulting bi-nucleation of cardiomyocytes vary from species to species. In mice, 85-90% of cardiomyocytes are very often bi-nucleated due to the inability to undergo cytokinesis (Paradis et al., 2014). Although cell cycle control is halted at the G2 phase, the reason for incompletion of this critical stage of cell division remains unknown (Ahuja et al., 2007). Nevertheless, the maintenance of the striated structure and signaling between cardiac myocytes is required for cell contraction and successful heart functioning.

| CELL TYPE | LOCALIZATION | FUNCTION |
|---|---|---|
| Cardiac Myocytes | Myocardium | Conduction Cells |
| Cardiac Fibroblasts | In Cardiac Skeleton and Within Myocardial Interstitium | Injury Response |
| Endothelial Cells | Endocardium | Line Interior of Blood Vessels and Cardiac Valves |
| Smooth Muscle Cells | Coronary Arteries | Cell Maintenance: Assists in Blood Flow |

**Table 1.1 The main cell types of the heart.** A chart of the 4 main cell types of the heart, where they are localized, and their function.

| E7 | E14 | E21/birth | P7 | P30 | Adult |
|---|---|---|---|---|---|
| MYOCYTE TRABECULATION AND COMPACTION | | | | | |
| | | | | | |
| CARDIOMYOCYTE PROLIFERATION | | | | | |
| | | | | | |
| | | | CARDIOMYOCYTE HYPERTROPHY | | |
| | | | | | |

**Table 1.2. Cardiomyocyte Developmental Time Points.** The developmental time points of a mice cardiomyocyte during cardiogenesis. Myocyte trabeculation, compaction, and proliferation occur to E14 **(green)** however , proliferation continues to birth **(purple)**. Although the myocyte continues to grow, it is by hypertrophy until P30 **(pink)**.

The phenotype of an adult cardiomyocyte is a rod shape with repeating striations across the cell (Manalo et al., in review; Kuo et al., 2012; Pantos et al., 2007; Ribeiro et al., 2015). Cardiomyocytes have a unique cytoarchitecture that allows for synergistic communication from cell to cell to ensure successful repetitive contraction of the heart. The main components are the myofibrils, made up of actin and myosin filaments which make up the striated muscle pattern, and the intercalated discs, responsible for cell-cell communication at the bi-polar ends of myofibrils. The formation of the myofibrils begins at the z-discs, followed by the M-line, and assembly of the thick and thin filaments (actin and myosin) (Hirschy et al., 2006). Proper patterning of the sarcomeric structure, organized by an extensive protein scaffold, makes up the mechanical component of a cardiomyocyte and the ability of sarcomere shortening to produce the appropriate force for heart function (Figure 1.1).

Functionally, cardiac-excitation contraction coupling is the series of events that links the electrical impulse (action potential) to the contraction of the heart chambers (Bers et al., 2002). The action potential is the entry of $Ca^{2+}$ entering the cell through depolarized-activation channels. The $Ca^{2+}$ entry triggers $Ca^{2+}$ in the sarcoplasmic reticulum to be released. This mechanism of $Ca^{2+}$ influx and release increases the intracellular calcium, which then binds to troponin C, enabling contraction to occur (Ferrier et al., 2001). In order for cardiomyocyte relaxation to take place, $Ca^{2+}$ must be removed from the cytosol. Ultimately, the ratio of bound:free $Ca^{2+}$ is the balancer of cardiomyocyte contraction (Bers, 2002).

When the heart muscle is stiff, ventricles cannot relax, making it difficult for the blood to flow normally (Westermann et al., 2008). The outer surface of a cardiomyocyte can be evaluated to detect the condition of mechanical properties by a nano-indentation technique (Borin et al., 2017). In isolated cardiomyocytes, abnormal stiffness has been associated with dilated cardiomyopathy, cardiac amyloidosis, diabetes, and heart failure (Bhupathi et al., 2011; Chew et al., 1976; Zile et al., 2004; Makarenko et al., 2004).

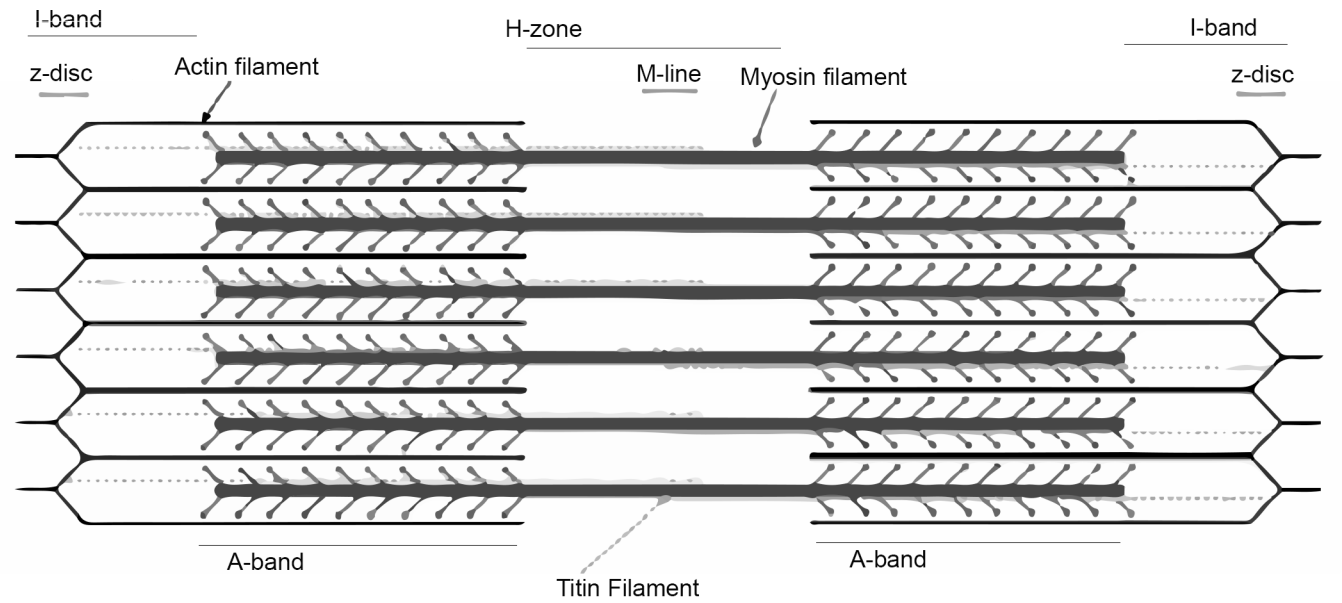


**Figure 1.1. The components of a sarcomere.** A relaxed sarcomere; z-discs - anchoring the ends of the sarcomere, I band - zone of thin filaments, A-band - contains the entire length of a thick filament, H zone - zone of thick filaments, M-line - middle of sarcomere, formed of cross-connecting elements of the cytoskeleton. (Modified from Luther, 2009).

**Microtubules in Cardiac Fibroblasts and Cardiomyocytes**

Microtubules are polarized structures comprised of alpha- and beta- tubulin heterodimers in a linear fashion. A single microtubule is composed of 13 protofilaments forming a 24-nm wide hollow cylinder. Classically, microtubules are bundled at the nucleus projecting outwards to the periphery of a cell (Poulain et al., 2010; Bowne-Anderson et al., 2013). The microtubule network undergoes dynamic instability, a constant growing and shrinking of the filaments length due to the addition of GTP and hydrolyzation of GDP, respectively (Burbank et al., 2006). Defined as dynamic instability, this polymerizing and depolymerizing event is critical for mitosis to occur in all cell types (Roostalu et al., 2017; Forth et al., 2017). Additionally, post translational modifications allow for the microtubules to serve as tracks for transport of cargo within the cell (Robison et al., 2016; Kerr et al., 2015). Proper functioning of the microtubule network is essential for proper cell division and cellular transport in most cell types (Figure 1.2).

The microtubule network is an essential component for many cells including the cardiac fibroblast. As mentioned above, cardiac fibroblasts have a similar appearance to fibroblasts of other organs and are critical for maintenance of normal cardiac function. Fibroblasts are an essential component of connective tissue elements throughout the body and are capable of compensating for damage within the heart by employing cardiac remodeling upon myocardial damage and/or dysfunction (Souders et al., 2009; Furtado et al., 2016; Camelliti et al., 2005). The microtubule network regulates proper and rapid cellular division in the cardiac fibroblast as with many other cell types. Microtubules are responsible for regulating the cell shape changes and motility, as well as allowing for the cardiac fibroblast to regulate actin polymerization/depolymerization (Baudino et al., 2006). With a disrupted microtubule network, fibroblasts lose cell shape regulation, have no directional persistence, and cell division is slowed (Pfaltzgraff et al., 2015). These studies alone justify exploring the potential importance of microtubules in heart health.

Cardiomyocytes, the work horse of the heart, are essential for proper functioning of the contractile machinery necessary for constant, involuntary contraction of the heart (Spater et al., 2014, Leone et al., 2015). The role of microtubules in cardiomyocytes, however, has not been well studied. Mice cardiomyocytes do not complete the final round of cytokinesis during development and thus a percentage of cardiac myocytes remain bi-nucleated (Paradis et al., 2014). With the most common understanding being that cardiomyocytes are terminally differentiated, the role of microtubules in the heart has been ignored (Senyo et al., 2014).

The microtubule network has a very different layout within the cardiac myocyte opposed to any other cell type (Figure 1.3). Cardiac myocyte microtubules are not bundled and do not appear to have a single point of nucleation. Instead, individual and loosely organized microtubules are longitudinally organized across the cell and in a grid like fashion around the costameres on the outer surface of the contractile apparatus. Even though microtubules are essential to cardiac myocyte function, their exact role in an adult cardiac myocyte is not clear (Figure 1.3).

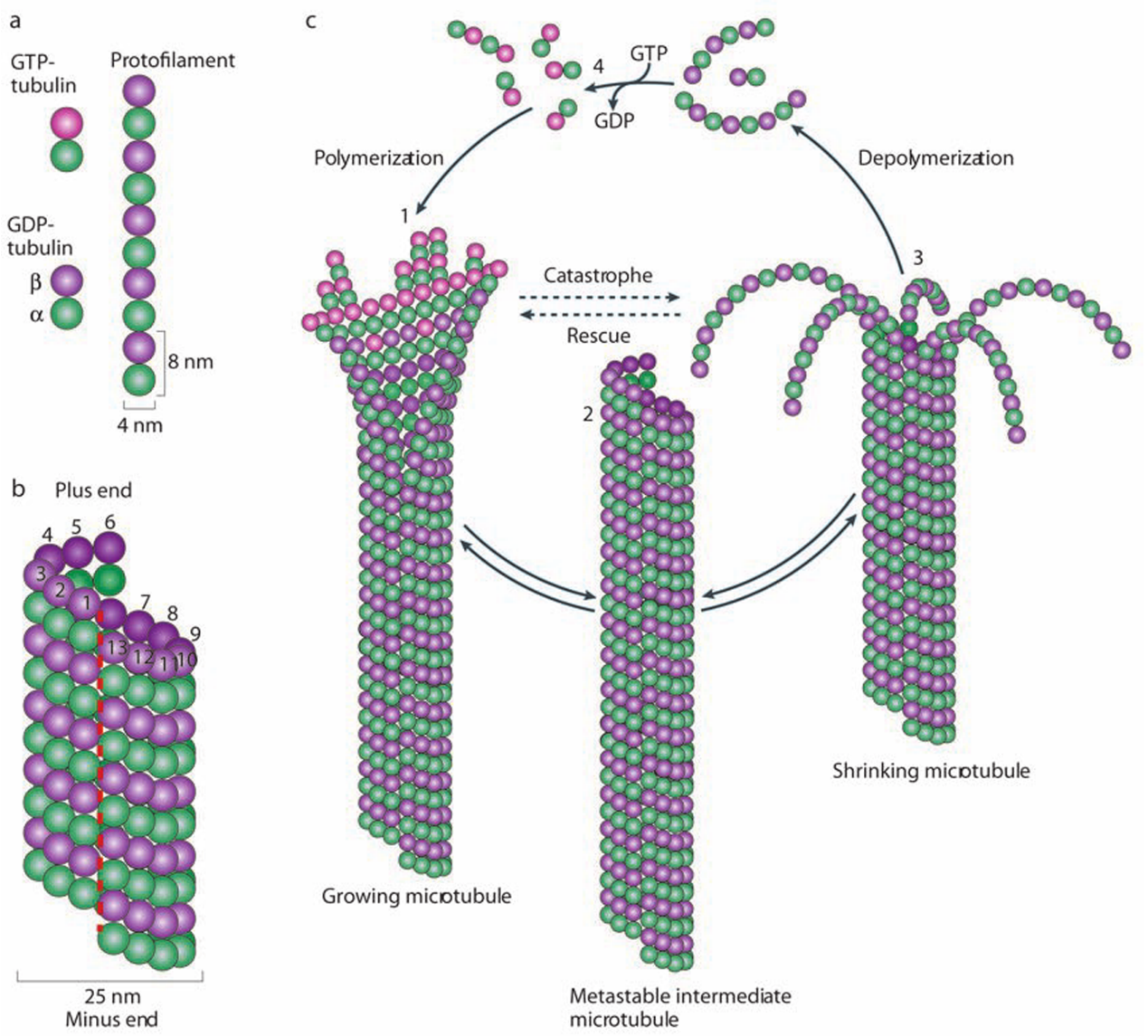


**Figure 1.2. Microtubule Instability and Structure.** Microtubules are composed of tubulin heterodimers that are aligned in a polar head-to-tail fashion to form protofilaments **(a)(b)**. Microtubles undergo dynamic instability, growing (1)(2) and shrinking (3). This process is a continous process. (Modified from Des Georges, 2008).

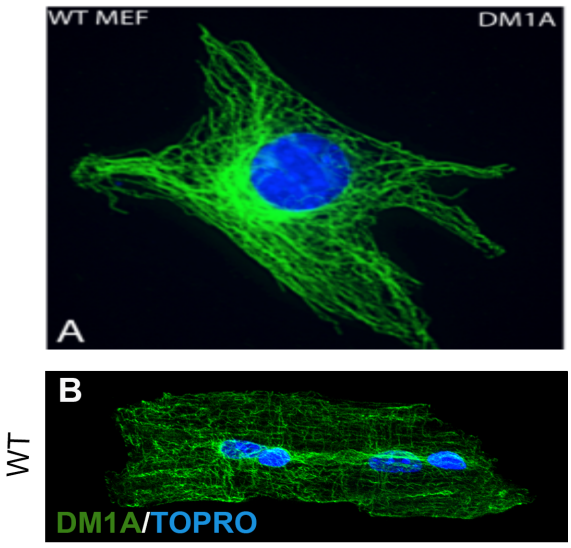


**Figure 1.3. Layout of the Microtubule Network in Mouse Embryonic Fibroblasts and Cardiac Myocytes.** Microtubules in an adult wild-type MEF originate perinuclear and are bundled, protruding out towards the periphery of the cell **(A).** Wild-type cardiomyocytes are loosely organized and grid-like with a lack of a radial array. Microtubule network is rod-shaped with distinct branching **(B)**.

**Microtubules in heart function and failure**

There is an array of evidence on the association of myofibrillar disassembly in heart failure (Machackova et al., 2006). During heart failure, troponin-t is decreased causing thin filaments to have a slower sliding speed when activating calcium concentration (Adamcova et al., 2006). However, there are no specifics on the precise microtubular contribution on heart disease. Recently, Robison et al. showed that post translationally modified microtubules "buckle and bear" to contribute to timely sarcomeric contraction. By controlling detyrosination, this study suggests that microtubules play a mechanical role in interacting with the sarcomeres and are thus associated with shortening and overall myocyte contraction (Robison et al., 2016). Lastly, there are a few reports that show an increase in the density of microtubules upon hypertrophy (Sequeira et al., 2014; Fassett et al., 2013). These reports are in an observation state and there are still many limitations in the available studies. However, it is clear that the microtubule network may have a very important role in cardiac health and that disruption of the network could lead to heart disease.

**Alteration of the microtubule network in the heart by Centromere Protein F**

Centromere Protein F (CENP-F) is a large microtubule binding protein that has a diverse set of binding partners and a myriad of cellular functions (Pooley et al, 2008). CENP-F is critical in mitosis and the loss of CENP-F function can result in mitotic delay and chromosome misalignment (Liao et al., 1998; Yang et al., 2003). Additionally, CENP-F is upregulated in esophageal and breast cancer and recent reports suggest a mutated CENP-F results in microcephaly phenotypes (Mi et al., 2013; O'Brien et al., 2007).

Our group made the first report of CENP-F having a role in cardiac function. More importantly, this was the first instance that showed a microtubule binding protein having implications in heart disease (Dees et al., 2012). The loss of CENP-F function resulted in arrhythmias, less trabeculation, and a thinned ventricular wall, characterizing dilated cardiomyopathy. Still, detailed analysis of the cellular components of the myocyte that were disrupted with loss of CENP-F function was not explored. A more thorough report on microtubular response to CENP-F was published shortly after (Pfaltzgraff et al., 2016). These results showed that in mouse embryonic fibroblasts (MEFs), loss of CENP-F resulted in hyper-stabilized microtubules with a great difference in dynamic stability (Table 1.3), cell motility, cell shape, and adhesion.

a

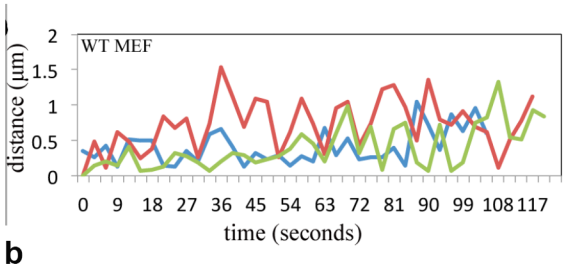


b

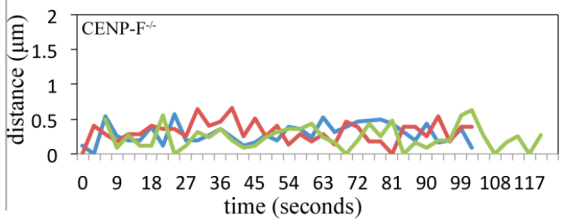


c

| DYNAMIC PARAMATER | WT n=15 | CENP-F$^{-/-}$ n=15 |
|---|---|---|
| Growth Rate (µm/s) | 0.2796 ± 0.025 | 0.15165 ± 0.00374 * |
| Shrink Rate (µm/s) | 0.2714 ± 0.008 | 0.18591 ± 0.0191 *** |
| Average pause duration (s) | 12.242 ± 1.09757 | 43.2889 ± 2.5005** |

**Table 1.3 Dynamic instability is decreased in *CENP-F*$^{-/-}$ microtubules.** Measurement of MT dynamics from MEFs transfected with 3xGFP-EMTB **(a)(b)**. Quantifications show the dynamics are severly paused **(c)**. *n*=15, **p*<0.01, ***p*<0.0005, ****p*<0.0002. Error = SEM.

However, microtubules in cardiomyocytes in *CENP-F*$^{-/-}$ hearts formed rings at the microtubule ends opposed to hyper-stabilization. Therefore, to fully understand the mechanisms that lead to heart disease with loss of CENP-F function, a comprehensive analysis of cardiac myocyte structure and function is necessary.

The following study further describes the consequences of a mutated CENP-F at the cellular level and provides evidence on the impact that disruption of the microtubule network has on the contractile components of a cardiomyocyte. Ultimately, this thesis provides a foundation to gain a greater understanding and appreciation of microtubules in the heart and, how disruption can lead to heart disease (Figure 1.4).

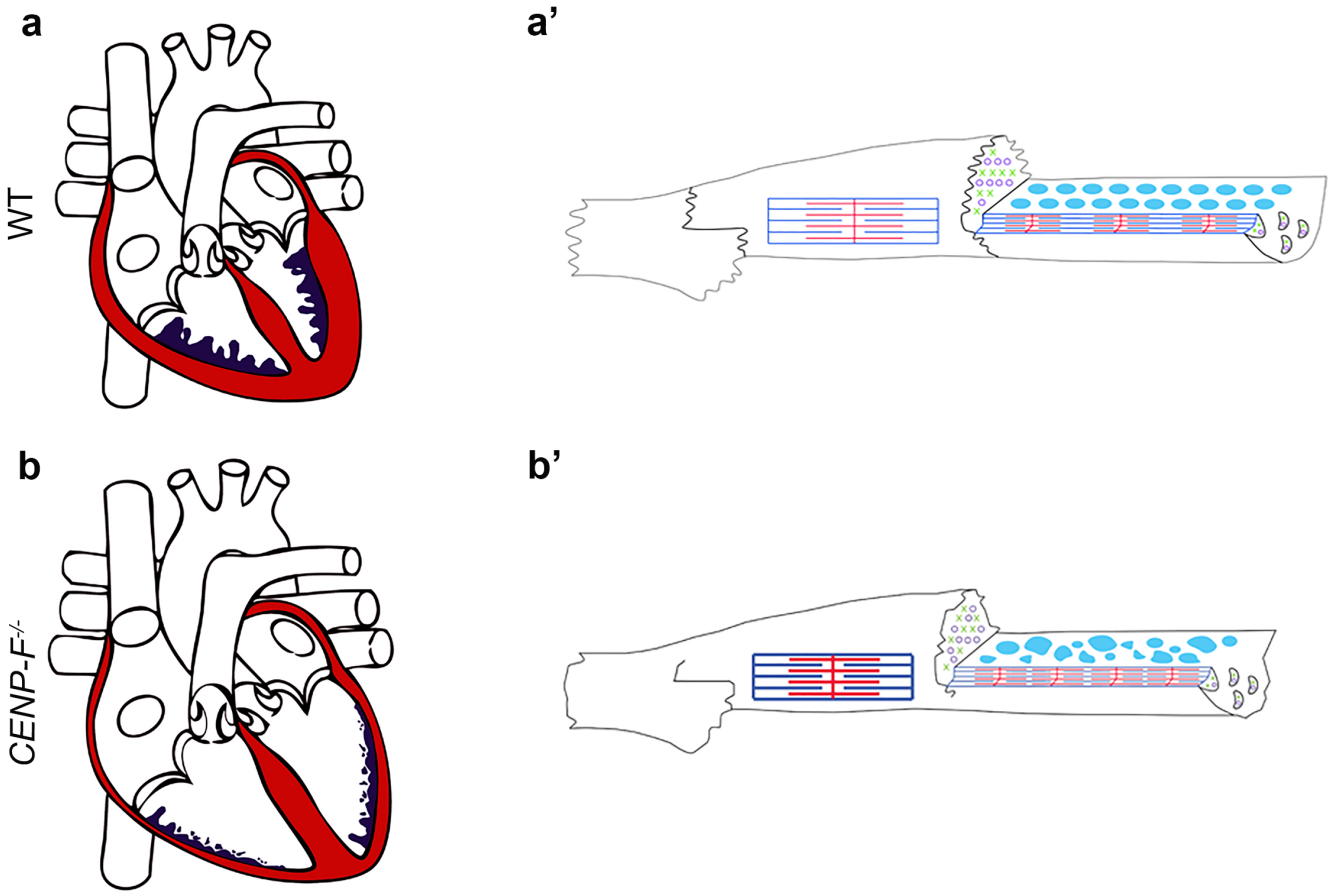


**Figure 1.4. A schematic comparing a normal vs CENP-F$^{-/-}$ heart with dilated cardiomyopathy and the resulting cardiomyocyte.** A normal developed heart **(a)** compared to a DCM schematic model that is enlarged, has fewer trabeculae **(purple)**, and thinner ventricular walls **(red) (b)**. A normal terminally differentiated cardiomyocyte has distinct sarcomeres **(red and blue)**, well aligned mitochondria **(light blue)**, and well defined intercalated discs **(green and purple) (a')**.The deletion of CENP-F results in complete cardiomyocyte disarray. Sarcomeres are thickened and closer together **(red and blue)**, mitochondria is misaligned and varied in size, and intercalated disc proteins are disintegrated **(b')**. (Modified from Liu, 2014).

**An additional study – the mesothelium**

In addition to the study described above, this thesis presents data from a study on the mesothelium, a simple squamous epithelium lining the body wall and organs of vertebrate coelomic cavities. The "accepted model" of generating mesothelial components through an extrinsic population, as identified in the heart, was the stand-alone paradigm for generation of mesothelial cell populations in organogenesis (Ho et al., 1978). During cardiogenesis, the newly formed heart tube needs to recruit a proepicardium (PE), an extrinsic population of mesothelial cells, in order for proper vasculature and cardiogenesis to occur. The PE migrates to and over the heart tube and provides the necessary mesothelium progenitors that are essential to generate the coronary vascular system (Dettman et al., 1998; Duenas, 2017). Using chick/quail chimeric grafting, developing digestive and respiratory systems were shown to have an intrinsic population of mesothelial progenitors (Chapter 5, current dissertation). These studies showed that in order to understand mesotheliogenesis in specific coelomic organs, it is important to individually observe each organ to identify whether they fit the newly discovered "organ intrinsic" model or follow the historical pattern of the heart. More importantly, the data presented here adds further support to how critical it is to analyze cardiomyocytes in our CENP-F studies in the heart.

# CHAPTER II

# MICROTUBULES IN THE HEART: A Review


## ABSTRACT

The microtubule network is fundamental to cellular division and has diverse roles within various cell types. Cardiac microtubules, however, have not been well defined and other than only a handful of publications nearly three decades ago, reports on the microtubule network in the heart have been minimal (Fassett et al., 2013; Takahashi et al., 1998; Webster, 1997; Robison et al., 2016; Dees et al., 2012; ter Keurs, 1998; Khairallah et al., 2012). The difference of the microtubular layout in the heart from cells of other organs has been noted but still, the clear-cut role and function of microtubules has not been deciphered. In mice, cardiomyocytes do not complete cytokinesis and a majority of the adult cells are terminally differentiated. Thus, perhaps the role of the microtubule network has been ignored since, in most cell types, microtubules are essential for constant cell division and turnover. Nevertheless, recent reports identify heart failure associated with a greater density of the microtubule network (Fassett et al., 2013; ter Heurs, 2013). These studies are not focused on the microtubules itself, though, and do not thoroughly evaluate the cause of this hyper-polymerization. The first report of the loss of a microtubule binding protein, Centromere Protein F (CENP-F), having implications in heart disease showed diverse changes in the heart (Dees et al., 2012). Whole pan hearts were dilated, cardiac function was greatly disrupted, and now, a detailed examination of CENP-F is under evaluation at the cardiomyocyte level. With promising results indicating that the microtubule network has a role in the cytoarchitectural structure and function of a cardiomyocyte, it is important to dial back and understand the role of the microtubule network in these cells. Here, a description on the view of the current field on cardiac microtubules and the need for a deeper understanding is reviewed.

**The developing cardiac myocyte and microtubule network organization**

The heart is one of the first functional organs to arise during heart development and the generation of the specific structural and functional components requires coordinated patterning during the correct time and space (Wilsbacher et al., 2015). At E7.5 the first and second heart fields are formed. At this point, the first heart field fuses to the midline, the crescent fuses, and a beating linear heart tube is formed (Brade, 2013). The sarcomere, the basic contractile unit of the cardiomyocyte, is assembled by the anchoring of actin filaments, titin, and many other contractile components to the z-disc. Alpha-actinin and the myosin fibers anchor to the M-line and alignment begins to occur (Deyne et al., 2013; Eldik et al, 2013). At first, the cardiomyocyte is organized in finger-like projections that emanate outwards towards the cell periphery and contain nearly mature myofibrils. The cardiomyocyte continues to proliferate and align until the completion of cytokinesis is interrupted (Wilsbacher et al., 2015). As mitosis never goes to completion in approximately 90% of mice cardiomyocytes (Paradis, 2013), a terminally differentiated cardiac cell is rod shaped in appearance and very often bi-nucleated (Figure 2.1).

There is a well-defined understanding of the role of microtubules in various cell types. In interphase, microtubules are responsible for intracellular transport and maintaining cell structure however, the most widely studied function of the microtubule network is in cell division (Meunier et.al, 2012; Karsenti et al., 1993). At the start of the cell cycle, microtubules assemble at opposite centrosomes and continue dynamic stability, growing and shrinking at the plus ends, at a more rapid pace towards the chromosomes. The microtubules become shorter and more dynamic as they attach to the kinetochores, forming an aligned mitotic spindle. It is important to note that the microtubules come in different subclasses, interpolar microtubules are the most dynamic but it is the k-fiber microtubules that shorten and promote chromosome segregration (Meunier et al., 2012). Upon completion of cell division, microtubules are in interphase, nucleating at the minus ends and protruding out to the cell surface.

In developing mice cardiomyocytes, the microtubule network first appears as a non-myocyte cell. The microtubules are bundled and nucleate from a single nucleus, protruding outwards. As the contractile apparatus is completing assembly in neonatal cardiomyocytes, the microtubule network bundling appears to separate. It is during this neonatal stage that a large population of post-translationally modified microtubules, specifically Glu tubulin with moderate dynamics, has been identified (Webster, 1997). By post-natal day 7, the cardiomyocyte is bi-nucleated and microtubules are individually elongated across the cell in a longitudinal manner. Adult cardiomyocytes have an abundant population of microtubules around the nuclei with the remaining microtubule network loosely organized in a grid-like fashion (Figure 2.2).

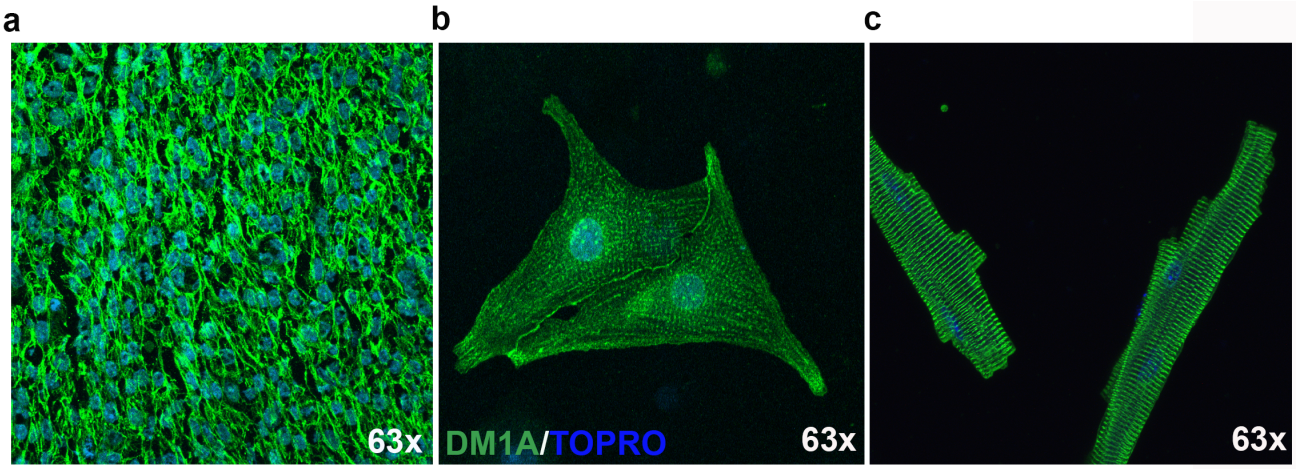


**Figure 2.1. Sarcomere development in cardiomyocytes.** In 14 day embryonic tissue (E14.5), alpha-actinin staining is beginning to pattern into striations **(a)**. By P7, alignment of the striations can now be detected in conjunction with the cell change in shape **(b)**. In adult cardiomyocytes, alpha-actinin is distinctly defining the sarcomeric structure **(C)**. Nuclei are indicated in blue (TOPRO).

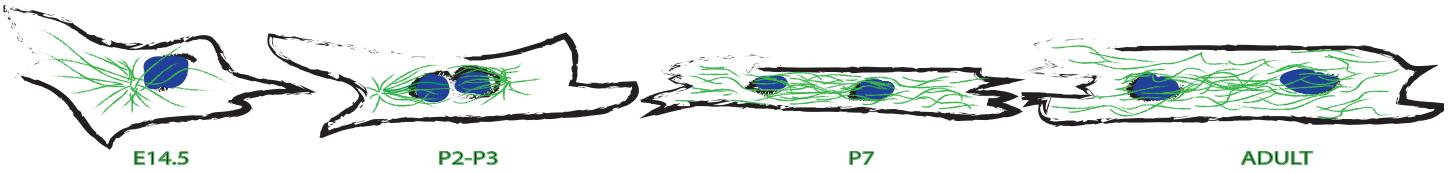


**Figure 2.2. Schematic of the organizational layout of microtubules in a cardiomyocyte throughout development**

Goldstein et al, showed electron microscopy images of microtubular layout consistent with current immunohistochemical images (Goldstein et al., 1979). And, although this layout has been established, understanding how the microtubule network assists in formation of the cytoarchitecture of a cardiomyocyte needs thorough examination. Identifying the phenotype can explain the recent studies reported on microtubule densification and the microtubular role in cardiac disease.

**Heart disease and the microtubule network**

Cardiomyocytes rely on the ability of the sarcomeric apparatus to develop force and rapidly shorten in a repetitive fashion (Henk & Granzier, 1998). Disruption of this process can occur in a variety of ways and can result in heart failure. Several reports of both the sarcomere and cytoskeleton have been implicated in cardiac hypertrophy and cardiomyopathies (Mcnally et al., 2013; Herman et al., 2012; Mohaptra et al.,2003; Eldik et al., 2013; Hein et al., 2000). However, only a few studies have mentioned the microtubule network in heart disease (Webster, 2002; Sequeira et al., 2013; ter Keurs et al., 1998). Since the only studies to pinpoint the function of microtubules in cardiomyocytes are very early mentions that state the network may be important in housekeeping functions, such as maintenance of the sarcoplasmic reticulum (Ioshii et al., 1994) and secretion (Larsen et al., 1993), understanding the application behind the observations of microtubules in disease has been challenging.

The most common investigation of the microtubule network in heart failure is the abundance of microtubules. In cardiac hypertrophy, an overload in microtubules has been noted as having a possible role in decompensation of the cardiomyocyte mechanics (Henk et al., 1998), increased systolic pressures (Tagawa et al., 1997), and an inability of the cardiomyocyte to shorten (Tsutsui et al., 1993). Ultimately, all of these observations have been associated with heart failure however, whether or not the microtubules are a part of the cause or, if the phenotype is a result of the disease has not been clear.

More recent studies have relied on newly available single cell assays and advanced imaging techniques to understand cardiac toxicity and disease (Webster, 2002; Robison et al., 2016; Dees et al., 2012). First, microtubules may have the ability to alter cardiomyocyte morphology in response to shear stress (Nishimura et al., 2006) and detyrosinated microtubules reportedly have a significant role in cardiomyocyte shortening, thus contraction (Robison et al., 2016). There is therefore a need for understanding which types of microtubules exist in cardiomyocytes in relation to function (Goldstein et al., 1979; Keurs et al., 1998; Robison, 2016). Nevertheless, Dees et al. reported the first study on a microtubule binding protein in the heart, which showed disruption of Centromere Protein F (CENP-F), resulting in dilated cardiomyopathy (DCM). *CENP-F*$^{-/-}$ hearts underwent arrhythmias, are much larger in size, and have lessened trabeculation (Dees, 2012). Furthermore, electron microscopy and single cell studies reported here on loss of CENP-F thoroughly show a disruption in cardiomyocyte architecture and function (Figure 2.3).

These results have also been tied to heart failure in a human bioview study where, a single nucleotide polymorphism (snp) of CENP-F was identified (Manalo et al., in review)(Figure 3.14, Chapter 3 of this dissertation). With these new studies, a new emerging field has opened up for the discovery of the importance of microtubules in cardiac function and disease.

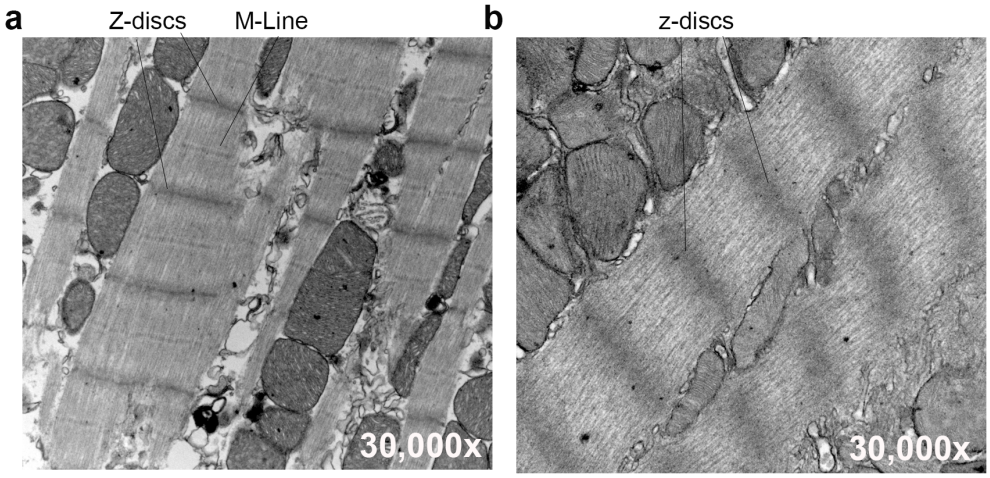


**Figure 2.3. Comparison of a healthy vs. diseased heart in adult mice.** A healthy adult heart shows patterned sarcomeres with distinct z-discs and aligned mitochondria **(a)**. Loss of microtubule-binding protein CENP-F results in misaligned mitochondria and thickened/disintegrated z-discs, with no distinct M-line **(b)**.

# CHAPTER III

# Loss of CENP-F Results in Dilated Cardiomyopathy with Severe Disruption of Cardiac Myocyte Architecture

This chapter is under current review under this title in *Scientific Reports* (Manalo et al., 2017)


## ABSTRACT

Centromere-binding protein F (CENP-F) is a very large and complex protein with many and varied binding partners including components of the microtubule network. Numerous CENP-F functions impacting diverse cellular behaviors have been identified. Importantly, emerging data have shown that CENP-F loss- or gain-of-function has critical effects on human development and disease. Still, it must be noted that data at the single cardiac myocyte level examining the impact of CENP-F loss-of-function on fundamental cellular behavior is missing. To address this gap in our knowledge, we analyzed basic cell function and structure in cardiac myocytes devoid of CENP-F. We found many diverse structural abnormalities including disruption of the microtubule network impacting critical functions of the cardiac myocyte. This is the first report linking microtubule network malfunction to cardiomyopathy. Importantly, we also present data demonstrating a direct link between a CENP-F single nucleotide polymorphism (snp) and human cardiac disease. In a proximate sense, these data examining CENP-F function explain the cellular basis underlying DCM in this genetic model and, in a larger sense, they will hopefully provide a platform upon which the field can explore diverse cellular outcomes in wide-ranging areas of research on this critical protein.


## INTRODUCTION

Dilated cardiomyopathy (DCM), the most common form of cardiomyopathy in humans, can arise from mutations in over 50 genes (McNally et al., 2013). There is expansive divergence in these genetic components as well as in the architectural abnormalities seen in the hearts of patients suffering from DCM (Herman et al., 2012; Mohapatra et al.,2003; Du et al., 2007). We were the first to report an implication for any microtubule binding protein in the development of DCM (Dees et al., 2012). With cardiac specific deletion of Centromere Protein F (CENP-F), a protein known to interact with microtubules (Vergnolle et al., 2007; Volkov et al.,2015; Moynihan et al., 2009), the resulting animals exhibited enlarged ventricles with thinner walls, fewer trabeculae, increased fibrosis, and arrhythmia (all

hallmarks of DCM), as well as death in 20% of outcomes (Dees et al., 2012). While extensive work, including our own, has been reported on this pervasive disease, significant gaps in our understanding of the underlying alterations in cellular mechanisms driving dysfunction remain.

CENP-F is a very large (380 KD), multi-faceted protein with a myriad of cellular functions (Pfaltzgraff et al., 2016; Pooley et al., 2008). CENP-F is critical in mitosis and disruption of its function can result in mitotic delay and misalignment of chromosomes (Liao et al., 1995; Yang et al., 2003; Yang et al., 2005). Additionally, CENP-F has been shown to have important interphase actions including regulation of ciliary function, vesicular transport, cell migration, cell shape, and organelle positioning (Pfaltzgraff et al., 2016; Pooley et al., 2008; Waters et al., 2015). A recurring theme in CENP-F function is interaction with the microtubule (MT) network and it is important to note that CENP-F loss of function has been shown to disrupt this cytoskeleton structure (Holt et al., 2005; Liao et al., 1995; Vergnolle et al., 2007). Recently and importantly, Waters *et* al have identified a human mutation which leads to severe ciliopathy and microcephaly-related phenotypes leading to prenatal death (Waters et al., 2015). Conversely, over-expression of CENP-F also has lethal effects on the human condition as recent studies have demonstrated that CENP-F is the leading prognostic indicator of poor outcomes in specific forms of esophageal and breast cancers (Mi et al., 2013; O'Brien et al., 2007; Aytes et al., 2014). Even from this brief review of the literature, it is abundantly clear that gain and loss of CENP-F function can have devastating outcomes in development and disease.

From the work of several laboratories, it is clear that CENP-F is a critical and complex regulator of basic cellular function. Still, it should be noted that almost all reports, including our own, examining the effect of CENP-F loss of function at the unicellular level have used cells grown for a prolonged period in an in vitro setting. With this in mind, we used our genetic *CENP-F*$^{-/-}$ murine model to isolate and immediately analyze fundamental properties of individual cardiac myocytes to determine whether and which myogenic properties might be changed with loss of CENP-F function. Our data at the unicellular level demonstrate that loss of CENP-F function in cardiac myocytes leads to fundamental changes in the regulation of the cytoskeleton, contractile apparatus, cell junctions, mitochondrial positioning and shape, and calcium influx. Importantly, our studies also demonstrate *CENP-F*$^{-/-}$ cardiac myocytes have loss of cellular stiffness while *CENP-F*$^{-/-}$ fibroblasts isolated from the same hearts have amplified stiffness. These data reveal that different cell types with the identical disruption of CENP-F may respond differently to this genetic challenge and have interesting implications for the analysis of DCM as wall stiffness is a hallmark of this disease. In this context, we also report human genomic studies linked to de-identified patient files identifying a CENP-F single nucleotide polymorphism (SNP) that is highly associated with human heart disease. Thus, concerning DCM, the current data reveal the basic cellular mechanisms underlying this murine form of cardiomyopathy and are the first to link CENP-F to human heart disease. In a broader sense, this study on the reaction of individual cells to loss of CENP-F may serve as a platform in the analysis of the numerous, diverse, and devastating responses of cells to fluctuation in CENP-F expression and function.

## MATERIALS AND METHODS

### Mouse lines

Mice were previously described (Moynihan, et al., 2009). *CENP-F*$^{fl/-}$, *CMV-CRE* animals (The Jackson Laboratory, Bar Harbor, ME) were crossed to generate *CENP-F*$^{-/-}$; *CMV-CRE animals*. *CENP-F*$^{+/+}$; *CMV-CRE* animals were used to generate control cardiac myocytes. Cardiac myocytes were isolated from adult mice aged 3-4 months to assure maturity. All animal care and experimental procedures were approved and performed in accordance with the ethical standards set by the Institutional Animal Care and Use Committees of Vanderbilt University and by the National Institute of Health (NIH).

### Cardiac Myocyte Isolation

Adult *CENP-F*$^{+/+}$; *CMV-CRE* and *CENP-F*$^{-/-}$; *CMV-CRE* mice were terminally anesthetized by inhalation of isofluorane five minutes after heparin injection (Moynihan et al., 2012). Hearts were suspended from a Langendorff perfused column via cannulation of the aorta and perfused with cell isolation buffer containing in mM: NaCl 113, KCl 4.7, $MgSO_4$ 1.2, $Na_2HPO_4$ 0.6, $KH_2PO_4$ 0.6, $NaHCO_3$ 12, $KHCO_3$ 10, Taurine 30, HEPES 10 to which Liberase TM 2.7mg (Roche cat.#05 401 127 001). Tissue was then minced and subject to further digestion followed by $CaCl_2$ dilution and bovine serum albumin (2mg ml $^{-1}$ until myocytes were liberated easily by titration with a sterile Pasteur pipette and filtered). Cardiac myocytes were then reintroduced to physiological $CaCl_2$ in increasing increments. Experiments were performed at 37 degrees C. Cardiac myocytes were plated on Laminin (10micrograms/ml) coated dishes and incubated for a minimum of one hour prior to manipulation or fixation with 4% paraformaldehyde. After a 15 minute fixing, cardiac myocytes were washed with 1x PBS and stored at -20 degrees C for further observation.

### Cardiac Fibroblast Isolation

Adult *CENP-F*$^{+/+}$; *CMV-CRE* and *CENP-F*$^{-/-}$; *CMV-CRE* mice were terminally anesthetized by inhalation of isofluorane five minutes after heparin injection (Moynihan, 2012). Hearts were suspended from a Langendorff perfused column via cannulation of the aorta and perfused with cell isolation buffer containing in mM: NaCl 113, KCl 4.7, $MgSO_4$ 1.2, $Na_2HPO_4$ 0.6, $KH_2PO_4$ 0.6, $NaHCO_3$ 12, $KHCO_3$ 10, Taurine 30, HEPES 10 to which Liberase TM 2.7mg (Roche cat.#05 401 127 001). Tissue was then minced and subject to further digestion followed by $CaCl_2$ dilution and bovine serum albumin (2mg ml $^{-1}$ ) until myocytes were liberated easily by titration with a sterile Pasteur pipette and filtered). The supernatant containing nonfibroblasts were removed and plated on 4 well slides or uncoated plates for further observation.

**Antibodies for Immunofluorescence**

Cardiac myocytes were fixed for 15 minutes at 37 degrees Celsius in 4% paraformaldehyde with 0.01% Triton-X100 prior to antibody labeling:

DM1A: mouse monoclonal (ab7291; Abcam).
Alexa Fluor 488 Phalloidin (A 12379; Invitrogen, Carlsbad, CA).
Alpha-Actinin (A7811; Sigma-Aldrich).
Beta-Catenin (C7207; Sigma-Aldrich).
TO-PRO-3 Iodide (T3605; ThermoFisher Scientific) was used to visualize DNA.

**Confocal Microscopy**

Cells were imaged on Zeiss LSM 510 Meta inverted confocal microscope in the Vanderbilt Cell Imaging Shared Resource Core at 40x (Plan-NEOFLUAR OIL), 63x (Plan-APOCHROMAT OIL), and 100x (Plan-NEOFLUAR OIL). Projections were created from 0.3 micrometer slices through the full thickness of the cardiomyocytes. The imaging mode used was a 3-D "Z-series" technique.

**Quantification of Microtubule/Nuclear Relationship**

From z-stack confocal images of cardiomyocytes, individual slices were analyzed using a point-line method in ImageJ (Abramoff et al., 2004). The line was specifically drawn throughout the nucleus from each end of the cardiomyocyte. The fluorescence of DM1A (microtubules) and TOPRO (nuclei) was calculated in ImageJ. The relationship of microtubule- and nuclear-associated fluorescence was quantified from analysis of 50 or greater individual fluorescence images per group. The tubulin concentration within 10 micrometers of the nucleus relative to the maximum tubulin concentration found throughout the cell was measured for specificity of the relationship and to avoid any imaging noise.

**Western Blot Analysis**

For Western blot, pelleted *CENP-F+/+* and *CENP-F*$^{-/-}$ cardiomyocytes were solubilized in Laemmli sample buffer in the presence of protease inhibitors (Lim et al., 2004). Equivalent amounts of extracts were run on 3–8% SDS gels using standard methodologies and transferred to nitrocellulose paper in the presence of 20% methanol, 10 mM β-mercaptoethanol, and 0.1% SDS. Blots were washed with phosphate-buffered saline (PBS) and blocked with 5% bovine serum albumin (BSA) in PBS for 1 h, followed by a 1-h incubation with anti–beta-catenin antibody and diluted 1:3000 in 5% BSA/PBS. Blots were washed in PBS with 0.1% Triton X-100, followed by reaction with goat anti-mouse (IRDye 800CW; Li-Cor) and similar washing for imaging on an Odyssey system. Controls for loading equivalence were conducted under similar conditions with GAPDH.

**PheWas Study**

To determine whether CENP-F is relevant to cardiac dysfunction in humans, we utilized BioVU, the Vanderbilt University Medical Center biorepository that links a de-identified version of the electronic health record to DNA samples and genotype data (Roden et al., 2008). The study cohort included 25,579 adults of European descent genotyped on the Illumina HumanExome BeadChip array v.1.0 (exome chip) as part of several BioVU research initiatives (Table 3.1).
The exome chip contains ~250,000 rare and common coding single nucleotide polymorphisms (SNPs), including 26 missense variants in CENP-F with a minor allele frequency >0.05% (http://genome.sph.umich.edu/wiki/Exome_Chip_Design). Variants in CENP-F were tested for association with heart failure with reduced ejection fraction (HFrEF) in BioVU using a phenome-wide association study (PheWAS) based phenotype (PheCode 428.3). PheWAS is a validated approach to interrogate the medical phenome that uses a validated, curated medical phenome that hierarchically groups International Classification of Disease (ICD-9) billing codes into ~1,800 phenotypes, each with defined control group (Denny et al., 2010). Variants in CENP-F were tested for association with HFrEF using logistic regression with an additive model adjusted for age and sex, and analyses were restricted to individuals of white European descent to limit population stratification. The Benjamini-Hochberg correction was applied to account for multiple testing with a $q<0.1$ considered statistically significant.

Clinical cohorts genotyped on exome chip

1. An elderly cohort (patients over age 75) with at least 3 years of follow-up
2. A rare-diseases cohort, including patients with FDA-defined rare diseases (no cardiomyopathies are included among the FDA-defined rare diseases)

3. A healthy longitudinal cohort including patients with 1-2 notes per year for at least 5 years

4. A sick longitudinal cohort including patients with 3-6 notes per year for at least 5 years
5. The Vanderbilt Electronic Systems for Pharmacogenomic Assessment Cohort, created to investigate drug response phenotypes.
6. A cancer cohort consisting of patients within the Vanderbilt Tumor Registry
7. A pediatric cohort consisting of patients under 18 years of age with at least one pediatric visit

| **Table 3.1: BioVu** | |
|---|---|
| Transcript | Amino Acid Change |
| NM_016343 | R300C |
| NM_016343 | H494Q |
| NM_016343 | M701V |
| NM_016343 | Q754E |
| NM_016343 | M793R |
| NM_016343 | R815H |
| NM_016343 | Y1018D |
| NM_016343 | G1033R |
| NM_016343 | T1105I |
| NM_016343 | E1145D |
| NM_016343 | A1208V |
| NM_016343 | L1412S |
| NM_016343 | A1515T |
| NM_016343 | K1539R |
| NM_016343 | N1703S |
| NM_016343 | D1768N |
| NM_016343 | R1879C |
| NM_016343 | D1978G |
| NM_016343 | E2011A |
| NM_016343 | S2044L |
| NM_016343 | A2139T |
| NM_016343 | Q2225R |
| NM_016343 | A2356V |
| NM_016343 | N2396D |
| NM_016343 | R2729Q |
| NM_016343 | N3106K |

**Table 3.1. Illumina HumanExome BeadChip array v.1.0 (exome chip).** The study cohort, including 25, 579 individuals on the above exome chip. ~250,000 snps can be found.

**Quantification of Cardiac Myocyte Mitochondrial Persistence**

For further analysis of mitochondrial population in EM images, a box was placed over a given area and assessed for mitochondrial persistence in Imagej (Abramoff et al, 2004). In five or more images, a line was drawn through the number of mitochondria in a row. The differences in mitochondrial persistence were quantified.

**Quantification of Cardiac Myocyte Sarcomere Structure**

Using Imagej, a fast Fourier transform was run on a trace along the length of the sarcomere structure from a series of z-stack images of cardiac myocytes stained for alpha-actinin. The position of the peak of the normalized phase plot was used to calculate the sarcomere length. A 2D FFT transform was run to observe differences in the frequency distribution, plotted as a 2D power spectrum. For further analysis of z-discs in EM images, a 1.5' x 0.12" box was placed over 50 or more individual z-discs in Imagej (Abramoff et al., 2004). If any part of the z-disc could not fit within the area of the box, the z-disc was considered disintegrated. Additionally, in twenty images or more, a line was drawn through the number of z-discs in a row. The differences in z-disc structure and linear persistence were quantified.

**Transmission Electron Microscopy**

Hearts were removed from adult mice and immediately perfused in 2.5% gluteraldehyde in 0.1M cacodylate buffer, pH7.4 at room temperature (RT), then further dissected for optimal transmission electron microscopy processing. The samples were washed in 0.1M cacodylate buffer, then incubated 1 hour in 1% osmium tetraoxide at RT, then washed with 0.1M cacodylate buffer, followed by a 30-minute incubation in 1% potassium ferrocyanide for additional membrane contrast. Subsequently, the samples were dehydrated through a graded ethanol series and then 3 exchanges of 100%

ethanol. Next, the samples were incubated for 5-minutes in 100% ethanol and propylene oxide (PO) followed by 2 exchanges of pure PO. Samples were then infiltrated with 25% Epon 812 resin and 75% PO for 30 minutes at RT. Next, they were infiltrated with Epon 812 resin and PO [1:1] for 1 hour at RT then overnight at RT. Next day, the samples went through a [3:1] (resin: PO) exchange for 3-4 hours, then incubated with pure epoxy resin overnight. Samples were then incubated in two more changes of pure epoxy resin than allowed to polymerize at 60°C for 48 hours.
70-80nm ultra-thin sections were cut and collected on 300-mesh copper grids and post-stained with 2% uranyl acetate and then with Reynold's lead citrate. Samples were subsequently imaged on the Philips/FEI Tecnai T12 electron microscope at various magnifications.

**Quantification of Cardiac Myocyte Stiffness by AFM**

A Bruker biocatalyst AFM system was used to measure the stiffness of isolated cardiac myocytes, cardiac fibroblasts and MEFs. The quantitative nano-mechanical mapping mode was used to assess both the topography and elastic modulus of wild-type and *CENP-F*$^{-/-}$ cells. This mode uses a blunted pyramidal tip to indent and gather mechanical information from about a micron below the cell surface. Between 4 and 10 cells were scanned per group and the median elastic modulus calculated from 1-2 approximately 10x10 micron scans for each cell (>10,000 measurements per scan). The average median cell stiffness was calculated and compared between wild-type and *CENP-F*$^{-/-}$ with a student t-test.

**RNA isolation**

RNA was isolated using mRNeasy mini kit (Qiagen) following manufacturer instructions and was quantified using Take3 micro-volume plates with Synergy Mx plate reader and Gen5 software.

**Real-Time PCR**

Total RNA was reverse transcribed, using TaqMan RT kit (Applied Biosystems) with random hexamers following manufacturer instructions. Individual transcript levels were quantified with real-time PCR TaqMan probes, and relative quantitation values (RQV) were calculated with normalization to the housekeeping gene, GAPDH.

**Measurement of Intracellular Ca**

Cardiomyocytes were loaded with Fura-2 acetoxymethyl ester, Fura-2AM (Molecular Probes Inc, Eugene, OR) as described previously (Feaster, 2015). After an 8-minute incubation in Fura-2AM at room temperature, cardiomyocytes were washed twice for 10 minutes with Tyrode's solution. Fura-2AM loaded Ca transients were recorded during spontaneous beating or 0.2 Hz field stimulation in 2mmol/L Ca Tyrode's solution. Ca transients were recorded and analyzed using commercially available data analysis software (IonOptix, IonWizard Milton, MA). All experiments were conducted at room temperature. Tyrode's solution containing (in mmol/L): $CaCl_2$, NaCl 134, KCl 5.4, $MgCl_2$ 1, Glucose 10, and HEPES 10, pH adjusted to 7.4 with NaOH.

## RESULTS

**Deletion of CENP-F disrupts the microtubule network in adult cardiac myocytes**

There are no reports on the effect of CENP-F loss of function at the level of the individual cardiac myocyte. Additionally, we found only one report analyzing the potential changes in the microtubule network in DCM (Takahashi et al., 1998). Thus, in order to gain a clear understanding of the possible effect that loss of CENP-F may have on the cardiac microtubule network, a thorough characterization of microtubules in wild-type adult cardiac myocytes was first conducted using anti-alpha tubulin antibody DM1A. All cells reported below were analyzed within one hour after isolation from healthy or diseased hearts. Slices of z-stack images obtained through confocal microscopy were individually measured for microtubule density throughout the entirety of the cardiomyocyte. The microtubule network in these wild-type cardiac myocytes had a distinct and highly ordered pattern as seen in reconstructed z-stack images (Fig 3.1). In agreement with previous studies on adult skeletal myocytes (Folker et al., 2013; Tassin et al., 1985; Oddoux et al., 2013), a concentration of the microtubule network around the nuclei of cardiac myocytes was observed (Figs 3.1. a, a', c). Quantification of this association confirmed this result and demonstrated a high concentration of microtubules in association with the myocyte nucleus (Fig 3.1. e). In the non-nuclear domain, a lattice of individual longitudinally- and circumferentially-oriented microtubules was readily detected along the entirety of the cell (Figs 3.1. a', a"). Again, this is in agreement with studies on skeletal myocytes that show microtubules distributed in this fashion along the entire length of the cell (Oddoux et al., 2013). Thus, the organization of microtubules is largely preserved in both skeletal and cardiac myocytes. These results establish a baseline for comparing the potential effect that loss of CENP-F might have on the microtubule network in cardiac myocytes.

Figure 3.1 shows the dilation of the heart in the global knockout of CENP-F. In adult cardiac myocytes isolated from these *CENP-F*$^{-/-}$ hearts, the overall structure of the microtubule network was severely disrupted. First, the concentrated association of the microtubules with the nucleus seen in wild-type myocytes was completely lost
in knockout cells (Figs 3.2. b, d). The relationship of the microtubule network around the nuclei of wild-type and *CENP-F*$^{-/-}$ cells was quantified using a point-line method on individual z-stack slices obtained by confocal microscopy (see Methods). These data confirmed the microtubule-nucleus relationship in wild-type cells (Figs 3.2. c, c') and the nearly complete loss of this association in *CENP-F*$^{-/-}$cardiomyocytes (Figs 3.2. d, d'; note the complete loss of overlap between blue (nuclear scan) and green (microtubule scan) in Fig 3.2 d' which is seen in Fig 3.2 c'). Next, the non-nuclear component of the microtubule network was also disrupted with major aberrations. While the longitudinal array of non-nuclear microtubules was preserved, the circumferential component was reduced and significantly altered. The ends of these microtubules formed tight circles which were never seen in wild-type cardiac myocytes (Figs 3.2. b, b'). Interestingly, acute treatment of wild-type cardiac myocytes with nocodazole (a microtubule destabilizer) produced similar alterations of microtubules seen in adult *CENP-F*$^{-/-}$ cardiac myocytes (Fig 3.2. b"). These data demonstrate that CENP-F loss of function has a significant and cell-specific (discussed below) effect on the microtubule network and are the first to show disruption of microtubules in any model of DCM.

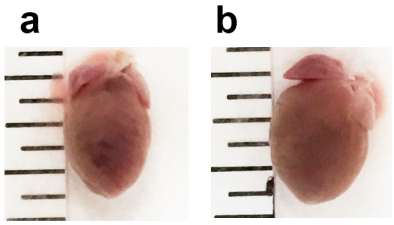


**Figure 3.1. The loss of CENP-F leads to cardiac dilation in adult mice.** Isolated adult hearts from wild-type mice are measured in inches **(a)**. In a global knockout of CENP-F, hearts are dilated/ enlarged when compared to wild-type hearts **(b)**. n=8 per group.

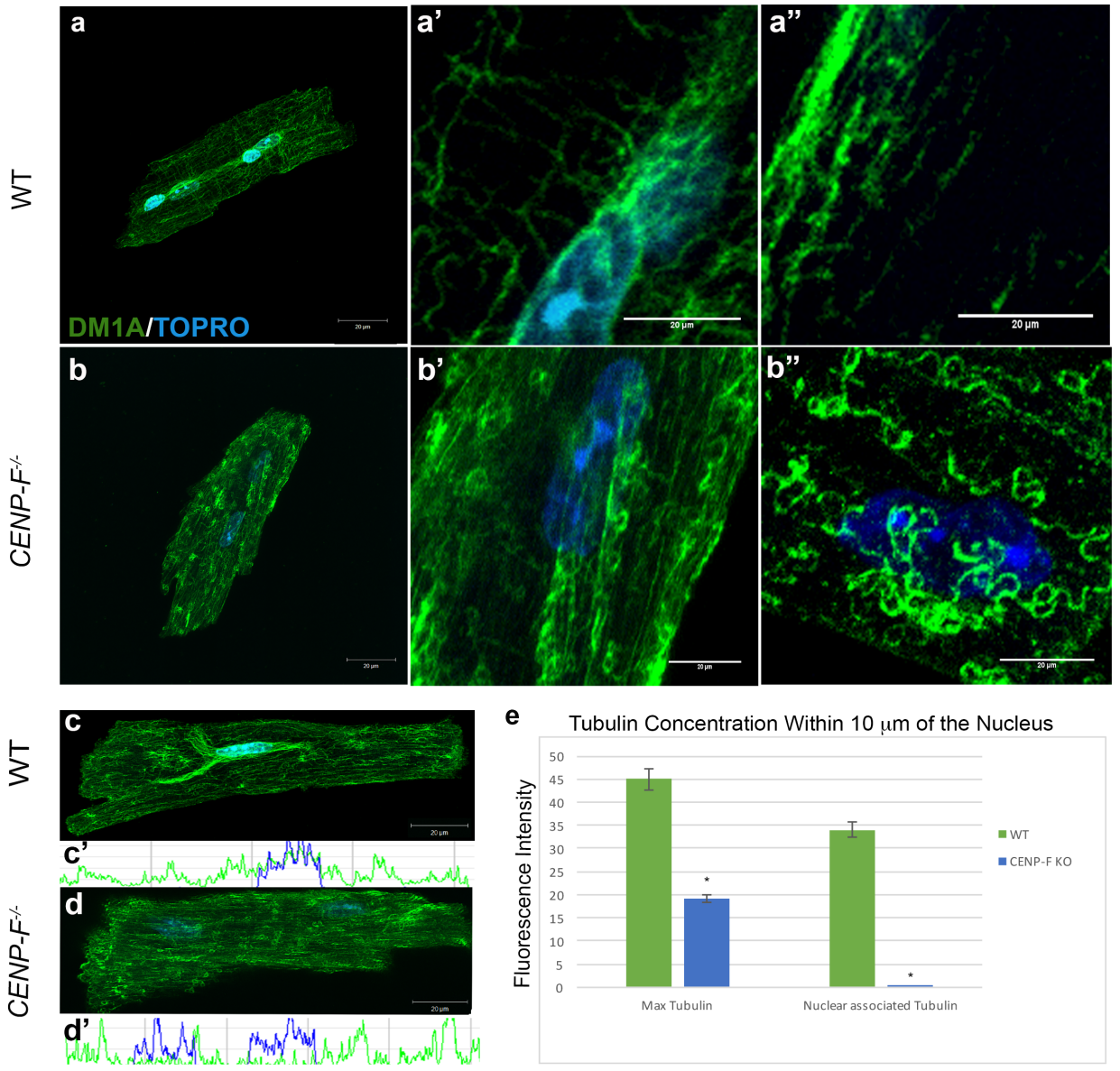


**Figure 3.2. Microtubules (MTs) form rings at plus ends and lose connection with nucleus in *CENP-F*$^{-/-}$ cardiomyocytes.** Cardiomyocytes isolated from wild-type **(a)** and *CENP-F*$^{-/-}$ **(b)** mice were fixed and immunostained with DM1A antibody (green) and TOPRO (blue). A zoom in of the circumferentially-oriented MT network **(a')(b')** and longitudinal array of MTs **(a'')** are shown in wild-type and *CENP-F*$^{-/-}$ mouse cardiomyocytes, respectively. Cardiomyocytes were treated with nocodazole to destabilize microtubules for phenotype comparison **(b'')**. Immunostaining of MTs (green) and nucleus (blue) in wild-type cardiomyocytes show a microtubule-nuclei relationship **(c)**, accompanied by a representative scan **(c')**.This relationship is completely gone in *CENP-F*$^{-/-}$ cardiomyocytes **(d)**, accompanied by a representative scan **(d')**. In **(e)**, quantification of the maximum tubulin and nuclear associated tubulin of wild-type vs. *CENP-F*$^{-/-}$ cardiomyocytes, show a tight relationship between microtubules and nuclei in wild-type cells opposed to a complete loss of association in *CENP-F*$^{-/-}$ cells. In wild-type and *CENP-F*$^{-/-}$ cells, n=50 or more z-stack images analyzed for maximum tubulin. In wild-type and *CENP-F*$^{-/-}$ cells, n=50 or more z-stack images analyzed for nuclear associated tubulin **(e)**. Scale bars: 20 µm. *$p$<0.001. Error bars indicate SEM.

**Basic cardiac myocyte structure is preserved in *CENP-F*$^{-/-}$ cells but with an alteration at the cell junctions**

Intercalated discs connecting adjacent cardiac myocytes are essential for intercellular synchronization and transmission of force for proper contraction of the heart (Kostetskii et al., 2005; Olson et al., 2002). Kostetskii *et al*. have reported that disruption of the intercalated disc results in modest dilated cardiomyopathy (Kostetskii et al., 2005). In this context, the cell junctions in isolated wild-type and knockout cardiac myocytes were evaluated. First, an anti-alpha-actinin antibody (staining z-discs) was used to visualize the overall structure of these cardiac myocytes to provide context for the analysis of intercalated discs. In images of wild-type myocytes, the cell termini displayed a stacked/multilayered arrangement of myocyte/myocyte junctional domains in the terminal regions of the cells (Fig 3.3. a). Figure 3.3a demonstrates the generalized prominence of these cell termini that abruptly end perpendicular to the long axis of the myocyte (these domains indicated by * in this figure). Next, anti-beta-catenin staining was used to identify the adherens junction component of the z-disc and confirmed the multilayered arrangement in wild-type myocytes (Fig 3.3. b). Ultrastructurally, transmission electron microscopic (TEM) analysis further demonstrated the highly-ordered, well-defined structure of intercalated discs of wild-type cardiac myocytes (Fig 3.3. c).

While significant changes in z-disc structure were seen with loss of CENP-F function (discussed below), anti-alpha-actinin staining illustrated that the basic structure of the myocyte is maintained in the absence of CENP-F. However, the multi-layered structure of the cell termini of these cells was completely lost in the absence of CENP-F. The sharp, perpendicularly-arranged cell termini observed in wild-type cells were not seen in single cell analysis of *CENP-F*$^{-/-}$ myocytes (Fig 3.3. a'). Instead, these myocytes have singularly-arranged cell termini (Fig 3.3. a'). Anti-beta-catenin staining was concentrated at this terminal domain and was not seen in the stepwise arrangement observed in wild-type cells (Fig 3.3. b'). Additionally, the staining in this single cell assay suggested that the terminal domain of *CENP-F*$^{-/-}$ myocytes was thicker than their wild-type counterpart. TEM images of the intercalated discs of these myocytes showed
that this terminal domain was widened and lacked the "sharpness" of discs observed in wild-type cells (Figs 3.3. c, c'). RT/PCR analyses were conducted on cell junction components, N-cadherin and beta-catenin, and decreased expression levels were noted for both gene products (Fig 3.3. d and Figure 3.4. a). Furthermore, western blot analysis on beta-catenin protein was performed and the cropped images revealed a significant decrease in this intercalated disc component of *CENP-F*$^{-/-}$ myocytes as compared to wild-type cells (Fig 3.3. e and Figure 3.4. b). Full-length blots are presented in Figure 3.5. Therefore, although the beta-catenin images appear thickened, quantitative analyses at the RNA and protein levels show that these intercalated disc components are down-regulated with loss of CENP-F. Taken together, these data demonstrate the disruption of intercalated discs in hearts where DCM is induced with the loss of CENP-F function.

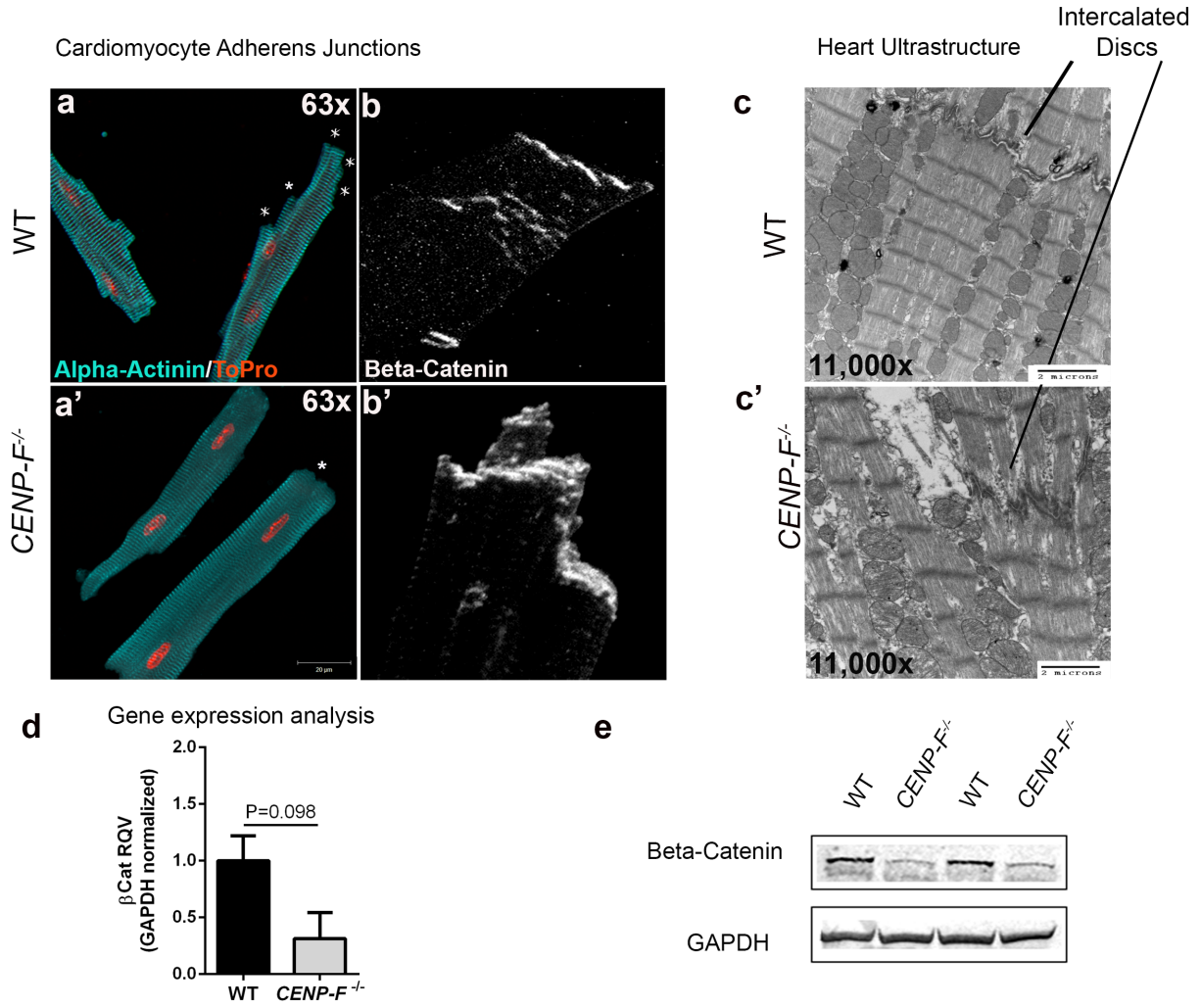


**Figure 3.3. Intercalated disc organization is disrupted with the loss of CENP-F in cardiomyocytes.** Cardiomyocytes isolated from wild-type**(a)** and *CENP-F*$^{-/-}$ **(a')** mice were fixed and immunostained with alpha-actinin 2 antibody (teal) and TOPRO (orange). In CENP-F$^{+/+}$ cardiomyocytes, there are multiple junction ends, as indicated by * **(a)**. However, in *CENP-F*$^{-/-}$ cardiomyocytes, the cell termini is blunted, indicated by * **(a')**. The intercalated discs were immunostained with beta-catenin antibody (white) and the images are zoomed in to depict the lining of the cardiomyocyte junctions. In wild-type mice, there is thin and distinct junction staining **(b)** opposed to disintegrated and thickened junction staining of the mutant cardiomyocytes **(b')**. An EM image of wild-type heart shows a clear depiction of an intercalated disc, see horizontal structure pointed to by line **(c)**, In *CENP-F*$^{-/-}$ cardiomyocytes, the intercalated disc is highly disintegrated **(c')**. A gene expression analysis of beta-catenin in wild-type versus *CENP-F*$^{-/-}$ cardiomyocytes **(d).** A western blot analysis of beta-catenin in wild-type versus *CENP-F*$^{-/-}$ cardiomyocytes showed significant decrease in beta-catenin. 2 cropped samples are presented and n=5, $p<0.05$. Full-length gels are presented in Supplementary Figure 3.**(e)**. Scale bars: (a), 20 mm**;** (a)', 20 mm; (c), 2 microns; (c)', 2 microns. Error bars in (e) represent standard error of the mean (SEM).

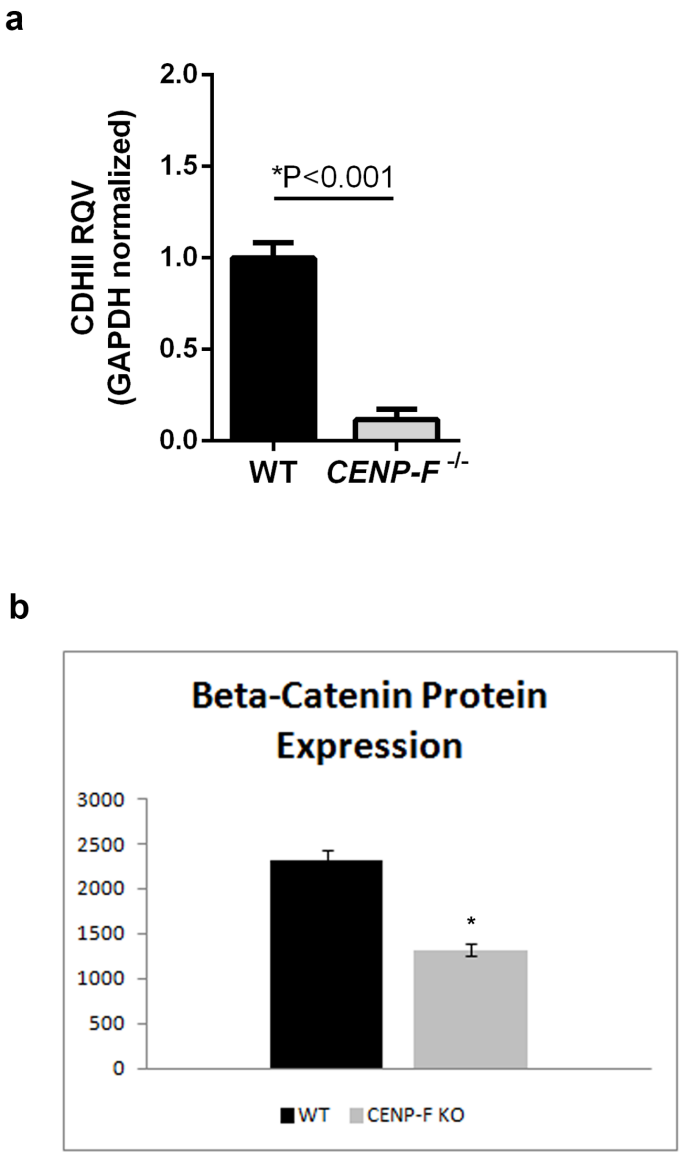


**Figure 3.4. Gene expression changes of the cardiomyocyte junction with loss of CENP-F.** The level of n-cadherin is significantly decreased in C*ENP-F*$^{-/-}$ cardiomyocytes when compared to wild-type **(a)**. A western blot analysis of beta-catenin protein expression is significantly decreased in *CENP-F*$^{-/-}$ vs. wild-type cardiomyocytes **(b)** $p<0.05$, n=5, error bars = (SEM).

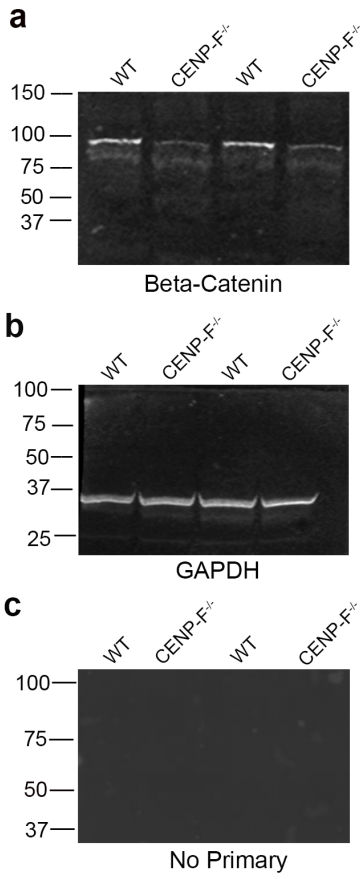


**Figure 3.5.**
**Full-length Western Blot of Beta-Catenin shows a significant decrease in *CENP-F*$^{-/-}$ cardiomyocytes.**
A western blot anaylsis (n=5) shows that loss of CENP-F results in a decrease of beta-catenin **(a)**. GAPDH represents a positive control for all western blot analysis **(b)**. No primary represents a negative control for all western blot analysis **(c).**

**Severe alteration of the sarcomeric network is observed in *CENP-F*$^{-/-}$ hearts**

To date, there are no reports linking the disruption of microtubule network components to structural deficits in the sarcomeric architecture in heart disease. Obviously, maintenance of the sarcomeric network is essential for cardiac function. To determine whether loss of CENP-F function impacted this fundamental unit of the cardiac myocyte, quantitative immunofluorescence was performed on isolated wild-type and knockout cardiac myocytes. Alpha-actinin antibodies were employed to mark the borders of sarcomeres (ie., z-discs). Electronic microscopic analysis of myocytic architecture was also conducted in parallel.

Using confocal microscopy, the z-discs in wild-type myocytes displayed the distinctive periodic and recurring structure previously reported for this cell type with anti-alpha-actinin antibodies (Fig 3.6. a). These results were quantified using a 2-D fast fourier transform technique and showed precise periodic banding (Fig 3.6. b). Additionally, a breakdown of individual z-stack slices confirmed the precise spacing of z-discs seen in wild-type cardiomyocytes and the precision of this optical technique (Fig 3.6. a, b). An ultrastructural view of a wild-type heart also displayed crisp sarcomere structure with a distinct M-line, z-discs, and actomyosin network at lower (Fig 3.6. e) and higher (Fig 3.6. e') power imaging.

Pervasive and widespread changes in the structure of the contractile apparatus were readily observed in *CENP-F*$^{-/-}$ myocytes. Specifically, a very diffuse appearance of z-discs in the *CENP-F*$^{-/-}$ cardiac myocytes was readily apparent when compared to wild-type cells (Figs 3.6. a, a'). 2-D fast fourier analysis of the alpha-actinin staining showed a lack of regularity in the z-discs of *CENP-F*$^{-/-}$ cardiac myocytes (Fig 3.6. b'). A breakdown of individual z-stack slices confirmed that the blurred structure seen in *CENP-F*$^{-/-}$ cardiac myocytes was of disintegrated z-discs rather than an issue of image quality (Fig 3.7. c, d). Additionally, a 3D movie further displayed the difference in z-disc precision and overall cardiomyocyte structure (Movie 3.1). Sarcomere length in knockout and wild-type cells was also quantified and the distance between the z-discs was reduced by 0.2 microns in the knockout myocytes representing a 10% decrease in length (Fig 3.6. c). Additionally, the z-discs were two-fold wider in *CENP-F*$^{-/-}$ cardiac myocytes in comparison to wild-type z-discs (Fig 3.6. d). These results are consistent with other reports on sarcomere shortening in other forms of cardiac disease (Sequeira et al., 2014; Hamdani et al., 2008). Transmission electron microscopy also demonstrated the overall disorganized nature of the contractile apparatus in *CENP-F*$^{-/-}$ myocytes (Fig 3.6 f, f'). The area and lineal persistence of z-discs in myofibrils of wild-type and knockout cells was also quantified using statistical analysis of ultrastructural images (Figure 3.7). These data confirm that z-discs of *CENP-F*$^{-/-}$ myocytes were widened, lacked persistence, and were variable in shape with compared to contractile apparatus in wild-type cells. Taken together, these data using different analytical tools demonstrate the essential nature of CENP-F in maintenance of the contractile apparatus.

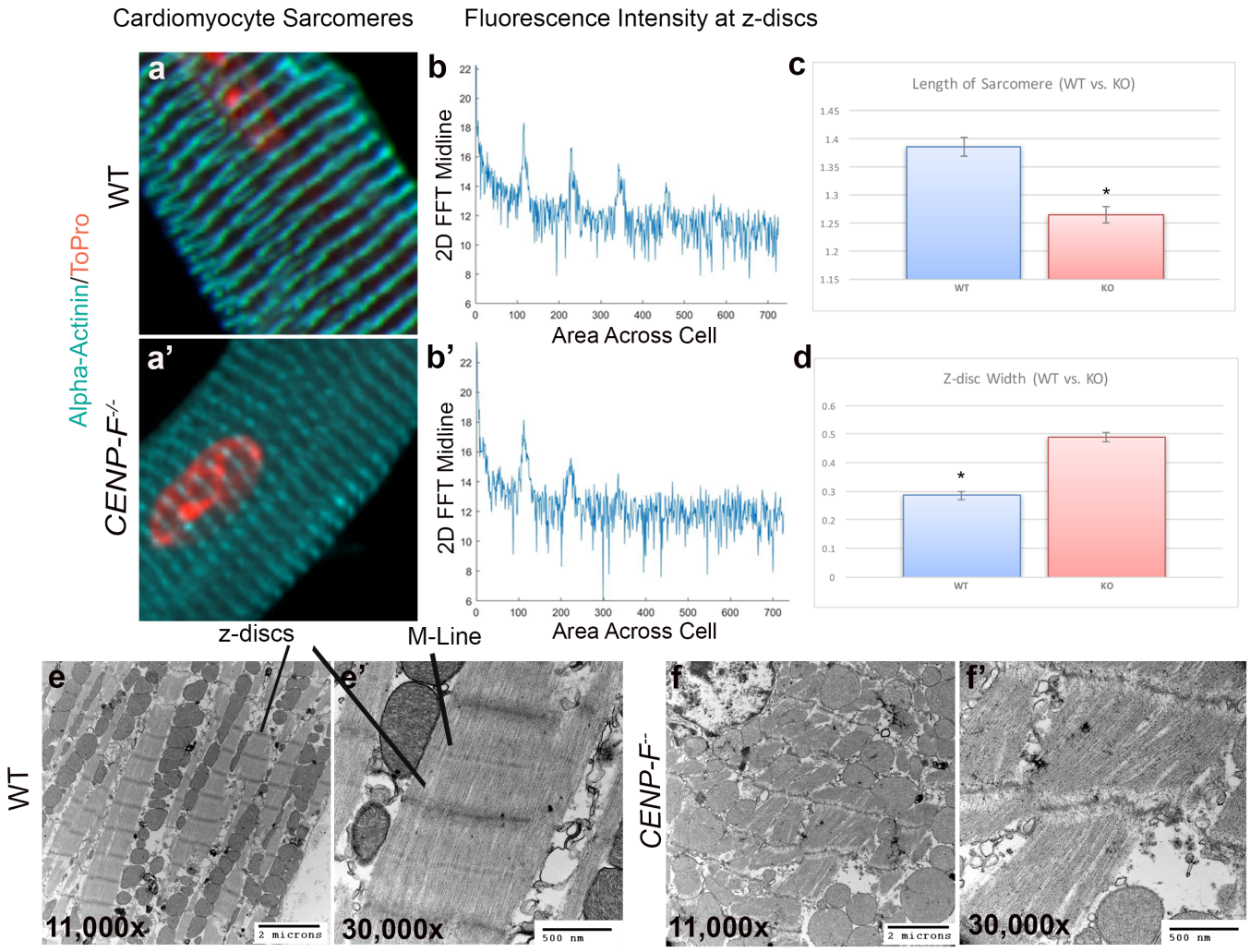


**Figure 3.6. Sarcomere architecture is disrupted with the loss of CENP-F in cardiomyocytes.** Cardiomyocytes isolated from wild-type **(a)** and *CENP-F*$^{-/-}$ **(a')** mice were fixed and immunostained with alpha-actinin antibody (teal) and TOPRO (orange). A zoom in view of the sarcomere structure displayed a distinct patterning in wild-type cardiomyocytes **(a)** versus a diffuse and thickened z-disc patterning in *CENP-F*$^{-/-}$ cardiomyocytes **(a')**. A 2-D spectrum analysis of the fluorescence regularity in alpha-actinin stained cardiomyocytes displayed high intensity points at regular positioning in wild type cardiomyocytes **(b)**. There is much more variability in the fluorescence staining of the *CENP-F*$^{-/-}$ cardiomyocytes **(b')**. The distance between the z-discs is much shorter in *CENP-F*$^{-/-}$cardiomyocytes in comparison to the wild-type population, *$p$<0.001 **(c)**. Additionally, the width of the z-discs is much wider in the mutant cardiomyocytes opposed to the wild-type,*$p$<0.001 **(d)**. A TEM of an wild-type adult mouse heart **(e)**. The z-discs and M-lines are well defined, as depicted in a higher magnification **(e')**. In a CENP-F deleted mouse heart, the z-discs are disintegrated and there are breaks within the actomyosin network **(f)(f')**.Scale Bars: (e), 2 microns; (e'), 500 nm; (f), 2 microns; (f'), 500 nm. Error bars in (c) and (d) represent standard error of the mean (SEM).

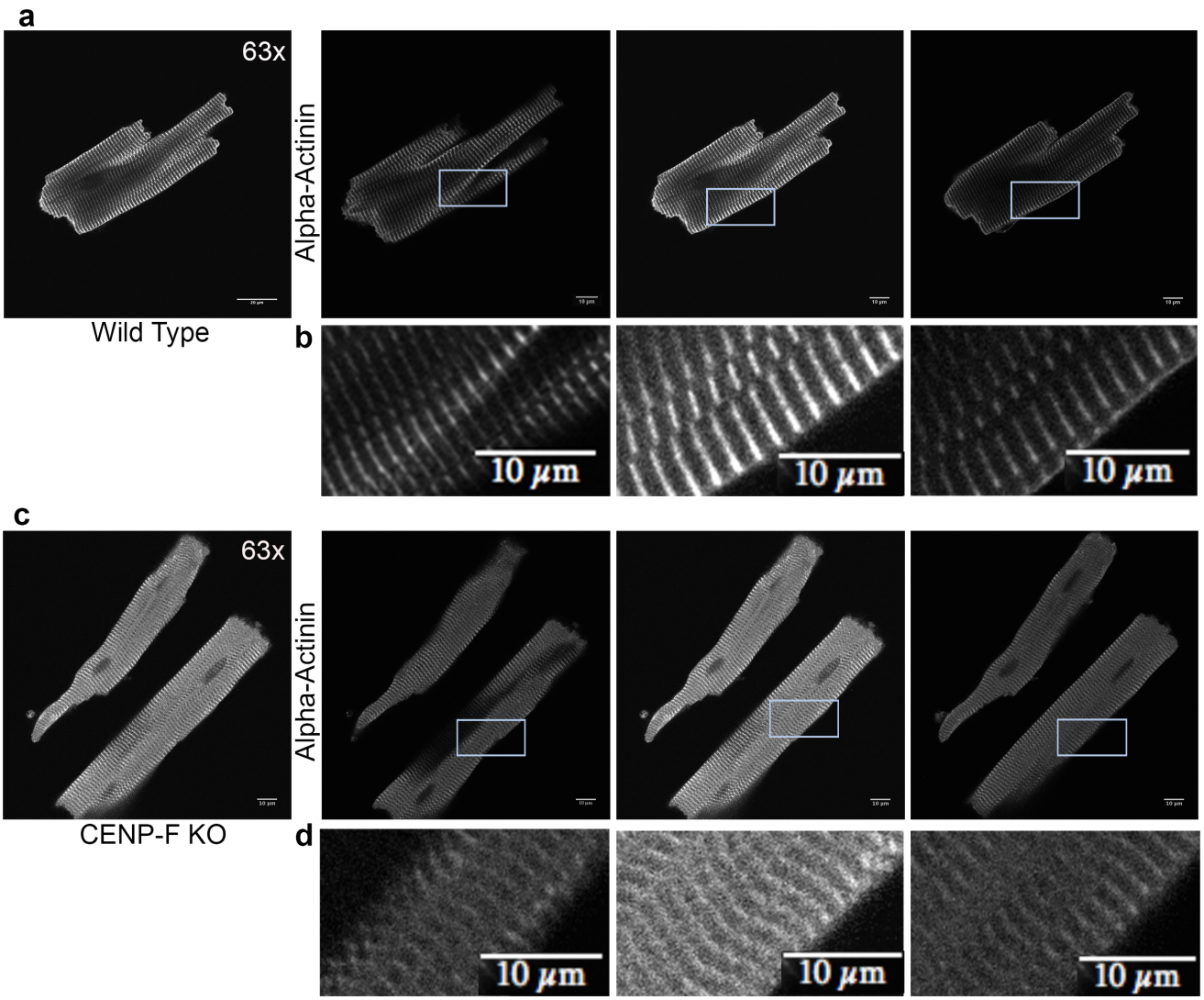


**Figure 3.7. *CENP-F*$^{-/-}$ cardiomyocytes have less alpha-actinin expression and are disorganized compared to wild type cardiomyocytes.** Individual slices of z-stack images in wild type cardiomyoctes show distinct z-disc staining with anti-alpha-actinin antibody **(a,b)**. In *CENP-F*$^{-/-}$ cardiomyocytes, alpha-actinin staining is dim, indicating less alpha-actinin expression. Additionally, z-discs are widened and severly disintegrated **(c,d)**. All images are adjusted at the same brightness and contrast levels. Images are in greyscale for proper comparison of image quality. Scale bars: (a), 20 mm; (b), 10 mm; (c), 20 mm; (d), 10 mm.

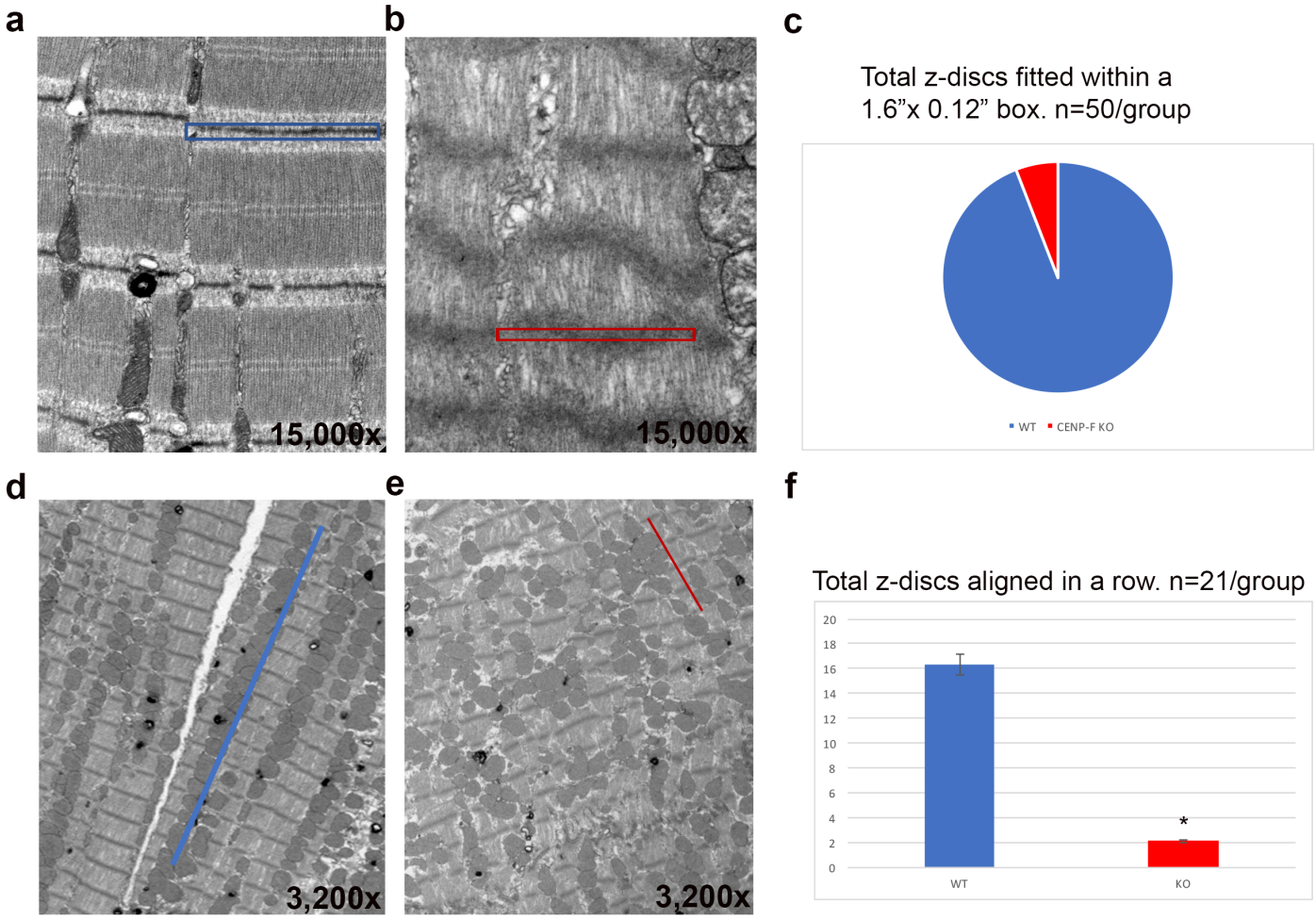


**Figure 3.8.. Z-discs lose straight and aligned phenotype in *CENP-F*$^{-/-}$ cardiomyocytes.** A 1.6” x 0.12” box can fit 96% of wild-type z-discs **(a)** and only 3 out of 50 of the *CENP-F*$^{-/-}$ z-discs could fit **(b)(c)**. As many as 17 z-discs can be counted in a row in wild-type TEM heart images **(d)**. No more than 4 z-discs are aligned in *CENP-F*$^{-/-}$ sarcomeres **(e)(f)**. n=21, *$p$<0.005. Error bars represent SEM.

**Mitochondria are misaligned and varied in size with the loss of CENP-F**

Recent reports have determined that mitochondrial disorganization is a precursor to DCM (Arbustini et al., 1998). There is an intimate relationship between the structural integrity of the cytoskeleton and mitochondrial organization within a cardiac myocyte (Vincent et al., 2016; Wang et al., 2015; Yancey et al., 2015). Having identified ultrastructural changes in *CENP-F*$^{-/-}$ cardiac myocytes, transmission electron microscopic analysis was used to image and compare mitochondria in wild-type and knockout cardiac myocytes. As previously reported, the similarly sized mitochondria of wild-type mouse myocytes are aligned in long sequences between adjacent myofibrils (Liao et al., 1995) (Fig 3.9. a). This arrangement was greatly disrupted in *CENP-F*$^{-/-}$ hearts as mitochondria were rarely seen arranged in the long rows observed in wild-type myocytes (Fig 3.9. b). A quantification of mitochondrial persistence revealed an approximately 5-fold decrease in lineal persistence with the loss of CENP-F (Figure 3.10). Additionally, these misaligned mitochondria varied in shape and size in a random manner throughout the myocyte (Fig 3.9. b). These results are consistent with other models of DCM (Wang et al., 2015; Fearnley et al., 2011) and, for the first time, link disruption of the microtubule network in the heart with abnormal mitochondrial size and alignment.

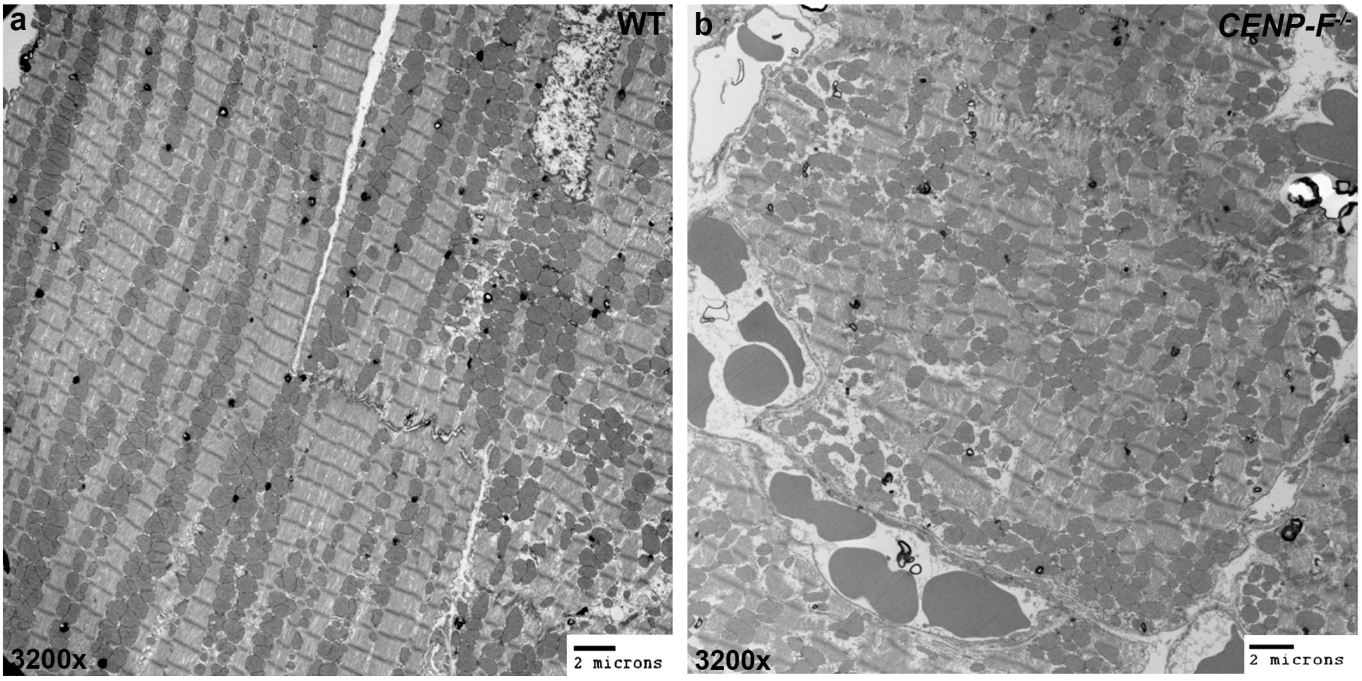


**Figure 3.9. Mitochondria are misaligned and varied in size with the loss of CENP-F.** Mitochondria are ordered, aligned, and relatively the same size in wild-type hearts **(a)**. In *CENP-F*$^{-/-}$ hearts, mitochondria have no alignment and are varied in size **(b)**. Scale bars: (a), 2 microns; (b), 2 microns.

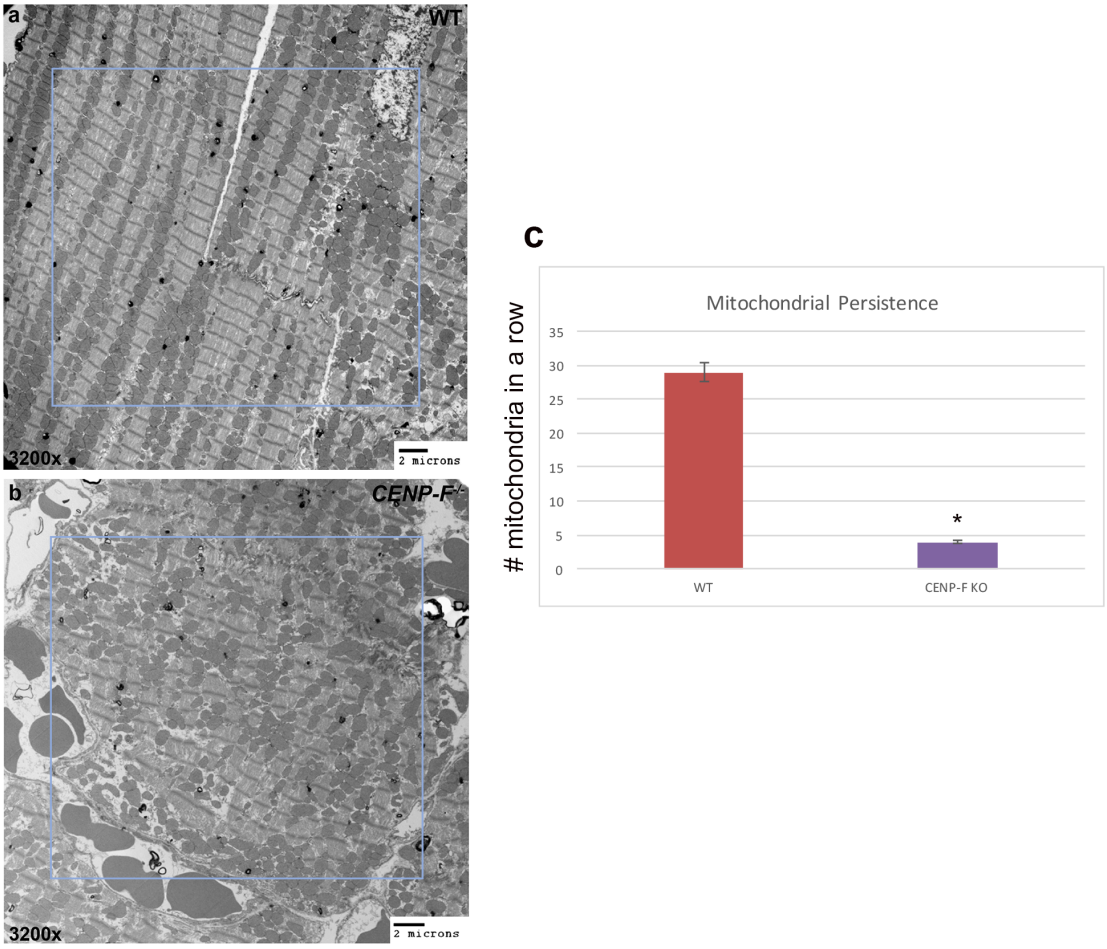


**Figure 3.10. Mitochondria are misaligned with loss of CENP-F in TEM images of the heart.** In a given area (box), the persistence of mitochondria in wild-type hearts that are aligned within the sarcomeric structures averages at 29 in a row **(a)(c)**. Without CENP-F, there is a significant decrease in mitochondrial alignment averaging only 4 in a row **(b)(c).** *$p$<0.001, Error bars represent (SEM).

**CENP-F deletion results in softened cardiac myocytes and thus a reduction in mechanical force**

There is increased fibrosis and loss of myocytes in DCM hearts that lead to overall myocardial stiffness (Nagueh et al., 2004). Interestingly and conversely, recent reports have identified that isolated myofibrils and myocytes of hearts with specific forms of DCM have a decreased stiffness in comparison to wild-type cells (Chaturvedi et al., 2010; Neagoe et al., 2002). While our previous report showed increased extracellular matrix in *CENP-F*$^{-/-}$ hearts (Dees et al., 2012), there are no studies that have directly examined the effect of CENP-F loss of function on the physical properties of single live cardiac myocytes.

To measure cell stiffness, Atomic Force Microscopy (AFM) was performed on wild-type and *CENP-F*$^{-/-}$ cardiac myocytes immediately after isolation (Collaboration with David Merryman Lab, Vanderbilt University; See methods). A 10 x 10 micron area of the cell was scanned for cell stiffness (Fig 3.11. a). In wild-type cardiac myocytes, there was a consistent stiffness of the scanned area (Figs 3.11. c, d). The cell recorded a stiffness of approximately 35 kpa (Fig 3.11. e.) The stiffness (elastic modulus) of the *CENP-F*$^{-/-}$ cardiac myocytes was significantly less than that of wild-type cells (Figs 3.11. c-e). Additionally, stiffness fluctuated in different areas of the knockout cell which was not observed in wild-type cells (Fig 3.11. c). Further, these cells were unable to withstand the ongoing tapping of the cantilever for longer than 1 hour which wild-type cells were able to endure. Interestingly and conversely, concurrent AFM analysis of cardiac fibroblasts isolated from the same *CENP-F*$^{-/-}$ hearts detected significantly stiffness than that observed in the wild-type population (Figure 3.12).

These data reveal that specific cell types react differently to the same loss of CENP-F function genetic model and that wall stiffening in this model of DCM is not the result of myocyte stiffening.

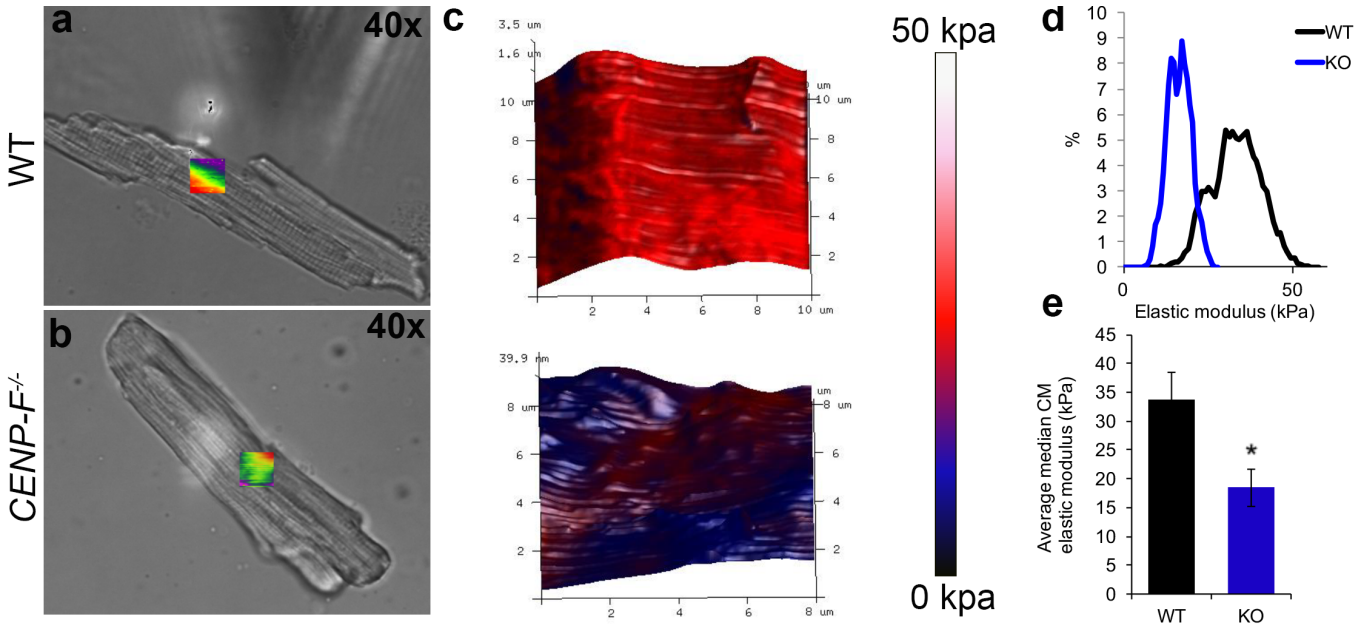


**Figure 3.11. Cardiomyocytes are softened with the loss of CENP-F.** Live cardiomyocytes isolated from wild-type **(a)** and *CENP-F*$^{-/-}$ **(b)** mice were plated on laminin and analyzed for the elastic modulus of the cell surface. Representative topography plots **(colorbar)** show a stiff surface across the 3D rendering of the wild-type cardiomyocyte **(red),** while, the *CENP-F*$^{-/-}$ cardiomyocyte **(blue)** is significantly softened **(c)**. Distribution of cell stiffness from representative scans **(d)**.The average median calculation of the elastic modulus of wild-type vs. *CENP-F*$^{-/-}$ cardiomyocytes is measured less (kpa) by an approximate 2-fold difference, $p$=0.0124 **(e)**. Error bars in (e) represent the SEM.

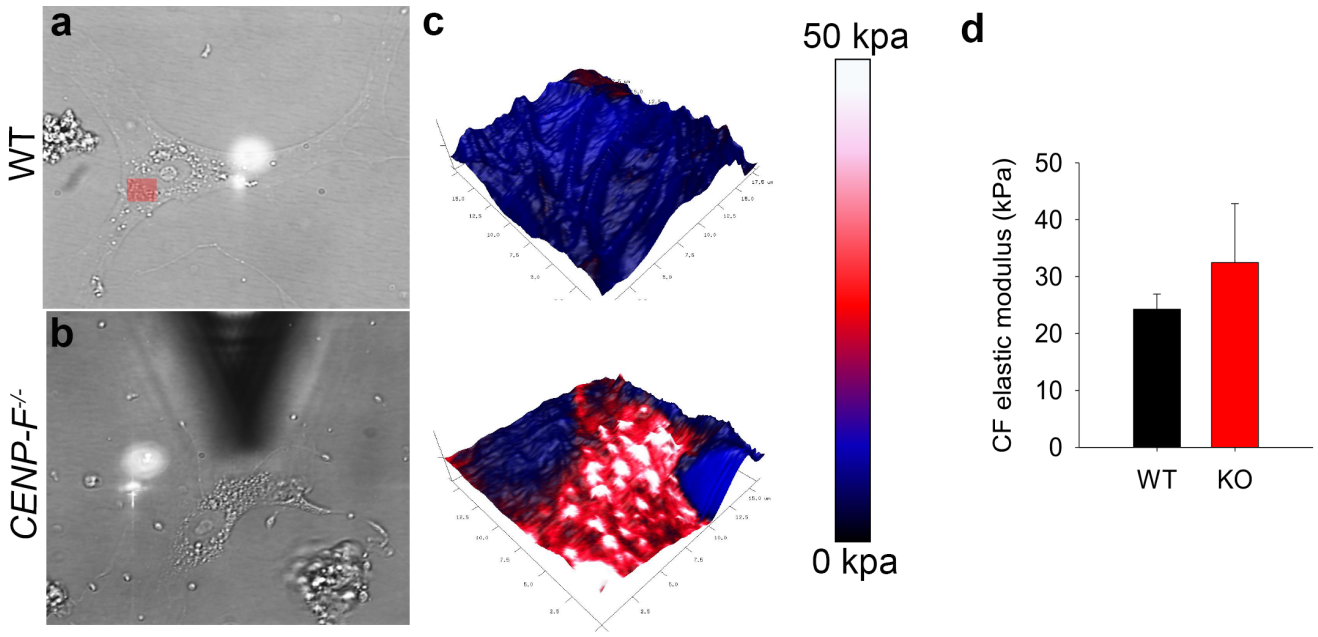


**Figure 3.12. Cardiac Fibroblasts are stiffened with the loss of CENP-F.** Live cardiac fibroblasts isolated from wild-type **(a)** and *CENP-F*$^{-/-}$ **(b)** mice were plated and analyzed for the elastic modulus of the cell surface. Representative topography plots **(colorbar)** show a soft surface across the 3D rendering of the wild-type cardiac fibroblast **(blue),** while, the *CENP-F*$^{-/-}$ cardiac fibroblast **(red)** is significantly stiffer **(c)**. The average median calculation of the elastic modulus of wild-type vs. *CENP-F*$^{-/-}$ cardiac fibroblasts results in an increase (kpa) **(d)**. Error bars represent (SEM).

**Calcium influx is decreased in *CENP-F*$^{-/-}$ cardiomyocytes**

In heart failure, calcium entry and removal are critical functions that are severely altered affecting cardiac action potential (Fearnley et al., 2011). In turn, the ability of heart to adequately pump sufficient blood is lost. The gravity of cellular parameters that are disrupted with loss of CENP-F led us to conduct a functional evaluation of isolated individual wild-type and *CENP-F*$^{-/-}$ cardiac myocytes. During the contraction-relaxation cycle, the calcium transients of single wild-type and knockout cells were measured using Fura-2AM calcium detection dye with Ionoptix. These studies revealed that the calcium transients in *CENP-F*$^{-/-}$ myocytes were significantly decreased when compared to wild-type cells (Fig 3.13. a). In conjunction to these results, significant changes in parameters that influence the calcium influx were seen. The percent of calcium released over multiple phases was decreased in *CENP-F* myocytes (Fig 3.13. b). The overall baseline peak was greatly lessened in each transient phase (Fig 3.13. c). All of the differences seen in calcium influx with loss of CENP-F function affect the overall physiological ability of a single contractile cell.

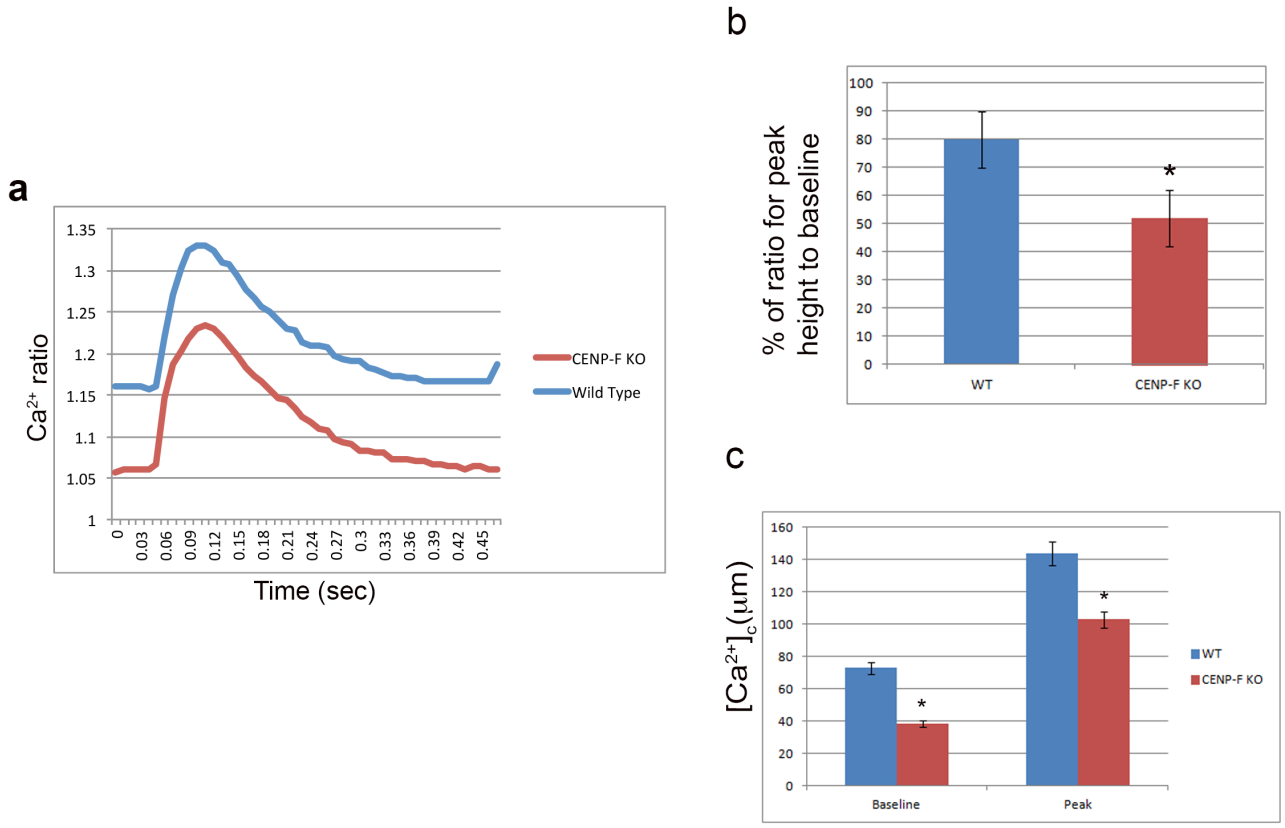


**Figure 3.13. Calcium transients are decreased in *CENP-F*$^{-/-}$ live cardiomyocytes.** Physiological analysis of live cardiomyocytes using Ionoptix Experimentation. Fluorescence ratio of FURA-2 binding to calcium was recorded from myocytes isolated from wild-type and *CENP-F*$^{-/-}$ hearts. Calcium ratio was measured during contraction/relaxation cycle resulting in a decreased ratio in *CENP-F*$^{-/-}$ cardiomyocytes **(a)**. Calcium released during the contraction/relaxation cycle was decreased in *CENP-F*$^{-/-}$ cariomyocytes, $^{*}p<0.001$ **(b)**. In phases of the transient, both the pre-stimulation baseline value and maximal deflection from baseline (peak) was less, $*p<0.05$ **(c)**. Each bar represents mean SEM, n=5-10 cardiomyocytes.

**Loss of CENP-F is associated with human heart failure**

CENP-F is the first microtubule binding protein to be linked to heart disease in a model organism. Given the diversity of genetic backgrounds influencing cardiac disease in humans, a Phewas Manhattan Plot Study was performed to correlate the results of the *CENP-F*$^{-/-}$ mice hearts with that of humans. In a biorepository that links 25, 579 patients at Vanderbilt University Medical Center, CENP-F single nucleotide polymorphisms (snps) were probed for their association with heart failure in patient populations (Figure 3.14). One common variant (MAF 45%) in CENP-F, rs7289, was associated with Heart Failure with Preserved Ejection Fraction (HFrEF) (OR=1.12, 95% CI 1.04 to 1.20, q=0.09). This variant encodes an amino acid substitution (N3106K), which is in the farnesylation domain/motif of CENP-F. This domain is located directly adjacent to the microtubule binding domain of CENP-F at the C-terminus (Hussein et al., 2002), and farnesylation of CENP-F is key for the localization of CENP-F to the nuclear envelope and for CENP-F degradation or turnover (Hussein et al., 2002)(Figure 3.14). This targeted PheWAS study suggests that common variants in CENP-F may modulate risk of heart failure with systolic dysfunction in humans and is consistent with the systolic dysfunction identified in *CENP-F*$^{-/-}$ murine hearts (Dees et al., 2012).

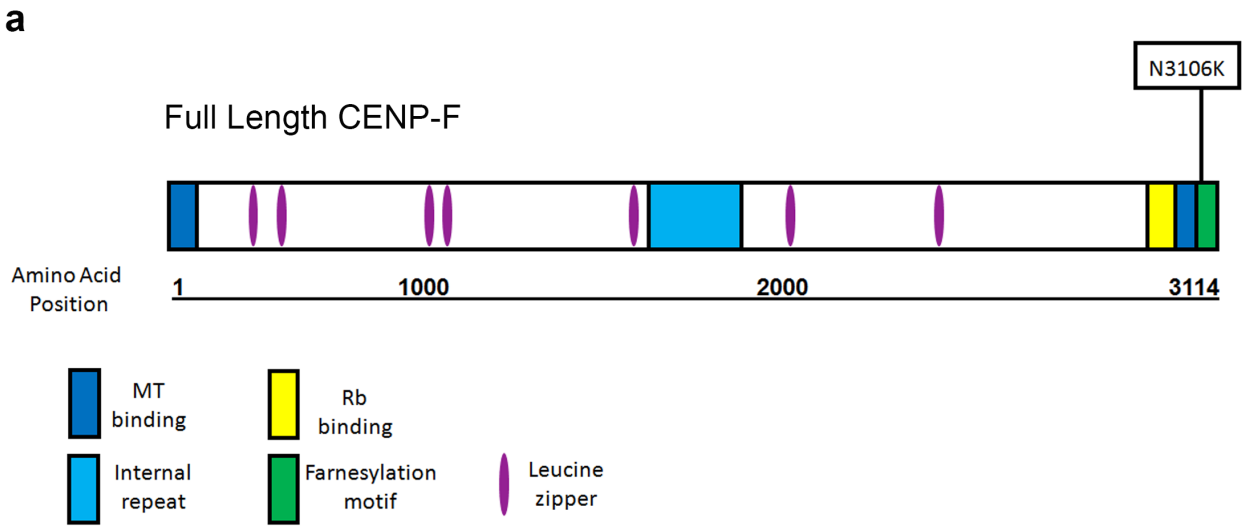


**Figure 3.14. CENP-F is relevant in human cardiac disease.** In BioVu, which includes 25,579 adult DNA samples, a PheWas study identified one common CENP-F variant (rs7289) associated with heart failure with reduced ejection fraction (HFrEF). The CENP-F variant (rs7289) encodes an amino acid substitution, N3106K, at the farnesylation motif (above in green) **(a)**.

## DISCUSSION

The current study addresses two interrelated and evolving areas of study: the genetic basis of cardiovascular disease and the regulation of basic cell function by CENP-F. These data reveal the fundamental reaction of cardiac myocytes to loss of CENP-F function and lay the groundwork for future studies focusing on individual cellular components in diverse cell types regulated by this complex and multifunctional protein.

Dilated cardiomyopathy (DCM) is a devastating disease with diversity and complexity in its genetic origins and subsequent cellular responses causing approximately 10,000 deaths and 46,000 hospitalizations each year in the United States alone. Interestingly, while more than 50 genes have been linked to this disease (McNally et al., 2013), no gene encoding a microtubule-binding protein has been identified as a cause of DCM until our recent study. Classic signs of the disease with ventricular wall thinning, arrhythmia, tissue scarring, contractile dysfunction, and death are detected in our mice model. Still, the underlying cellular and sub-cellular structural changes resulting from loss of CENP-F function which underlie this form of DCM had not been determined until the current study. Thus, in-depth analyses of single, isolated individual were needed for a comprehensive understanding of this model of DCM and, in a larger sense, to understand the potential role of microtubule network dysfunction in cardiac disease.

The current data generated from analysis of individual wild-type and knockout cardiac myocytes clearly demonstrate that loss of CENP-F function results in significant disruption of the microtubule network. Analysis of microtubule network structure in all genetic models of DCM has been very limited (Takahashi et al., 1998) to this point. With loss of CENP-F function, the perinuclear domain of the microtubule network in myocytes was completely lost. In the non-nuclear domain of the network, the longitudinal domain remained intact but its horizontal/lateral component was disrupted and replaced by highly coiled ends. Importantly, a disorganization of the grid-like microtubule network of skeletal myocytes is also seen in Duchenne muscular dystrophy (Khairallah et al., 2012). Conversely, it is interesting and important to note that the one study focused on MT network structure in DCM reported that no differences in the density or distribution of MTs were detected in their tachycardia-induced DCM (Takahashi et al., 1998). Thus,
retrospectively and going forward, it will be interesting to determine whether disruption of the microtubule network is a hallmark of DCM, is only associated with disruption/mutation of microtubule components, or is restricted to disruption/mutation of CENP-F alone. Further, given that DCM is a frequent occurrence in chemotherapeutic treatment of cancers and that many of these drugs target microtubules (Yvon et al., 1999; Rowinsky et al., 1997., El-Hattab et al., 2016) careful, broad, and ongoing investigation of the role of microtubule network dysfunction in cardiac disease may be warranted.

Confocal, immunochemical, and electron microscopic analyses of individual *CENP-F*$^{-/-}$ myocytes clearly demonstrate dramatic alterations in overall cell structure, especially in contractile, junctional, and mitochondrial domains when compared to normal myocytes. These changes were quantitatively significant and underlie physiological defects noted in

this genetic model of disease. Disruption of the myofibril and its sarcomere components is a common phenotype in DCM and can be caused by mutation of genes coding for both sarcomeric and non-sarcomeric proteins (Herman et al., 2012). Additionally, breakdown of the intercalated discs with concurrent decrease in N-cadherin and beta catenin expression is seen in *CENP-F*$^{-/-}$ myocytes (Figs 3.3 and 3.4) and is consistent with the report demonstrating that loss of N-cadherin leads to disc aberration (Kostetskii et al., 2005). Still, Kostetskii *et al* reported only modest DCM with disruption of intercalated discs while the current disease model results in severe DCM with a 20% death rate of *CENP-F*$^{-/-}$ animals (Kostetskii et al., 2005). The mitochondrial disruption seen with loss of CENP-F function is also a trait of several forms of DCM resulting from mutations in the mitochondrial or nuclear genomes (El-Hattab et al., 2016). While we found only one other publication attempting to decipher the functional role of microtubules in the heart, physiological disruption of calcium influx in single cells with loss of CENP-F also demonstrates the functional relevance for a microtubule associated protein in the heart physiology (Fig 3.14). Taken together, it is important to reiterate that in this first model of cardiac disease resulting from loss of a microtubule-binding protein, these hallmark disturbances (Herman et al., 2012; Olson et al., 2002; Yvon et al., 1999; Rowinsky et al., 1997) and the resulting "final common pathway" that is DCM are observed. But, at the same time, it is important to emphasize that loss of CENP-F function is not identical to any specific form of heart disease previously reported and that loss of other microtubule-associated proteins may or may not produce the phenotypes seen here.

It is important to note that differing models of CENP-F disruption can lead to differing results with the same cell type. For example, the field has reported varying *in vitro* results concerning the promotion of aneuploidy with disruption of CENP-F; one model using RNA interference technologies demonstrated resulting aneuploidy (Yang et al., 2005) while another genetic deletion model did not (Pfaltzgraff et al., 2016). The present study is the first to examine the reaction of two different cell types, isolated from the same organ, with identical and simultaneous disruption of gene function. Deletion of CENP-F in this genetic model results in cardiac myocytes displaying a more softened profile in atomic force analyses, whereas cardiac fibroblasts isolated from the same hearts exhibited a stiffened phenotype (Figs. 3.11 and 3.12). Revealing this diversity of reaction may be specifically important to the cardiovascular field, as heart wall stiffening is widely observed in DCM (Du et al., 2007; Nagueh et al., 2004). Knowing which cells and tissues underlie this phenotype may prove of importance in future therapeutic strategies. In a broader sense, the current data demonstrating the exact opposite responses of two cell types derived from the same organ to loss of CENP-F function would predict a diversity of response of other cell types in reference to the many and varied cellular behaviors governed by this gene product.

# CHAPTER IV

## Adult Mice Cardiomyocyte Isolation Protocol

### Introduction

The isolation of mice adult cardiomyocytes is a very tedious and fragile experiment. There are many different ways to implement this process, as well as many different choices of reagents however, we found no protocols consistently successful. After many failed attempts, all reagents should be made fresh for each isolation experiment. It should be noted that every Langendorff set up is different and timing should be tested on one wild-type heart. The following protocol is derived from a combination several different reports on the isolation of cardiomyocytes (Li et al., 2014; Roth et al., 2014; Louch et al., 2011; Pinz et al., 2011).

1. Prepare 500 ml of **Stock Perfusion Buffer (1X)**

**Table 4.1.**

| | **Catalog #** | **M.W.** | **mM** | **g/500 ml** |
|---|---|---|---|---|
| NaCl | Sigma S-5886 | 58.4 | 113 | 3.3 |
| KCL | Sigma P-5405 | 74.55 | 4.7 | 0.175 |
| $MgSO_4$ | Sigma M-2643 | 120.4 | 1.2 | 0.07 |
| $Na_2HPO_4$ | Sigma S-5136 | 142 | 0.6 | 0.042 |
| $KH_2PO_4$ | Sigma P-5655 | 136.1 | 0.6 | 0.041 |
| $NaHCO_3$ | Sigma S-5761 | 84 | 12 | 0.505 |
| $NHCO_3$ | Sigma P-9144 | 101.12 | 10 | 0.505 |
| Taurine | Sigma T-8691 | 125.1 | 30 | 1.875 |
| | | **Stock** | **mM** | **Volume** |
| Hepes @ 4° | GIBCO 15630-080 | 1M | 10 | 5 ml |

- Weigh all reagents into a 500 ml beaker; use Milli-Q water (directly from purification system) and stir.
- Bring to final volume 500 ml.
- Filter the solution (Millipore filter cat #SCGPU05RE); label with date.
- Store the solution at 4°C for up to 1 week.

2. Prepare 50 ml of **1 M Ca Stock solution**

- Weigh 7.35g of $CaCl_2$ *$2H_2O$ (M.W. 147.02; Sigma; cat #C7902) into 100 ml beaker.
- Add 50 ml Milli-Q water and stir until dissolved.
- Filter, label with date and store at 4°C.

3. Prepare 50 ml of **100 mM Ca Stock solution**

- Measure 5 ml of 1 M Ca stock into a 150 ml beaker and add 45 ml of Milli-Q water.
- Filter, label with date and store at 4°C.

4. Prepare 50 ml of **10 mM Ca Stock solution**

- Measure 5 ml of 100 mM Ca Stock solution into a 150 ml beaker and add 45 ml of Milli-Q water.
- Filter, label with date and store at 4°C.

5. Prepare **5, 1, 0.5 and 0.1 N NaOH solutions**

The following solutions are used to adjust the pH of the Control Solution (1X) on the day of experiment:

- **5 N NaOH**: weigh 10 g of NaOH (Sigma; cat #S8045) into a 100 ml beaker with 50 ml Milli-Q water. Stir, label with date and store at room temperature.
- **1 N NaOH**: measure 10 ml of 5 N NaOH into a beaker and add 40 ml Mill-Q water. Stir and label with date.
- **0.5 N NaOH**: measure 25 ml of 1 N NaOH into a beaker and add 25 ml Mill-Q water. Stir and label with date.
- **0.1 N NaOH**: measure 10 ml of 0.5 N NaOH into a beaker and add 40 ml Mill-Q water. Stir and label with date.

Use these solutions for up to 1 month.

6. Prepare 50 ml of **500 mM BDM** (M.W. 101.1; Sigma; cat #B0753) solution

- Weigh 2.53 g of BDM into 50 ml Milli-Q water and stir until dissolved.
- Filter the solution, label with date and store at 4°C.
- Use this stock for up to 2 weeks.

7. Prepare **200 ml Control Solution (10X stock)**

**Table 4.2**

**Control Solution 10X Stock**

| | Catalog # | mM | M.W. | g/200 ml |
|---|---|---|---|---|
| NaCl | Sigma S5886 | 1335.0 | 58.44 | 15.603 |
| KCl | Sigma P5405 | 40.0 | 74.55 | 0.596 |
| $NaH_2PO_4$ | Sigma S5011 | 12.0 | 120.00 | 0.288 |
| HEPES | Sigma H4034 | 100.0 | 283.31 | 4.777 |
| $MgSO_4$ | Sigma M2643 | 12.0 | 120.40 | 0.289 |

- Weigh chemicals into a 250 ml beaker; add Milli-Q water and stir.
- Bring to final volume 200 ml.
- Filter the solution (Millipore filter cat #SCGPU02RE); label with date.
- Store the solution at 4°C for up to 1 week.

**THE DAY OF THE EXPERIMENT**

1. Turn on the circulating water bath and allow enough time for it to reach the required temperature. Turn on the temperature probe. The temperature of the water bath has to be adjusted so that the final temperature of perfusion reaching the heart will be 37°C.
2. Make solutions for the day: **Perfusion buffer, Digestion buffer, Stop Solution 1, Stop Solution 2,** and **Control Solution (1X)** to wash out BDM and raise $Ca^{2+}$ at the end of the protocol.

3. Make 300 ml of **Perfusion buffer**

- Pour about 300ml of **Stock Perfusion Buffer** into a 250 ml beaker.
- Add 0.30 g glucose.
- Add 6 ml of **500 mM BDM** solution.
- Stir; bring to final volume 300 ml in graduate cylinder.
- Filter and label; check pH (pH should be 7.46); adjust with a few drops 1 N HCL; label bottle.

4. Make 20 ml of **Stop Buffer 1**

- Pipette 18 ml of **Perfusion buffer** into a 25 ml beaker.
- Add 2 ml bovine calf serum (BCS) (HyClone; cat #SH30073).
- Add 25 µl of **10 mM Ca** solution.
- Stir and filter into a 15 ml conical tube; label tube.

5. Make 20 ml of **Stop Buffer 2**

- Pipette 19 ml of **Perfusion buffer** into a 25 ml beaker.
- Add 1 ml bovine calf serum (BCS).
- Add 25 µl of **10 mM Ca** solution.
- Stir and filter into a 15 ml conical tube; label tube.

6. Make 54 ml of **Digestion buffer**

- Pipette 54 ml of **Perfusion buffer** into a 50 ml beaker.
- Add 5.4 mg **Liberase TM** (Roche; cat #05 401 127 001).
- Add 300 µl of 2.5% trypsin (Gibco; cat #15090-046).
- Add 6.75 µl of **100 mM Ca Stock**.
- Stir and filter into a 50 ml conical tube.

7. Make 500 ml of **Control Solution (1X)**

- Weigh 1.0 g of glucose (Sigma; G7021) and put into 600 ml beaker.

- Add 50 ml of **Control Solution (10X Stock)** into the beaker.
- Adjust volume to 400 ml with Milli-Q water.
- Adjust pH to 7.4 with **NaOH solutions.**
- Bring final volume to 500 ml with Milli-Q water in a graduated cylinder.
- Filter and label.

8. Make 100 ml of **Control Solution-BSA**

- Weigh 100 mg of albumin (Essentially Fatty Acid Free; Sigma A-6003) and put into 200 ml beaker.
- Add **Control Solution (1X)** into the beaker and stir.
- Check that pH is 7.4.
- Bring final volume to 100 ml with **Control Solution (1X)** in a graduated cylinder.
- Filter the solution; label **Control Solution-BSA.**

9. Make **Control Solution-BSA with Ca**

- Pipette 25 ml of **Control Solution-BSA** into three 50 ml conical tubes (Falcon; cat #352098).
- Label tubes and their caps: **CS-BSA 200 µM Ca, CS-BSA 500 µM Ca** and **CS-BSA 1 nM Ca.**
- Add 50, 125, and 250 µl of **100 mM Ca Stock** to the respective tubes.
- Put in 37°C water bath until ready to use.

10. Weigh the animal and inject with Heparin (5000u/kg b.w. i.p.) (200 µ; 1 mg/0.2 ml PBS). Wait approximately 10 minutes then anesthetize the animal. During the heparinization set up the dissection and cell dissociation areas.
11. Prepare the perfusion system

- Set the circulating bath at approximately 38°C so that the flow from the tip of the cannula is 37°C.
- Check the flow rate of the peristaltic pump. It should be **10 ml/minute.**
- Run 100 ml of Milli-Q water through the perfusion system.
- Fill the system with **Perfusion buffer** and eliminate air bubbles. It is important to perfuse the heart for 4 minutes at a pump rate of 3 ml/minute. Thus, a system volume of 12 ml is ideal. The tubing must be the same length each time it is replaced so that the volume of the system remains constant. If the system holds more or less than 12 ml, the uptake of Perfusion buffer from the conical tube must be started either early or late, as needed, so the heart is always perfused. If this adjustment is needed, stop the pump when moving the uptake tubing from Perfusion to Digestion buffers, to avoid introducing bubbles.
- After filling the system with **Perfusion buffer**, connect the pump inlet to the conical holding the **Digestion buffer**.
- Leave the outlet stopcock open and turn off the pump while cannulating.
- Set timer for 4 minutes.

12. Prepare the dissection, cell dissociation and microscope areas:

**Microscope Area:**

- Turn on chiller.
- Fill a 1 ml syringe with **Control Solution (1X)** and expel bubbles.
- Attach the syringe to a stopcock and metal cannula. Press the plunger to fill the stopcock and cannula with solution, then close the valve.
- Make a loop of about 4” suture and slip over the tip of the cannula.
- Prepare a notched petri dish filled with **Control Solution (1X)** on the stage of the microscope.

- Press the cannula and syringe into a block of modeling clay so that the cannula rests in the notch of the dish with the tip submerged in the cold buffer.
- 2 very fine curved forceps for the cannulation of the aortas.
- Sharp scissors to cut sutures.

13. **Dissect the heart**

- Anesthetize the animal with sodium pentobarbital (50 mg/kg b.w.) and check for reflexes.
- When completely anesthetized (no foot withdrawal reflex) open chest, hold sternum back with hemostat.
- Grasp heart with fingers and cut underneath to remove.
- Place heart in small beaker with **Control Solution (1X)**, pressing gently to expel blood.
- Transfer heart to 60 mm culture dish with **Control Solution (1X)** and trim excess tissue.

14. **Cannulate the aorta**

- Cannulate the aorta of the heart under the microscope with the cannula tip under the surface.
- Slip suture over aorta and tie off. Trim ends of suture.
- Press gently on the syringe plunger to perfuse the heart with a small volume of **Control Solution (1X)**. If the cannulation is successful, the blood will be expelled from the coronary arteries and replaced with the Control Solution.
- Close the syringe stopcock. Please note the difference in the color of the coronaries.

15. **Perfuse and digest the heart**

- Carry the ice bucket with dish and cannulated heart to the perfusion system.
- Detach the cannula from the syringe.


**Figure 4.1** Langendorff perfusion system. An in vitro technique that allows for retrograde perfusion of the rodent heart via the cannulated aorta.

- Start the pump and allow the top of glass coil to fill with **Perfusion buffer** until it overflows.
- Connect cannula to the system. This should be done in a way that prevents any bubbles from entering the cannula.
- Turn on the timer for **3 minutes**.

- Perfuse the heart for 3 minutes. At the end of this time the **Digestion buffer** will be in the cannula.
- Reset the timer for **8-10 minutes** and start.
- Move the lower chamber up over the heart. When it runs clear, collect into a 60 mm dish.

16. **Dissociate the cells**

- Remove the cannula and heart from the system and transfer to the bench in a 35 mm dish containing digestion buffer.
- Cut away the cannula and atria, leaving the ventricles in the dish.
- Set timer for **10 minutes** and start.
- Cut heart into small pieces with scissors.
- Use forceps to pull apart tissue to get small pieces.
- Gently triturate with a transfer pipette until clumps disappear.
- Filter the cell suspension through a mesh collector on a 50 ml canonical tube.
- Use a transfer pipette to place suspension in a falcon tube.

17. Stop enzyme, wash out BDM and increase cell Ca tolerance

- Add an equal volume of **Stop Buffer 1** solution, mix and allow cells to settle up to **15 minutes.**
- Remove supernatant and resuspend in 10 ml of **Stop Buffer 2.**
- Mix with transfer pipette and divide into 2 falcon tubes.
- Add 25 µl of **10 mM CaCl** to each tube. Mix well and wait **4 minutes.**
- Add 25 µl of **10 mM CaCl** to each tube. Mix well and wait **8 minutes.**
- Remove supernatant and resuspend in **CS-BSA 200 µM Ca** to 5 ml; wait **7 minutes.**
- Remove supernatant and resuspend in **CS-BSA 500 µM Ca** to 5 ml,;wait **7 minutes.**
- Remove supernatant and resuspend in **CS-BSA 1 mM Ca** to 5 ml; **spin 5 minutes**.
- Aspirate supernatant in the cell culture hood following spin. Add 5 ml of culture media to each tube.

# CHAPTER V

## Resident progenitors, not exogenous migratory cells, generate the majority of visceral mesothelium in organogenesis

This chapter is was published under this title in *Developmental Biology* (2nd author Manalo, 2014)


### ABSTRACT

Historically, analyses of mesothelial differentiation have focused on the heart where a highly migratory population of progenitors originating from a localized "extrinsic" source moves to and over the developing organ. This model long stood alone as the paradigm for generation of this cell type. Here, using chick/quail chimeric grafting and subsequent identification of mesothelial cell populations, we demonstrate that a different mechanism for the generation of mesothelia exists in vertebrate organogenesis. In this newly discovered model, mesothelial progenitors are intrinsic to organs of the developing digestive and respiratory systems. Additionally, we demonstrate that the early heart stands alone in its ability to recruit an entirely exogenous mesothelial cell layer during development. Thus, the newly identified "organ intrinsic" model of mesotheliogenesis appears to predominate while the long-studied cardiac model of mesothelial development may be the outlier.


### INTRODUCTION

Mesothelium is the simple squamous epithelium that lines the body wall and organs of the coelomic (pleural, pericardial, and abdominal) cavities in vertebrates. During organogenesis, mesothelial cells throughout the organism generate the visceral vasculature, provide stromal cell populations through epithelial to mesenchymal transition (EMT) (Que et al., 2008; Asahina et al., 2011;, Wilm et al., 2005; Dettman et al., 1998), and influence the growth (Li et al., 2011) and differentiation (Yin et al., 2011) of the organs they cover. In the adult, mesothelial cells modulate many characteristics of the coelomic cavities including fluid and immune cell content (Mutsaers et al., 2002), angiogenesis (Mandl et al., 2002), and rates of fibrinolysis (Tieze et al, 1998). These features in turn regulate ischemic injury repair and adhesion formation, influence cancer metastasis, and promote fibrotic disorders (Aroeira et al., 2005).

Our understanding of the basic biological functions of mesothelium in the embryo and adult has incited interest in the therapeutic potential of this cell type. Applications currently under exploration include the modulation of EMT of

the mesothelium to prevent fibrotic disorders (Loureiro et al., 2011) as well as the induction of mesothelial proliferation and migration to repair injured coelomic surfaces (Djafarzadeh et al., 2012) or even replacement of damaged cells within the organs themselves (Kovacic et al., 2012). However, the fundamental mechanisms at work in mesothelial differentiation are still largely unknown.

For decades, cardiac mesothelium (epicardium) was the only mesothelial population extensively studied during development. This intense research focus stemmed from the identification of the proepicardium—an isolated cell population that originated near the liver and sinus venosus (Ho et al., 1978). This structure migrates to the heart giving rise to the epicardium, coronary vasculature, and stroma (Dettman et al., 1998). Cardiogenic splanchnic mesoderm itself does not have the capacity to generate mesothelium (Gittenberg et al.,2000). Identification of the origin of the epicardium opened the floodgates for research and now we understand many of the cellular and molecular mechanisms leading to epicardial and coronary differentiation and are now beginning to understand important epicardial functions in the diseased or injured heart (von Gise A et al., 2012).

We recently set out to identify the origin of mesothelium to an additional coelomic organ—the intestine. We expected mesothelial formation to proceed in the intestine as it did in the heart. To our surprise, we instead determined that unlike the heart, the avian intestinal splanchnic mesoderm housed broadly distributed mesothelial progenitors that differentiated *in situ* rather than from an external migratory population. This provided the first experimental evidence of an alternative model of mesothelial formation (Winters et al., 2012).

A fundamental question arises, “Is the cardiac or intestinal model the predominant mechanism at work in the generation of mesothelia in coelomic organs?” Here, using chick-quail chimeras, we determined the origin of pleural and pancreatic mesothelial cells. Interestingly, while the lungs and pancreas, both gut tube derivatives, form in close proximity to the proepicardium, we found that pleural and pancreatic mesothelia were both derived almost entirely from cells resident to the lung and pancreatic primordia. Conversely, we found that cardiogenic tissue is the only mesoderm capable of recruiting exogenous mesothelia during organogenesis. Thus, the current data suggest that the new “organ intrinsic” model of generating mesothelia prevails in organogenesis of the respiratory and alimentary tracts while recruitment of exogenous progenitors observed in the heart appears to be the outlier in this critical developmental process.

## MATERIALS AND METHODS

### Windowing

Chick (Gallus gallus) eggs incubated 2.5 days were windowed by withdrawing 4 ml of albumin and cutting a hole in the top of the egg shell. The vitelline membrane over the posterior region of HH14–17 embryos was removed with a tungsten needle. A strip of neutral red/agar was placed over the embryo to lightly stain it red. A tungsten needle was used to pierce the somatopleure anterior to the vitelline artery. All animal procedures were performed in accordance with institutional guidelines and IACUC approval.

### Generation of chick-quail chimeras

Chick and quail (Coturnix japonica) embryos were staged according to Hamburger and Hamilton (Hamburger et al., 1992). Lung and pancreatic buds were isolated from HH13–15 quail embryos by dissecting free the somatopleure, transecting the embryo anterior and posterior to the lung buds using the heart tube as a landmark and then cutting dorsal to the lung buds at the junction of splanchnopleure and somatopleure to free the lung buds as a single unit. The dorsal pancreatic bud was isolated by removing the PE and liver bud ventrally, transecting the embryo posterior to the pancreatic bud, and then cutting dorsally at the junction of splanchnopleure and somatopleure freeing a small section of splanchnopleure with attached pancreatic bud. This strategy was used to remove potential contamination from PE cells which develop in association with the liver bud (Ishii et al., 2007; Viragh et al., 1993). The PE, liver, and ventral pancreatic bud were dissected away before isolating the dorsal pancreatic bud for transplantation. All of these transplants are completely devoid of a mesothelial covering at this time (Figure S5.2). Heart tubes were isolated from HH12–14 (without any visible PE attachment) or HH19–20 (after PE attachment and migration) quail embryos and then splayed open to expose the endocardium. Dissection was carried out in sterile Tyrode's salt solution. A single quail tissue isolate (lung buds were transplanted as a unit) was transplanted into the right lateral (future abdominal) cavity just anterior to the vitelline artery of a host chick embryo. Tyrode's salt solution with 1% penicillin/streptomycin was added to replace volume and chick eggs were sealed and incubated for 7 or 14 days.

### Immunohistochemistry (IHC) and co-localization analysis

Isolated grafts were fixed in 4% formaldehyde in PBS. Cryosections were cut at 5µm thickness. Immunohistochemical analysis of sectioned chick or quail tissue was as published (Osler et al., 2004). The following primary antibodies were applied overnight at 4°C: Anti-GFP (Invitrogen A11122, 1:200), Anti-smooth muscle actin (Sigma A2547 1:200), Anti-smooth muscle actin (Abcam Ab5694 1:200), Anti-sarcomeric myosin (MF20), QCPN (DSHB undiluted),

8F3 (DSHB 1:25), Anti-cytokeratin (Abcam Ab9377, 1:100), QH1 (DSHB, 1:200), Anti-insulin (Abcam Ab63820, 1:100) and Anti-glucagon (DAKO, A0565, 1:200). The following secondary antibodies were applied at a 1:500 dilution for 90 min at room temperature: Alexa fluor 488 or 568 Goat anti-rabbit (Invitrogen); Alexa fluor 488 or 568 Goat anti-mouse (Invitrogen). TOPRO-3 (Invitrogen T3605) at 1 µmol/L was applied with secondary antibody. Sections were imaged in Z-stacks using a LSM510 META Confocal with 0.4 µm optical slices. All IHC images presented in figures are Z-projections. The mesothelial layer was distinguished by morphology combined with cytokeratin staining. Nuclei within the mesothelial layer were manually identified and then subsequently identified as QCPN positive or negative.

## RESULTS

Chick-quail chimeras have been critical as a lineage tracing technique in embryology. In using this methodology, the tissue of interest is isolated from a quail embryo and transplanted into a host chicken embryo. The transplanted material may contribute to the host embryo while the host may in turn contribute to the graft. Graft and host cells are identified by quail- (QCPN) and chick- (8F3) specific antibodies. For generation of our chimeras, transgenic donor quail embryos expressing a nuclear eYFP protein in endothelial cells (Tie1:H2B-eYFP) were utilized (Sato et al., 2015). This allows the vasculature to be visualized in whole mount and facilitates identification of graft-derived structures. As previously noted in Winters et al. (2012) and seen below, remarkable organ morphogenesis occurs in these chimeras. To determine whether the cardiac (extrinsic origin) or intestinal (intrinsic origin) model of mesotheliogenesis is observed variant organogenic models, we generated heart, lung and pancreas chick-quail chimeras and examined the mesothelium of these chimeric organs.

**Ectopically transplanted hearts recruit an "exogenous" mesothelium**

Quail heart tubes were isolated prior to attachment of the PE (Hamburger and Hamilton stage 12–14) and were completely devoid of mesothelial progenitors. These grafts were transplanted into the developing right abdominal cavity of a host chick embryo to determine whether cardiogenic mesoderm could generate mesothelium from endo- or exogenous sources. This protocol results in the juxtaposition of grafted material with parietal peritoneum and its resident mesothelium.

At seven days post-transplantation (7DPT), cardiac grafts were tube-like in shape (Figure 5.1A, arrow) with a vascular attachment to the host (Figure 5.1B, arrowhead). It is important to note that all surviving grafts analyzed here, whether they be cardiac, pleural, or pancreatic in nature, had a mesenteric connection to the body wall establishing vascular continuity with the host cardiovascular system undergoing remarkable morphogenic differentiation (Figures 5.1-5.4). Mesothelium of the mesenteric connection was continuous with mesothelium of the parietal peritoneum. These hearts also underwent spontaneous, rhythmic contraction. Immunohistochemical analyses revealed the vast majority of QCPN-positive cells within the transplant were cardiomyocytes visualized by striated patterns of staining with antibodies to both myosin and actin (Figure 5.1C–H). Quail endothelial/endocardial cells were also identified within the graft-derived heart (Figure 5.1H, arrows). Interestingly, chick cells (QCPN-negative) made up the mesothelium/epicardium of these hearts (Figure 5.1I-L, arrowheads) and were arranged in a cytokeratin-positive epithelial layer (arrowheads) facing the coelom. The underlying sub-mesothelial layer (Figure 5.1J–L, asterisks) was also chick host-derived. The host origin of the mesothelial epicardium was further confirmed by staining for the chick cell marker 8F3 which co-localized with cytokeratin (Figure 5.1M–P, arrows).

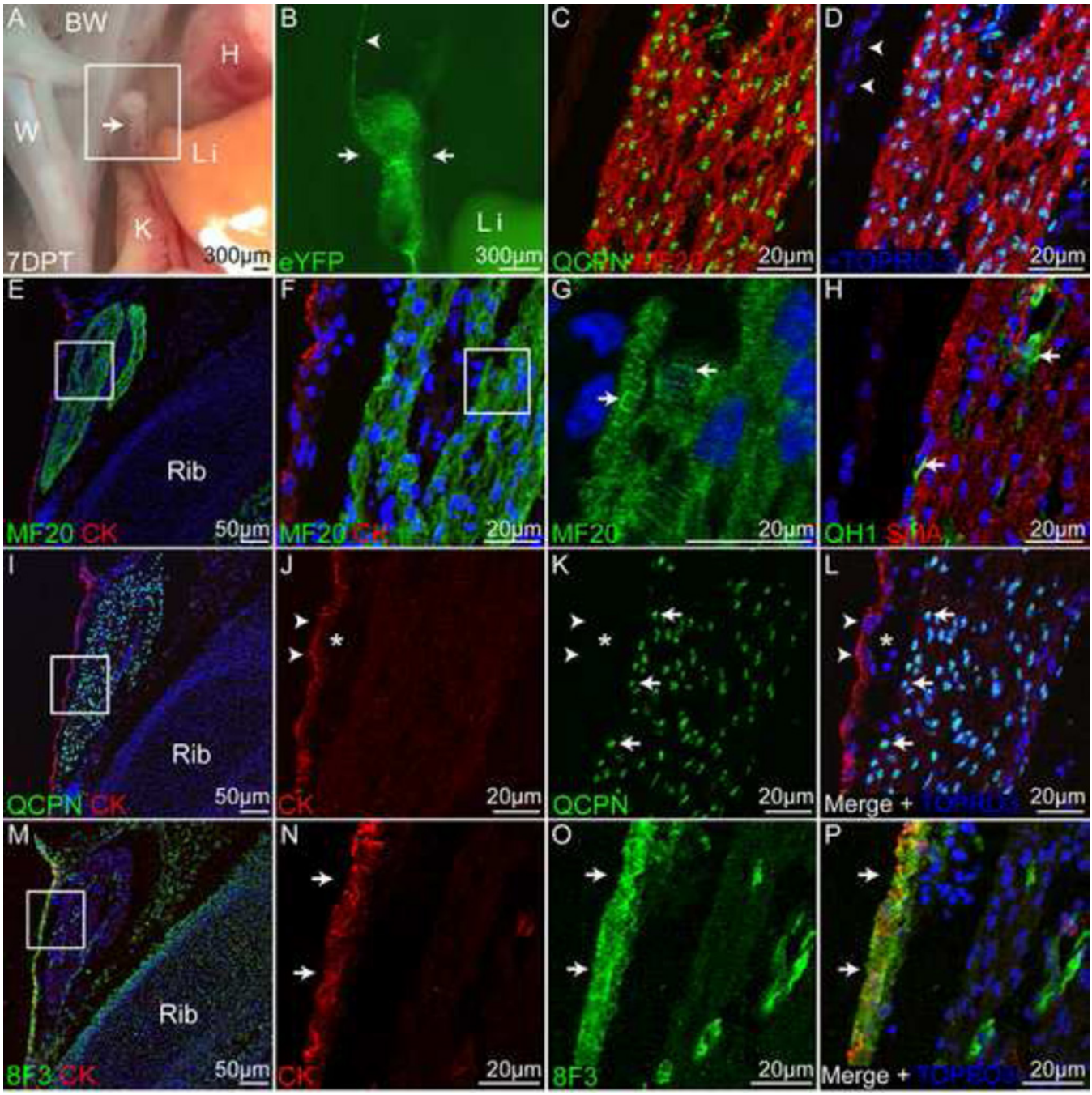


**Figure 5.1. Quail heart tube isolated without proepicardium 7DPT.** Representative 7DPT graft-derived heart. **A)** Graft developed within the coelomic cavity of the host in close proximity to the body wall (BW), liver (Li) and kidney (K) and was tube like in shape (arrow). **B)** Whole mount eYFP fluorescence. A blood vessel (arrowhead) extended from the graft (arrows) to the host. **C)** Quail cells (QCPN-positive) within the graft are myosin (MF20)-positive suggestive of cardiomyocyte differentiation. **D)** Neighboring QCPN-negative cells are also negative for MF20 (arrowheads). **E)** Low power image demonstrating myosin staining within the graft-derived heart. **F)** Higher power of boxed area in E). **G)** Higher power of boxed area in F) demonstrates striations consistent with sarcomere formation (arrows). **H)** Endocardial/endothelial cells marked by the antibody QH1 were found within the graft (arrows). **I)** Graft-derived heart was covered by a cytokeratin-positive surface mesothelial layer. **J–L)** Higher power of boxed area in I). The

surface mesothelium was QCPN-negative (arrowheads) and had an underlying mesenchymal layer of cells (asterisks). **M)** The graft-heart was surrounded on all sides by chick cells (8F3 positive). **N–P)** Higher magnification of boxed area in M). 8F3 co-localized with cytokeratin demonstrating the host origin of the graft mesothelium. BW, body wall; H, heart; K, kidney; Li, liver; W, wing.

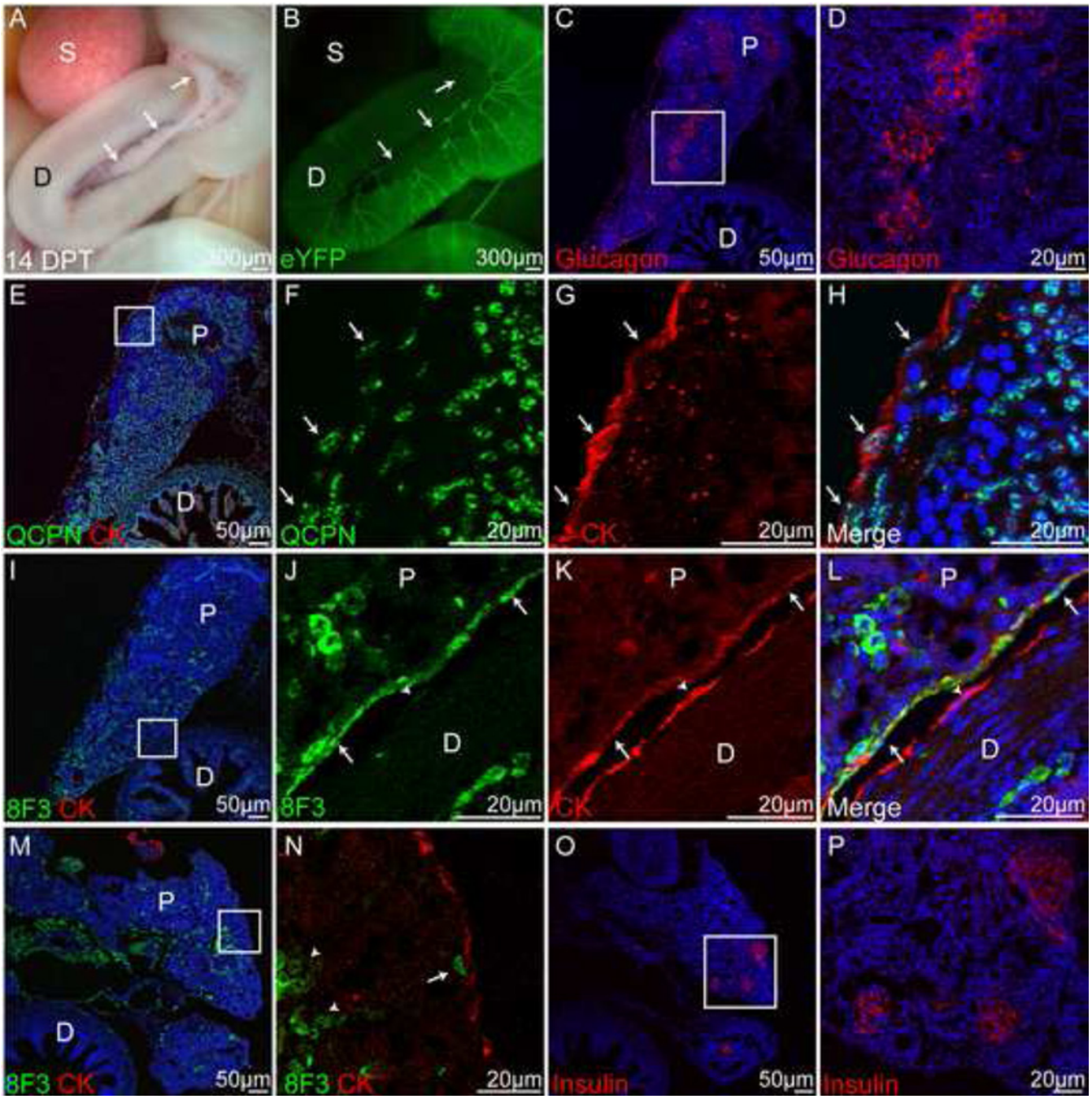


**Figure 5.2. Graft-derived pancreas 14 DPT.** The grafted tissue formed a duodenum (D) and pancreas (arrows). **B)** Whole mount eYFP fluorescence. **C)** Within the graft-derived pancreas there were islands of glucagon positive cells (red). **D)** Higher magnification of boxed area in C). **E)** Both the pancreas and duodenum were formed in large part by QCPN-positive cells. **F–H)** Higher magnification of boxed area in E). The surface cells were QCPN- and cytokeratinpositive (arrows) demonstrating their quail origin. **I)** Chick cells were also distributed throughout the graft. **J–L)** Higher magnification of boxed area in I). Rare patches of surface mesothelial cells were 8F3-positive (arrows). The mesothelial cells of the nearby duodenum were 8F3-negative (arrowhead). **M)** Low power view of another graft-derived pancreas and duodenum. **N)** In this graft, 8F3 cells were not found within the mesothelium (arrow) and most were within clusters deep within the pancreas (arrowheads). **O–P)** This graft also exhibited islet formation with insulin production (red). D, duodenum; P, pancreas; S, spleen.

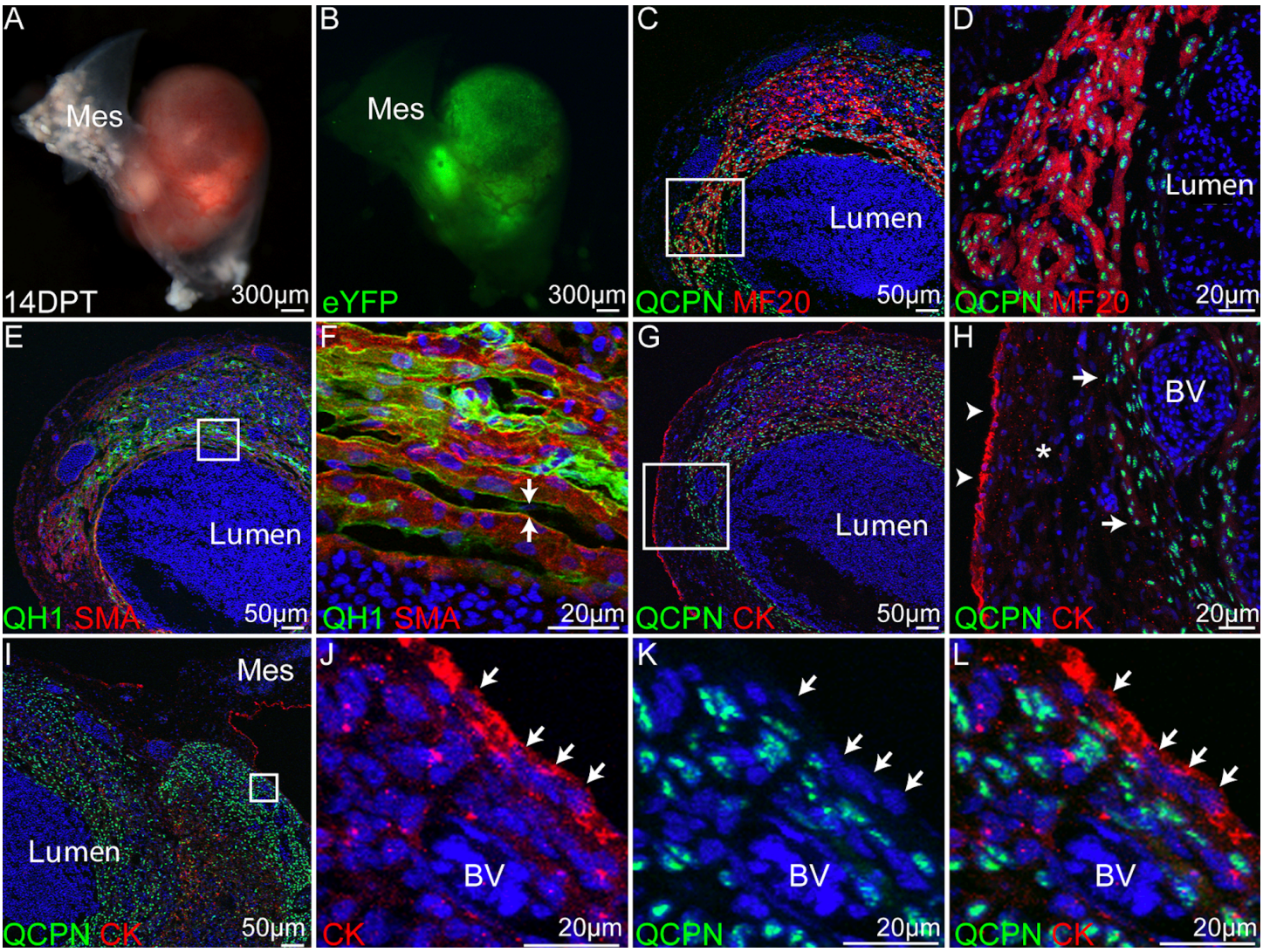


**Figure 5.3. Quail heart tube isolated without proepicardium 14DPT, related to Figure 5.1:**

Heart tubes were isolated at HH12–14, prior to PE attachment. **A)** At 14DPT, the graft-derived hearts were ball-shaped and were connected to the host via a mesentery (Mes). **B)** Whole mount eYFP fluorescence. Endocardial/endothelial cells were distributed throughout the graft. **C)** In cross-section, a large blood filled lumen was surrounded by QCPN-positive cells. **D)** Higher magnification of boxed area in C). Many of the QCPN-positive cells were also myosin (MF20) positive. **E)** Low power view of quail endothelial/endocardial cell distribution (QH1-positive). **F)** Higher magnification of boxed area in E). Endocardial cells lined the cardiomyocytes of the graft (arrows) in a trabecular-like pattern. **G)** Lowpower view demonstrating a cytokeratin-positive mesothelium surrounded the graft. **H)** Higher magnification of boxed area in G). The surface mesothelium (arrowheads) was QCPN-negative and separated from QCPN-positive cells (arrows) by a mesenchymal cell layer (asterisk). **I)** Low power view of the graft near the mesenteric (mes) connection to the host. **J–L)** Higher magnification of boxed area in I) (BV, blood vessel). In this region, the mesothelium is directly opposed to the quail myocytes but is host-derived (arrows).

We next incubated host embryos to 14 DPT to determine whether the observed mesothelial configuration was transient or retained throughout development. At 14DPT, the graft-derived hearts exhibited spontaneous contractions and were connected to the host via mesentery-like attachments (Figure 5.3A–B). Remodeling of the myocardium and endocardium was even more pronounced with myocardium surrounding a blood-filled lumen (Figure 5.3C–D) with extensive trabeculation (Figure 5.3E–F, arrows). It should be noted that quail graft-derived hearts while undergoing significant morphogenetic transition are smaller than age-matched host hearts. The difference in size of the host and graft hearts is likely due to the intrinsic difference in size of the two organisms and it is also possible that the grafting protocol impedes growth. Importantly, the epicardial mesothelium of grafted hearts (arrowheads) and an underlying sub-mesothelial layer (asterisk) were clearly host-derived (Figure 5.3G–H). MF20 staining of myocytes clearly delineates the epicardial/myocardial boundary (figures 5.1 and 5.3). The lack of QPCN staining of epicardial cells in both mesothelial and sub-mesothelial components of the epicardium indicates that this layer is host-derived (figure 5.1). In areas lacking a sub-mesothelial layer, the chick-derived mesothelium (arrows) was directly juxtaposed to quail-derived myocardium (Figure 5.3I–L). Thus, heart tubes isolated prior to PE attachment and grown ectopically were unable to generate a mesothelium endogenously but instead recruited these cells from host tissue and maintained them throughout development.

We next transplanted quail heart tubes isolated after PE attachment and initial epicardium formation (HH19–20) to determine whether these hearts retained the ability to recruit exogenous mesothelial cells. At 7DPT, the graft-derived hearts were organized with a lumen and surrounding myocardium (Figure 5.4A–B). Endothelial/endocardial cells were found throughout the myocardium and lining the lumen (Figure 5.4C–D, arrowheads). The mesothelium covering the surface of the graft-derived heart was QCPN-positive demonstrating it originated from the transplanted tissue (Figure 5.4E–H, arrows). Importantly, while chick cells were found scattered throughout the graft-derived heart tube demonstrating the ability of host cells to invade the graft (Figure 5.4I–J, arrows), none were observed within the mesothelium (arrowheads). Thus, once invested with a mesothelium, the transplanted heart losses its ability to recruit this cell type.

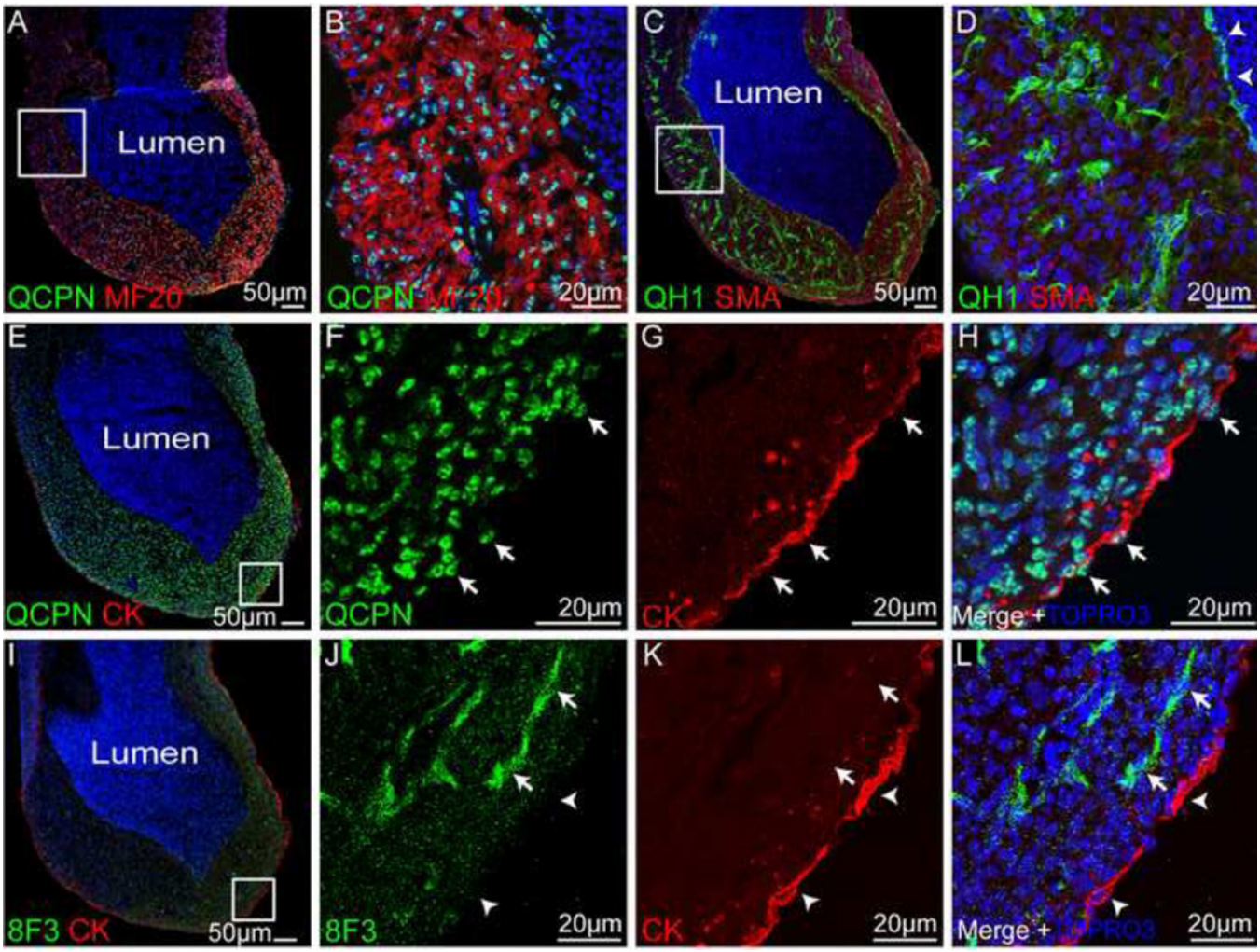


**Figure 5.4.** Quail heart tube isolated with attached proepicardium/epicardium 7DPT

Heart tubes were isolated from HH19–20 quail embryos after the PE had attached and the epicardium had partially formed. **A)** QCPN-positive myocytes encircled a blood-filled lumen. **B)** Higher magnification of boxed area in A. **C)** Quail endothelial/endocardial cells (QH1-positive) were distributed throughout the graft-derived heart. **D)** Higher magnification of boxed area in C. Endocardial cells lined the lumen (arrowheads). **E)** Low power view demonstrating cytokeratinpositive mesothelium lining the surface of the graft. **F–H)** Higher magnification of boxed area in E). The surface mesothelial cells were QCPN-positive (arrows). **I)** Low power view demonstrating scattered chick (8F3-positive) cells within the graft-derived heart tube. **J–L)** Higher magnification of boxed area in I). Chick cells were found within the graft (arrows) but not within the mesothelium (arrowhead).

**Pleural mesothelium is derived from an intrinsic source of progenitors**

We next transplanted HH13–15 quail paired lung buds into host chick embryos to determine the origin of respiratory mesothelium. Lung buds develop as endodermal outgrowths from the foregut that branch into the surrounding splanchnic mesoderm. Grafts obtained from HH13–15 stage embryos containing quail lung primordia consist of simple endoderm and splanchnic mesoderm and are completely devoid of a mesothelial covering as evidenced by the lack of a cytokeratin-positive simple squamous epithelium on the coelomic surface of the primordium (Figure 5.5). The epithelial endoderm in situ (arrows, Figure 5.5B) and of the graft (arrows, Figure 5.5C) is cytokeratin-positive. We have previously shown that mesothelial differentiation in gut derivatives occurs later in development at HH29 at which time this simple squamous epithelium is also cytokeratin-positive (Thomason et al, 2012). Thus, at day 0, transplanted tissue is remarkably simple in structure and lacks a mesothelial covering.

At 7DPT, the grafts had formed a central gut tube and two lungs. The graft-derived lungs appeared very similar to the host lungs at this time although smaller in size (Figure 5.6A–B). Upon sectioning, we found an ordered array of airways and vasculature derived from the grafted tissue (Figure 5.6C) similar to wild type avian lungs. Airways were lined with a continuous mucosal cell layer (arrows) and a broken smooth muscle cell layer (arrowheads), both of quail origin (Figure 5.6D). The blood vessels (arrowheads) resided in the mesenchyme of the lung encircling the airways (asterisks, Figure 5.6E–F). Grafts exhibited both esophageal (Figure 5.6G) and tracheal formation exemplified by cartilage differentiation with its characteristic perichondrium and developing lacunae (Figure 5.6H; See Bloom and Fawcett, Twelfth edition, pages 182–183 for description of cartilage development) within the central gut tube structure. Thus, lung differentiation in the grafted tissue mirrored that on seen with differentiation in situ.

The mesothelium in grafted lungs at 7DPT was derived almost completely (95% average) from QCPN-positive cells (Figure 5.6I–J, arrows). Very few chick cells were recruited into the graft at this time and those present were clearly not mesothelial in nature (Figure 5.6 K–L, arrows). By 14DPT, grafted lungs had acquired a dark pink color (Figure 5.7A) due to the intense vascularity (Figure 5.7B). The airways continued to be invested in a broken smooth muscle layer (Figure 5.7C, arrowhead) and vascular smooth muscle of quail origin had differentiated around the major blood vessels (Figure 5.7C–D, arrows). The mesothelium over the 14DPT lung was on average 84% QCPN-positive (Figure 5.7E–G, arrows) and 8F3 staining revealed only rare positive host-derived cells within the mesothelium (Figure 5.7H–J, double arrow). It should be noted that the mesothelium of control quail lung differentiated in situ at day 14 was on average 83% QCPN-positive suggesting that QCPN does not mark 100% of quail cells and/or that the perinuclear antigen is more difficult to detect in mesothelial cells flattened with differentiation or embryonic age. Taken together, these data demonstrate that the vast majority of avian lung mesothelium is generated and maintained from a population of progenitors intrinsic to the splanchnic mesoderm of the developing lung.

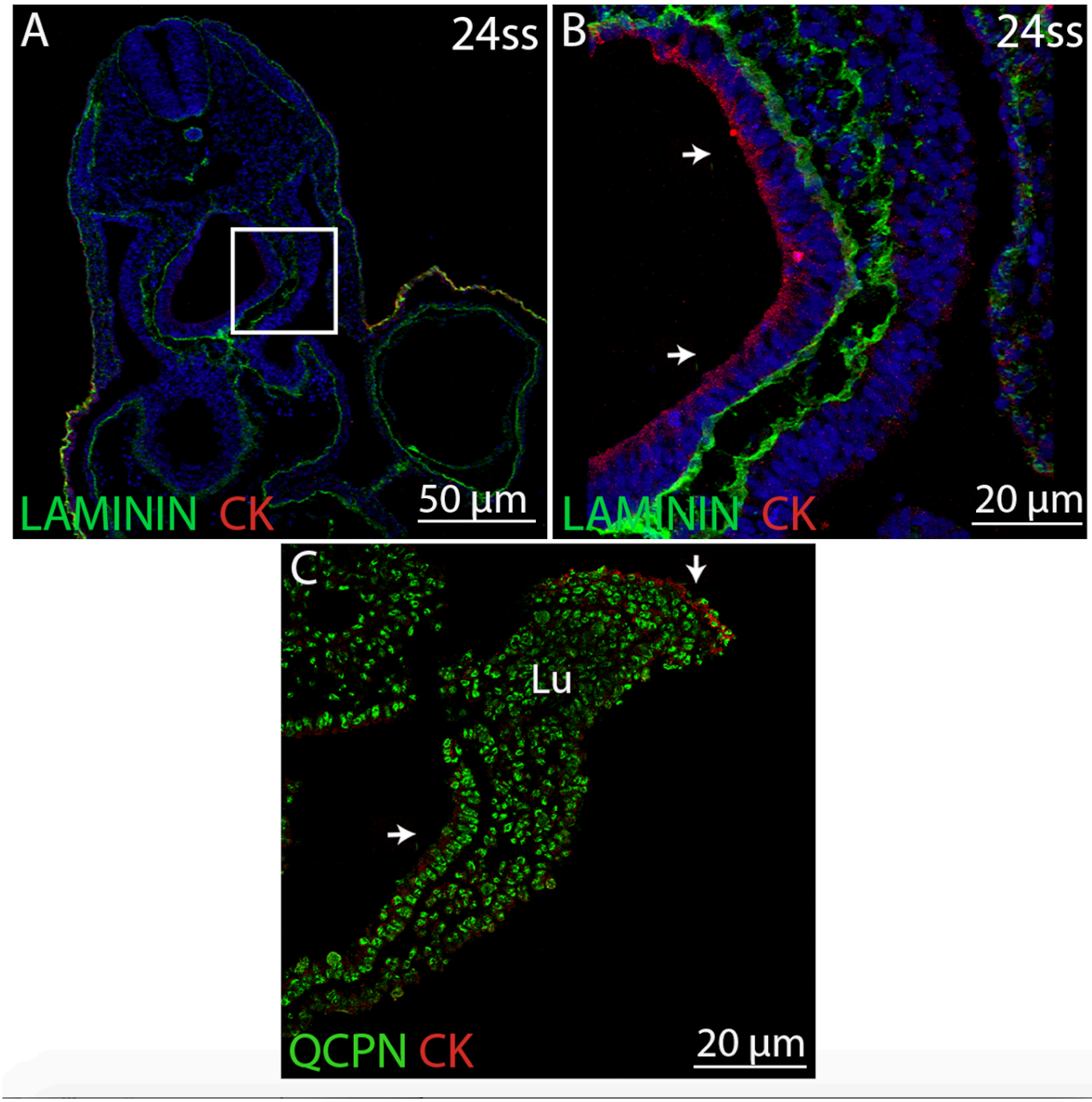


**Figure 5.5. Lung Graft at 0DPT/day of transplantation:** A cross-section of a quail embryo at the time of graft isolation is given. The boxed area shows the position of splanchopleure used to analyze lung morphogenesis as a transplant at 24ss (equivalent to Hamburger and Hamilton stage 14). The section was stained with anti-laminin, anti-cytokeratin (CK) and DAPI. **B)** Higher magnification of the boxed area A shows that splanchnopleure has inner endoderm which is CK-positive (arrows) with underlying splanchnic mesoderm. It is important to note that no simple squamous epithelium/mesothelium is seen at the outer surface of the mesodermal component. Similar embryos were dissected and used for grafting. **C)** A graft of lung primordium at 0DPT is pictured and demonstrates the simple structure of the isolate. QCPN and cytokeratin (CK) staining are given. Again, epithelial endoderm is CK-positive (arrows).

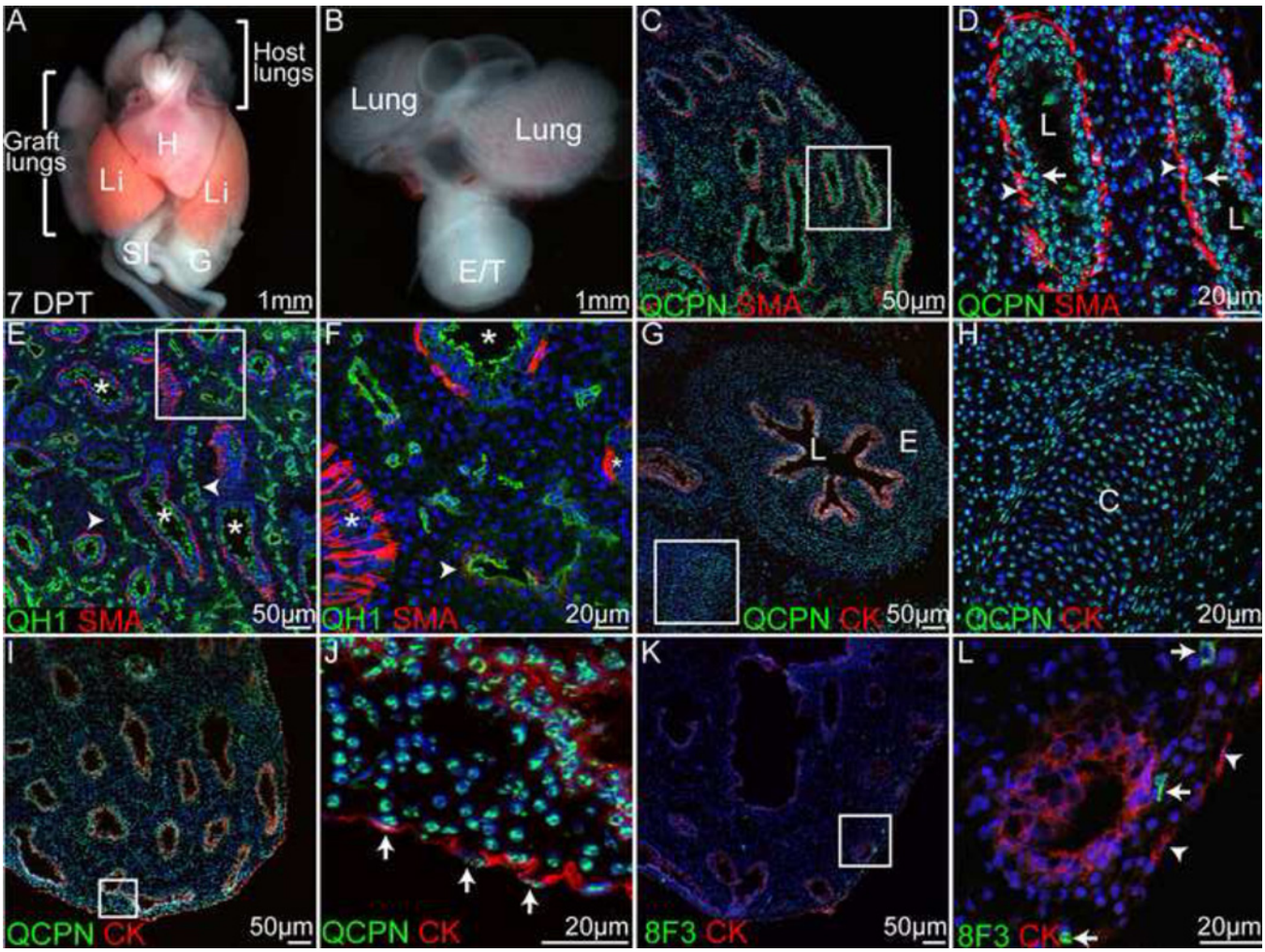


**Figure 5.6. Graft-derived lungs 7DPT.** Transplanted lung buds formed paired lungs within the coelomic cavity of the host embryo (H, heart, Li, liver, SI, small intestine, G, gizzard). **B)** A central esophagus/trachea (E/T) also formed from the grafted tissue. **C)** The graft-derived lungs were formed primarily of quail tissue and included a linear organization of airways. **D)** Higher magnification of boxed area in C) (L, lumen). The mucosal linings of airways were derived from quail (arrows) as was the encircling smooth muscle (arrowheads). **E)** Quail endothelial cells marked by QH1 surrounded the airways (arrowheads). The mucosal epithelium was also QH1-positive (asterisks) as previously reported. **F)** Higher magnification of boxed area in E). The major vessels exhibited limited vascular smooth muscle differentiation (arrowhead) and were localized centrally between airways (asterisks). **G)** Section through the lumen (L) of the graft-derived esophagus (E). **H)** Higher magnification of boxed area in G. Near the esophageal lumen, cartilage (C) differentiation was frequently observed. **I)** Low magnification demonstrating cytokeratin-positive surface epithelium. **J)** Surface mesothelium was QCPN-positive. **K)** Chick cells were scattered throughout the graft in low numbers. **L)** Chick cells (arrows) did not contribute to the mesothelium (arrowheads). E/T, esophagus/trachea; G, gizzard; H, heart; Li, liver; SI, small intestine.

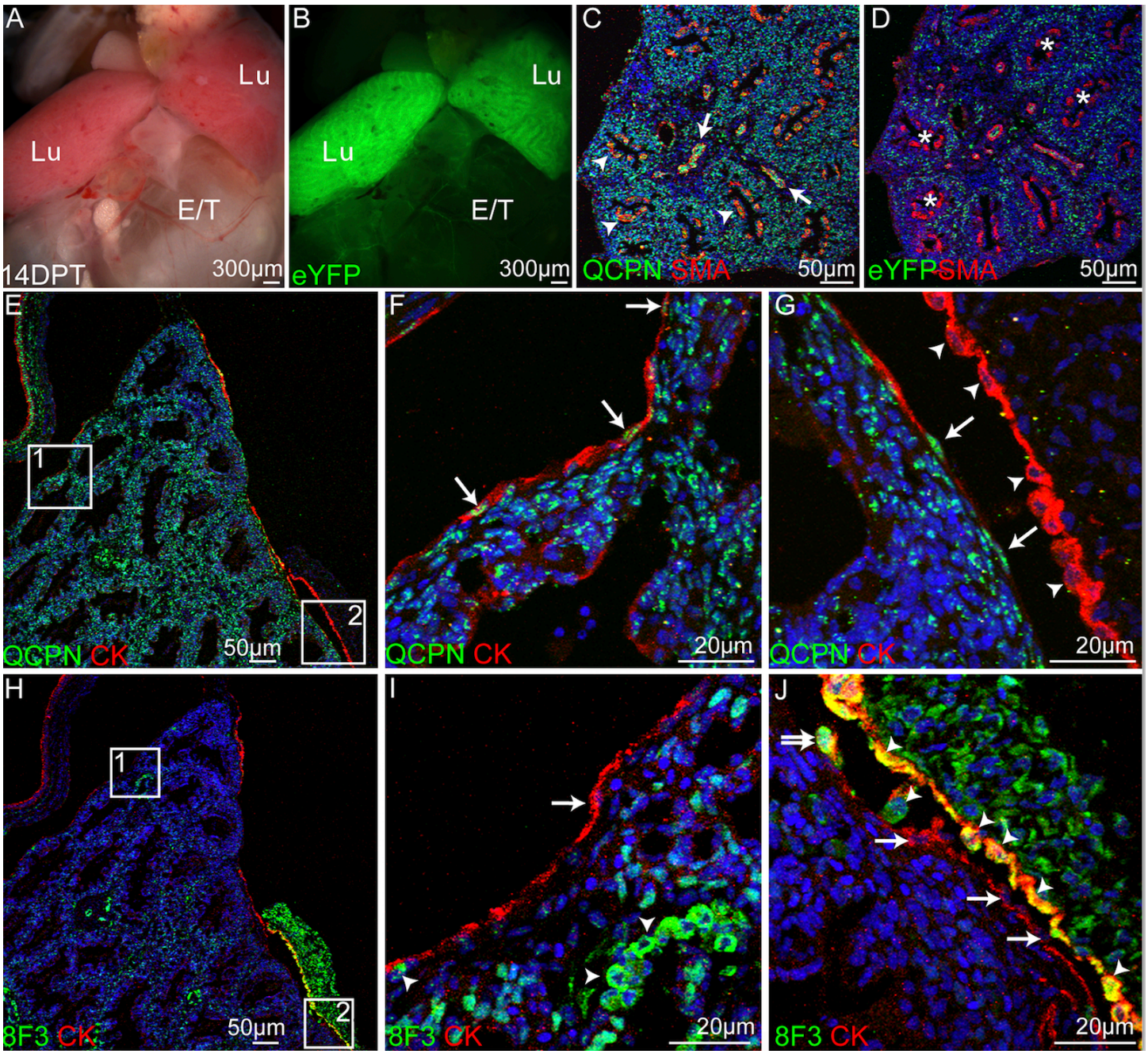


**Figure 5.7. Graft-derived lungs 14DPT.** At 14DPT, graft derived lungs (Lu) were pink in appearance due to the intense vascularity of the tissue. A centralized esophagus/trachea (E/T) was also apparent within the graft-derived structures. **B)** The lungs were highly fluorescent due to the large number of endothelial cells expressing eYFP. **C)**The airways were lined with a broken smooth muscle layer (arrowhead). The large centralized blood vessels were also lined with smooth muscle cells (arrows). **D)** The vasculature (green) is organized around the airways (asterisks). **E)** Low power view showing the cytokeratin-positive mesothelium that lines the surface of the lungs. **F)** Higher magnification of boxed area 1 in panel E). QCPN-positive mesothelial cells are indicated by the arrows. **G)** Higher magnification of boxed area 2. In this region, the graft-derived mesothelial cells (arrows, QCPN-positive) were in close proximity to host body wall mesothelium (arrowheads, QCPN-negative). **H)** Low power view demonstrating clusters of chick cells (green) throughout the graft-derived lungs. **I)** Higher magnification of boxed area 1. Over much of the graft, 8F3-positive cells were found in deep clusters (arrowheads) and not within the mesothelium (arrow). **J)** Higher magnification of boxed area 2. In the region of

the graft juxtaposed with host body wall mesothelium (arrowheads), scattered chick cells (double arrow) were identified within the graft mesothelium (arrows).

**Pancreatic mesothelium also arises from progenitors located within the organ primordium**

We next transplanted HH13–15 dorsal pancreatic buds into the coelomic cavity of host chick embryos. We specifically chose to investigate the origin of pancreatic mesothelium as a glandular derivative of the digestive system. At 7DPT, the grafts had formed an intestinal loop (D) in which the pancreas (arrowheads) was nestled similarly to the wild type configuration of duodenum and pancreas (Figure 5.8A–B). The mesothelium of the 7DPT pancreas was on average 98% QCPN-positive (Figure 5.8C–D, arrows). To determine whether host mesothelium transiently covered transplanted tissue, 4DPT grafts were examined for the presence of 8F3-positive surface cells. Interestingly, chicken-derived cells were never identified on the surface of transplanted pancreas (Figure 5.9) or lung tissue and examination of these grafts revealed the presence of cytokeratin-positive quail cells at the organ surface (Figure 5.9; arrows). Importantly, continuity of blood flow from the host and connection to the body wall were established in these 4DPT grafts. By 14DPT, pancreatic grafts had undergone significant growth and remained in the same duodenal-pancreatic configuration (Figure 5.2A–B). At this time, there was abundant glucagon and insulin expression within the graft indicating that pancreatic differentiation proceeded (Figure 5.2C–D, O–P). At 14DPT, pancreatic mesothelium was principally derived from QCPN-positive cells (88% average, Figure 5.2E–H, arrows), although occasional patches of host-derived mesothelium were observed in two of the five pancreatic grafts analyzed (Figure 5.2I–L, arrows). 8F3-positive cells were found in clusters subjacent to the mesothelium (Figure 5.2M–N, arrowheads) but the vast majority of pancreatic mesothelium, like that of the intestines and lungs, was derived from resident cells (Figure 5.10).

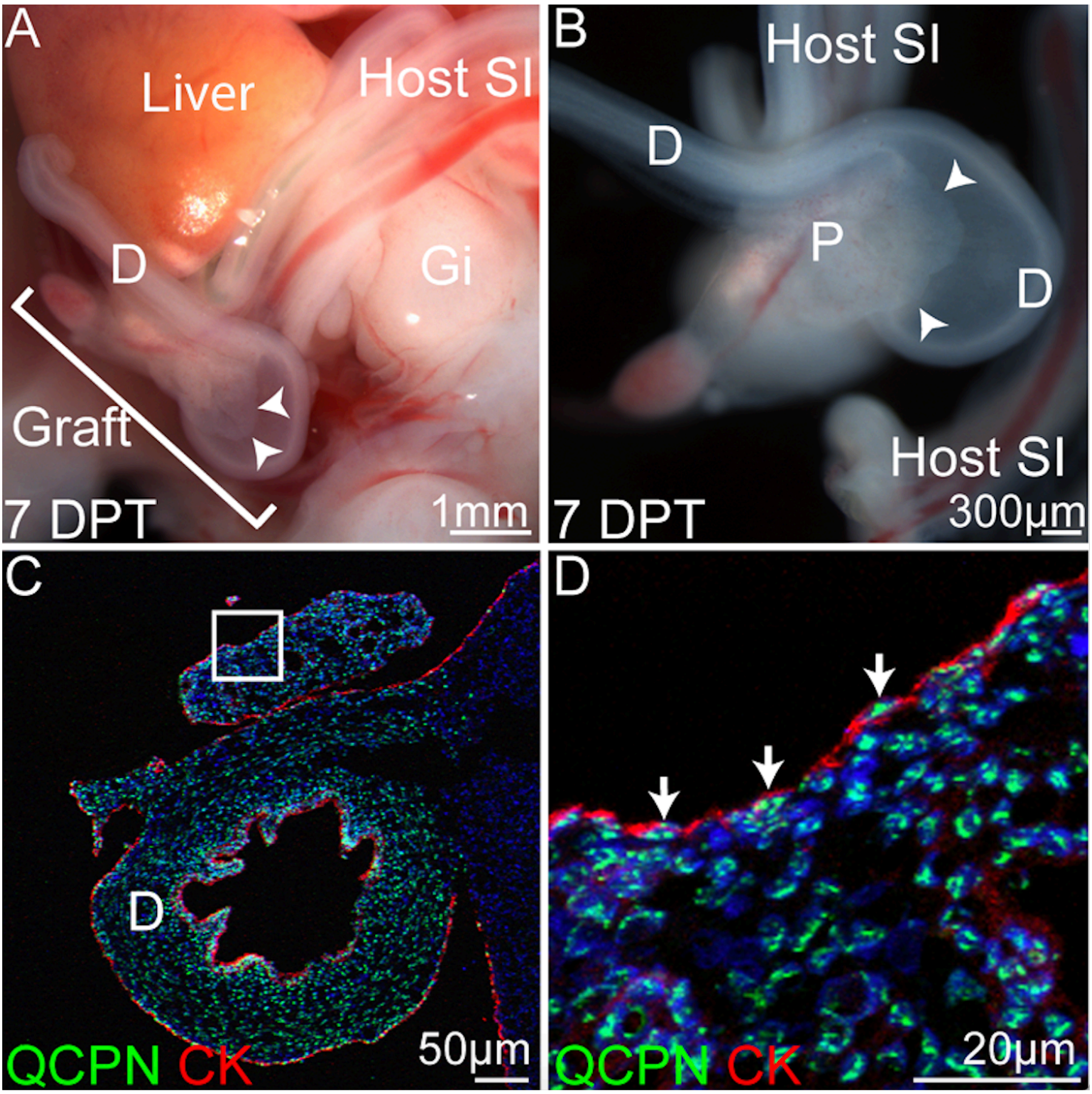


**Figure 5.8. Graft-derived pancreas 7 DPT.** Representative graft with a duodenum (D) wrapped around the pancreas (arrowheads). **B)** After isolation from the host, the pancreas (P, arrowheads) was easily visible within the duodenal mesentery. **C)** Lower power view demonstrates a cytokeratin-positive mesothelium lined the graft-derived pancreas and duodenum. **D)** Higher magnification of boxed area in C). The pancreatic surface mesothelium was QCPN-positive (arrows). D, duodenum; Gi, gizzard; P, pancreas; Host SI, host small intestine

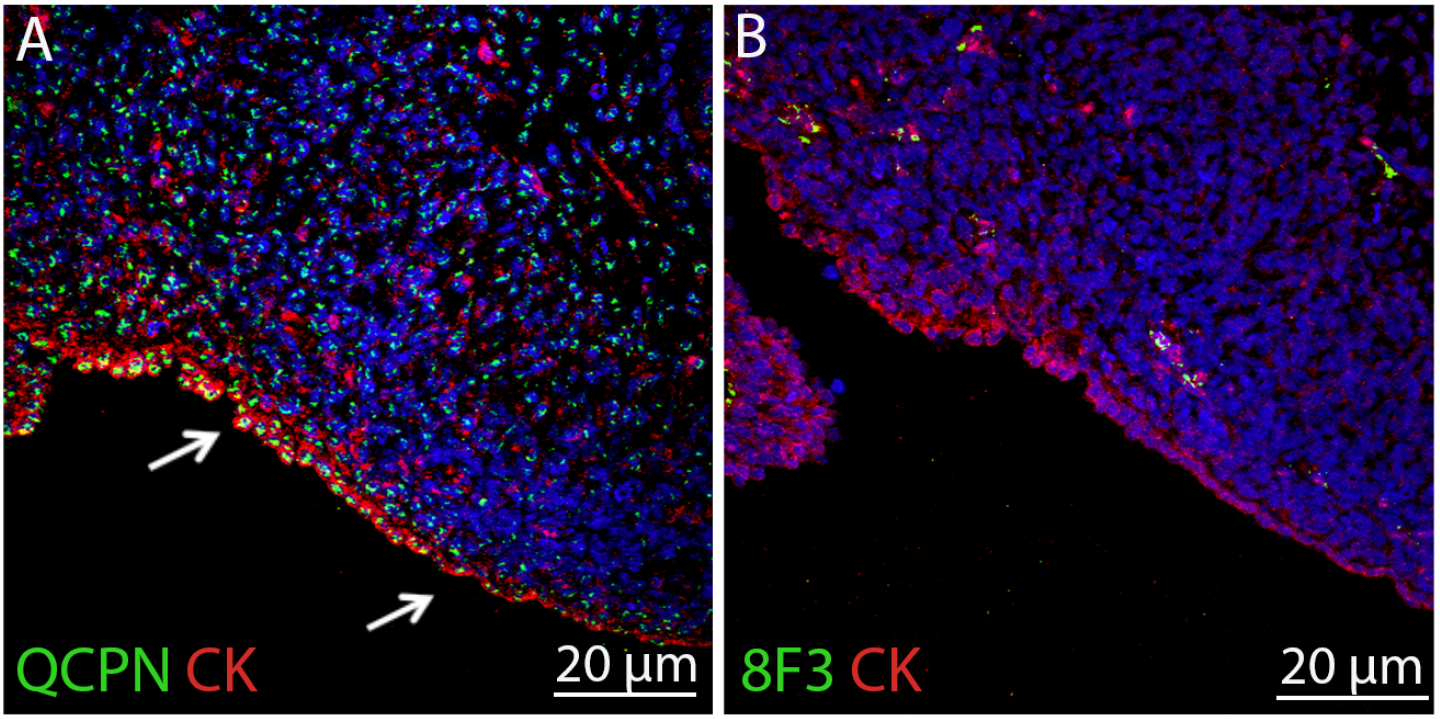


**Figure 5.9. Pancreatic graft at 4DPT.** A pancreatic graft is shown at 4 days after grafting. QCPN staining demonstrates that cytokeratin-positive (CK) quail cells are present at the surface of this graft. While not uniformly squamous in nature, this epithelium strongly resembles that observed for mesothelia in the intact quail embryonic embryo at this time of development (Thomason et al, 2012). **B)** An adjacent section was stained with 8F3 and cytokeratin. Note the complete absence of 8F3-positive cells at the graft surface indicating the lack of host contribution to this layer of the graft even while 8F3-positive cells are observed deep within the graft.

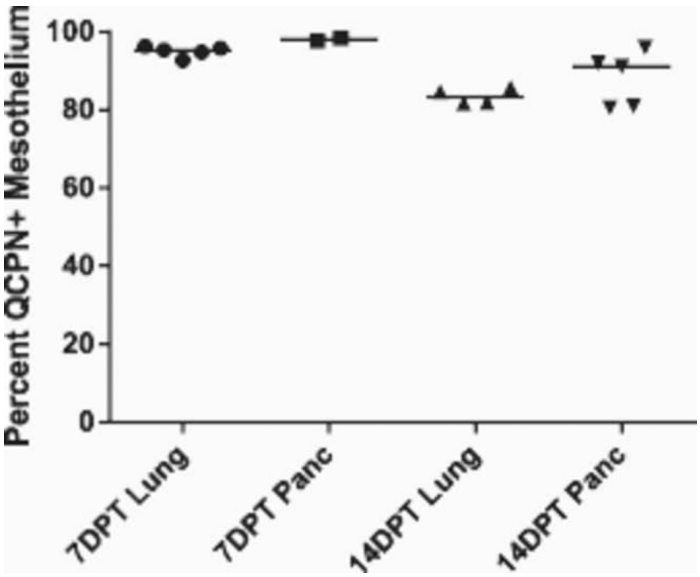


**Figure 5.10. Quantification of QCPN-positive mesothelium in graft-derived organs.** Each symbol represents a single experimental embryo. Horizontal line denotes mean value for each sample group. At 7DPT, lung and pancreatic graft mesothelia were between 93–98% QCPN-positive. At 14DPT, lung graft mesothelia were on average 84% QCPN-positive. Pancreatic graft mesothelia were on average 88% QCPN-positive at 14DPT.

## DISCUSSION

Mesothelia are essential cell populations that share specific functions in organogenesis and adult homeostasis. Mesothelial development has been studied for many years in the heart (Manasek et al., 1969). However, it is unknown whether the mechanisms of cardiac mesotheliogenesis, in particular the requirement to recruit exogenous mesothelial cell progenitors to the developing organ, are applied broadly throughout vertebrate organogenesis. We recently reported the intestine employed an alternative mechanism of mesothelial formation – generation of mesothelium from a broadly-distributed intrinsic population of progenitors (Winters et al., 2012). Still, the question remains as to whether a major conserved mechanism in this process is observed. The current study demonstrates that the lungs and pancreas of the respiratory and digestive systems respectively, also obtain the vast majority of their mesothelial lining from intrinsic progenitors. Thus, while mesothelial acquisition and differentiation in the heart is far better understood, that system appears to be the outlier being the only organ incapable of generating a mesothelium and capable of recruiting exogenous progenitors. Analysis of the small intestine, lung, and pancreas demonstrate that development of mesothelium in these settings is through the differentiation of progenitor cells intrinsic to the splanchnic mesoderm of the coelomic organ itself.

The heart has unique characteristics among coelomic organs that may offer potential explanations for this variation. All coelomic organs are derived at least in part from splanchnic mesoderm. However, the cardiac splanchnic mesoderm is specified very early in development and this early specification to a myocardial fate may prevent later mesothelial differentiation. Additionally, the lungs, liver, pancreas, and intestine include endoderm as a major component of the organ. As the cardiac splanchnic mesoderm forms a heart tube, the endoderm is excluded dorsally and thus, the heart tube would lack any positive signal originating from the endoderm required for mesothelial differentiation. Further research will be required to distinguish between these and other possibilities.

While studies on the recruitment and differentiation of mesothelia have long focused on heart development, the current study demonstrates that this model is not the principal mechanism driving development of this cell type in the intestines, lungs, and pancreas. Future studies on such organs as the gall bladder, liver and spleen will help determine whether the “organ intrinsic” model is indeed the conserved mechanism in coelomic organogenesis.

As the currently described mechanism in the generation of this cell type varies greatly from the system best understood, we must revisit the fundamental principles of mesotheliogenesis in these other coelomic organs. Currently available mouse models used for the analysis of mesothelial development in the heart may provide a rich starting point for these studies. Some of the molecular mechanisms driving this process might be broadly applied throughout the embryo regardless of the origin of the progenitors. Additionally, it will be of great interest to determine whether the signaling molecules important for coronary development apply to other coelomic organs and generation of their vasculature. We would also note that the experimental paradigm employed here can be modified to probe mouse/chick chimeras where

genetically modified graft tissue could be used to study the consequences of mesothelial malformation. The door is open to future research into the biology of this fascinating cell type.

# CHAPTER VI

# FUTURE DIRECTIONS

There is a clear need for further investigation into the role of microtubules in cardiomyocytes. With the work from the present studies, the importance of the relationship between the microtubule network and the contractile apparatus in cardiac myocytes has been established. CENP-F is critical in maintaining this relationship. In a large human study, a single nucleotide polymorphism (snp) was found to have implications in heart failure (Chapter 3 of this dissertation). In mice, the layout of the microtubules throughout development has now been thoroughly provided in immunohistochemical studies at the cellular level (Chapter 3 of this dissertation). Disruption of the microtubule network in the heart results in dilated hearts with a significantly altered sarcomere structure and disintegration of the intercalated discs. Additionally, the mitochondria are misaligned and vary in size. These phenotypic disruptions resulted in stiffened fibroblasts but softened cardiomyocytes, a disruption of calcium influx, and sarcomere shortening. All single cell studies were made possible by a new cardiomyocyte isolation protocol that was added here (Chapter 4, this dissertation). Now, a foundation for understanding molecular mechanism governing the relationship between these two systems can be explored, as loss of CENP-F clearly influences multiple processes in cardiac function. From the costamere to the sarcolemma, and to the intercalated discs, there is much to determine on the mechanistic role of not only CENP-F but more importantly, the microtubule network. These studies have opened the door and the field is now poised to bear down on how microtubules impact overall heart health.

An early and additional study has been added to the document describing a new model for recruiting a mesothelium (Chapter 5, this dissertation). The 'accepted model' of extrinsic mesothelial recruitment during embryogenesis has been contrasted by an organ intrinsic model in several organ systems. This study has changed the current belief on mesothelium development and further studies on the remaining organs need to be done. This study also ties into reports in Chapter 3 of this dissertation that shows that fibroblast stiffness is opposite of cardiomyocyte stiffness with the loss of CENP-F. With fibroblasts and cardiomyocytes having a different developmental lineage (Pinto, 2017), it is key to explore each cell type from each organ individually. The following discussion focuses on the impact of CENP-F in isolated cardiomyocytes and microtubules in heart health.

## ROLE OF MICROTUBULES IN CARDIOMYOCYTES

Prior to the current studies, the role of microtubules in cardiomyocytes was minimal. A few early studies noted the different layout of the microtubule network in a cardiac cell and, even with similarities with a skeletal muscle cell, no concrete reports which define the role of microtubules in cardiomyocytes were available. Microtubules have a loosely organized appearance and does not nucleate as a bundle, like in most cells. Along the costameres, the microtubule network is patterned like a grid and there are no reports of microtubular dynamic instability. Still, whether the microtubules are important in maintaining cardiomyocyte structure or serve as intracellular tracks is unknown. More recently, a few reports on the abundance of microtubules has been implicated in heart disease, however, no studies experimented on whether the microtubule density was a result of heart failure or part of the cause. With the current report on the impact of the loss of a microtubule binding protein on heart function at the cellular level, it is now clear that the microtubule network plays a role in cytoarchitectural maintenance and the functioning of a beating cardiomyocyte.

## MICROTUBULE BINDING PROTEIN CENP-F IS CRITICAL FOR PROPER HEART STRUCTURE AND FUNCTION

There are now two reports that show the disruption of multiple cardiomyocyte components when CENP-F is lost. CENP-F is a large microtubule binding protein that has been shown to have a critical role in the maintenance of heart structure and function. In whole, the loss of function of CENP-F results in a thinned ventricular wall, lessened trabeculation, and larger hearts indicating dilated cardiomyopathy (DCM). With diverse roles played by CENP-F in different cell types (Waters, 2015), it is now critical for further comparison studies on CENP-F in cardiomyocytes versus fibroblasts as well as in other cell types where CENP-F function has been shown to affect cell behaviors (Welner, 2013; Moghaddas, 2016; Haley et al., in review). There are additional studies that should be explored in order to identify the first mechanisms related to heart disease. First, the only other report on microtubules having a direct impact on dilated cardiomyopathy was tachycardia induced DCM in dogs (Takahashi, 1998). Although myocyte contraction depressed, microtubule immunohistochemical analysis showed no differences in distribution as no single cell assay was performed. In isolated cardiomyocytes, an additional study did show that stiffness against shear stress with a hyperpolymerized microtubule network in an animal model of heart failure was reported (Masaru, 1998). And recently, advanced imaging has resulted in better resolution of microtubular layout and insight on one way that the microtubule population may alter contraction. Robison et al. reported that detyrosinated microtubules interacted with desmin to “buckle” during contraction, assisting in modulation of the cell shape (Robison, 2016). Tying in these recent microtubule publications, along with the report here, with mechanisms known on the contractile properties of a cardiomyocyte will provide missing knowledge on the importance of microtubules in heart disease.

## THE EMERGING FIELD OF CARDIO-ONCOLOGY

Cardio oncology is the study of chemotherapies and their potential effects on heart disease. Beginning in 2005, respondent heart failure syndromes were detected with chemotherapeutic treatments using doxorubicin and trastuzumab (Ewer, 2005). As a result, a strategy to contrast the off-set effects of cardiomyopathies with continuous genetic and cellular experimentation was begun (Bellinger, 2015; Moslehi, 2017; Cubbon, 2016). A majority of studies highlight the cardiotoxic effects of anthracyclines, antineoplastics, and small molecule chemotherapies (Minotti, 2010; Menna, 2008). Our recent work on CENP-F poises questions for the impact of microtubule-targeted chemotherapies on the heart. In this context, it is also important to note our current findings that expression of a specific CENP-F snp may predict poor heart health (Chapter 3 in this dissertation). Thus, an additional component, the genetic background of the individual in question should be considered. Current cancer therapy regimens include pharmaceuticals that target the microtubule network to inhibit mitosis, such as paclitaxel and nocodazole (Zhou et al., 2005). Until our recent study, the importance of microtubules in the heart has never been explored. Early and unpublished observations of chemotherapy drugs treated on cardiac cells show a disruption in the microtubule network similar to that in loss of CENP-F. Therefore, the potential relationship between microtubule-targeted chemotherapies, induction of heart disease, and genetic background of the individual in the study of cardio-oncology should be explored.

## UNANSWERED QUESTIONS

Work from this dissertation provides the foundation for exploration of many unanswered questions. In regards to mitosis in cardiomyocytes, whether or not microtubules impact the failure of a cardiomyocyte to achieve cytokinesis would be of great impact in understanding cardiac development. And, in addition, where the individual microtubules nucleate from is of great importance. For instance, in the recent Robison study, the bundling and detyrosination of the individual microtubules are responsible for the sliding effect which is necessary for contraction (Robison et al., 2015). Understanding where the microtubules nucleate will initiate the mechanism of the role of microtubules in contraction.

The common belief that CENP-F has a role in mitosis alone, now has importance in the heart. Loss of CENP-F directly impacts every major component of the contractile apparatus and now, discerning the role of this interaction is important for heart health. Immediate analysis on pinpointing CENP-F localization and relationship with the microtubule network is critical. Additionally, in order to understand whole heart function, how CENP-F functions differently in a cardiac myocyte versus a cardiac fibroblast should be continued. Further investigation into these questions will generate a more comprehensive understanding of the role of CENP-F in the heart and the importance of microtubules in overall cardiac health and disease.

# REFERENCES


**1** Abramoff, M. et al., Image Processing with ImageJ. Biophotonics International. (July 2004).

**2** Adamcova, M. et al. Myocardial regulatory proteins and heart failure. Eur J Heart Fail 8, 333-342, doi:10.1016/j.ejheart.2005.09.007 (2006).

**3** Ahuja, P., Sdek, P. & MacLellan, W. R. Cardiac myocyte cell cycle control in development, disease, and regeneration. Physiol Rev 87, 521-544, doi:10.1152/physrev.00032.2006 (2007).

**4** Arbustini, E. et al. Mitochondrial DNA mutations and mitochondrial abnormalities in dilated cardiomyopathy. Am J Pathol 153, 1501-1510, doi:10.1016/S0002-9440(10)65738-0 (1998).

**5** Aroeira, L. S. et al. Mesenchymal conversion of mesothelial cells as a mechanism responsible for high solute transport rate in peritoneal dialysis: role of vascular endothelial growth factor. Am J Kidney Dis 46, 938-948, doi:10.1053/j.ajkd.2005.08.011 (2005).

**6** Asahina, K., Zhou, B., Pu, W. T. & Tsukamoto, H. Septum transversum-derived mesothelium gives rise to hepatic stellate cells and perivascular mesenchymal cells in developing mouse liver. Hepatology 53, 983-995, doi:10.1002/hep.24119 (2011).

**7** Aytes, A. et al. Cross-species regulatory network analysis identifies a synergistic interaction between FOXM1 and CENPF that drives prostate cancer malignancy. Cancer Cell 25, 638-651, doi:10.1016/j.ccr.2014.03.017 (2014).

**8** Banerjee, I., Fuseler, J. W., Price, R. L., Borg, T. K. & Baudino, T. A. Determination of cell types and numbers during cardiac development in the neonatal and adult rat and mouse. Am J Physiol Heart Circ Physiol 293, H1883-1891, doi:10.1152/ajpheart.00514.2007 (2007).

**9** Barrans, J. D., Allen, P. D., Stamatiou, D., Dzau, V. J. & Liew, C. C. Global gene expression profiling of end-stage dilated cardiomyopathy using a human cardiovascular-based cDNA microarray. Am J Pathol 160, 2035-2043, doi:10.1016/S0002-9440(10)61153-4 (2002).

**10** Baudino, T. A., Carver, W., Giles, W. & Borg, T. K. Cardiac fibroblasts: friend or foe? Am J Physiol Heart Circ Physiol 291, H1015-1026, doi:10.1152/ajpheart.00023.2006 (2006).

**11** Bellinger, A. M., et al. Cardio-Oncology: How New Targeted Cancer Therapies and Precision Medicine Can Inform Cardiovascular Discovery. Circulation 132(23): 2248-2258. (2015).

**12** Bers, D. M. Cardiac excitation-contraction coupling. Nature 415, 198-205, doi:10.1038/415198a (2002).

**13** Bhupathi, S. S., Chalasani, S. & Rokey, R. Stiff heart syndrome. Clin Med Res 9, 92-99, doi:10.3121/cmr.2010.899 (2011).

**14** Borbely, A. et al. Cardiomyocyte stiffness in diastolic heart failure. Circulation 111, 774-781, doi:10.1161/01.CIR.0000155257.33485.6D (2005).

**15** Borin, D., Pecorari, I., Pena, B. & Sbaizero, O. Novel insights into cardiomyocytes provided by atomic force microscopy. Semin Cell Dev Biol, doi:10.1016/j.semcdb.2017.07.003 (2017).

**16** Bowles, N. E., Bowles, K. R. & Towbin, J. A. The "final common pathway" hypothesis and inherited cardiovascular disease. The role of cytoskeletal proteins in dilated cardiomyopathy. Herz 25, 168-175 (2000).

**17** Bowne-Anderson, H., Zanic, M., Kauer, M. & Howard, J. Microtubule dynamic instability: a new model with coupled GTP hydrolysis and multistep catastrophe. Bioessays 35, 452-461, doi:10.1002/bies.201200131 (2013).

**18** Brade, T., et al. Embryonic heart progenitors and cardiogenesis. Cold Spring Harb Perspect Med 3(10): a013847. (2013).

**19** Bray, M. A., Sheehy, S. P. & Parker, K. K. Sarcomere alignment is regulated by myocyte shape. Cell Motil Cytoskeleton 65, 641-651, doi:10.1002/cm.20290 (2008).

**20** Brooks, G., Poolman, R. A. & Li, J. M. Arresting developments in the cardiac myocyte cell cycle: role of cyclin-dependent kinase inhibitors. Cardiovasc Res 39, 301-311 (1998).

**21** Burbank, K. S. & Mitchison, T. J. Microtubule dynamic instability. Curr Biol 16, R516-517, doi:10.1016/j.cub.2006.06.044 (2006).

**22** Burbank, K. S. & Mitchison, T. J. Microtubule dynamic instability. Curr Biol 16, R516-517, doi:10.1016/j.cub.2006.06.044 (2006).

**23** Camelliti, P., Borg, T. K. & Kohl, P. Structural and functional characterisation of cardiac fibroblasts. Cardiovasc Res 65, 40-51, doi:10.1016/j.cardiores.2004.08.020 (2005).

**24** Chaturvedi, R. R. et al. Passive stiffness of myocardium from congenital heart disease and

implications for diastole. Circulation 121, 979-988, doi:10.1161/CIRCULATIONAHA.109.850677 (2010).

**25** Cheng, H. & Force, T. Molecular mechanisms of cardiovascular toxicity of targeted cancer therapeutics. Circ Res 106, 21-34, doi:10.1161/CIRCRESAHA.109.206920 (2010).

**26** Chew, C., Ziady, G. M., Raphael, M. J. & Oakley, C. M. Proceedings: Functional defect in amyloid heart disease 'the stiff heart syndrome'. Br Heart J 38, 537 (1976).

**27** Cubbon, R. M. and A. R. Lyon. Cardio-oncology: Concepts and practice. Indian Heart J 68 Suppl 1: S77-85. (2016).

**28** De Deyne, P. G. Formation of sarcomeres in developing myotubes: role of mechanical stretch and contractile activation. Am J Physiol Cell Physiol 279, C1801-1811 (2000).

**29** Dees, E. et al. Cardiac-specific deletion of the microtubule-binding protein CENP-F causes dilated cardiomyopathy. Dis Model Mech 5, 468-480, doi:10.1242/dmm.008680 (2012).

**30** Denny, J. C. et al. PheWAS: demonstrating the feasibility of a phenome-wide scan to discover gene-disease associations. Bioinformatics 26, 1205-1210, doi:10.1093/bioinformatics/btq126 (2010).

**31** Dettman, R. W., Denetclaw, W., Jr., Ordahl, C. P. & Bristow, J. Common epicardial origin of coronary vascular smooth muscle, perivascular fibroblasts, and intermyocardial fibroblasts in the avian heart. Dev Biol 193, 169-181, doi:10.1006/dbio.1997.8801 (1998).

**32** Djafarzadeh, R. et al. Recombinant GPI-anchored TIMP-1 stimulates growth and migration of peritoneal mesothelial cells. PLoS One 7, e33963, doi:10.1371/journal.pone.0033963 (2012).

**33** Du, C. K. et al. Knock-in mouse model of dilated cardiomyopathy caused by troponin mutation. Circ Res 101, 185-194, doi:10.1161/CIRCRESAHA.106.146670 (2007).

**34** Duenas, A., et al. More than Just a Simple Cardiac Envelope; Cellular Contributions of the Epicardium. Front Cell Dev Biol **5**: 44. (2017).

**35** El-Hattab, A. W. & Scaglia, F. Mitochondrial Cardiomyopathies. Front Cardiovasc Med 3, 25, doi:10.3389/fcvm.2016.00025 (2016).

**36** Fassett, J. T. et al. AMPK attenuates microtubule proliferation in cardiac hypertrophy. Am J Physiol Heart Circ Physiol 304, H749-758, doi:10.1152/ajpheart.00935.2011 (2013).

**37** Fassett, J. T. et al. AMPK attenuates microtubule proliferation in cardiac hypertrophy. Am J Physiol Heart Circ Physiol 304, H749-758, doi:10.1152/ajpheart.00935.2011 (2013).

**38** Fearnley, C. J., Roderick, H. L. & Bootman, M. D. Calcium signaling in cardiac myocytes. Cold Spring Harb Perspect Biol 3, a004242, doi:10.1101/cshperspect.a004242 (2011).

**39** Feaster, T. K. et al. Matrigel Mattress: A Method for the Generation of Single Contracting Human-Induced Pluripotent Stem Cell-Derived Cardiomyocytes. Circ Res 117, 995-1000, doi:10.1161/CIRCRESAHA.115.307580 (2015).

**40** Ferreira-Cornwell, M. C. et al. Remodeling the intercalated disc leads to cardiomyopathy in mice misexpressing cadherins in the heart. J Cell Sci 115, 1623-1634 (2002).

**41** Ferrier, G. R. & Howlett, S. E. Cardiac excitation-contraction coupling: role of membrane potential in regulation of contraction. Am J Physiol Heart Circ Physiol 280, H1928-1944 (2001).

**42** Folker, E. S. & Baylies, M. K. Nuclear positioning in muscle development and disease. Front Physiol 4, 363, doi:10.3389/fphys.2013.00363 (2013).

**43** Forth, S. & Kapoor, T. M. The mechanics of microtubule networks in cell division. J Cell Biol 216, 1525-1531, doi:10.1083/jcb.201612064 (2017).

**44** Furtado, M. B., Costa, M. W. & Rosenthal, N. A. The cardiac fibroblast: Origin, identity and role in homeostasis and disease. Differentiation 92, 93-101, doi:10.1016/j.diff.2016.06.004 (2016).

**45** Furtado, M. B., Nim, H. T., Boyd, S. E. & Rosenthal, N. A. View from the heart: cardiac fibroblasts in development, scarring and regeneration. Development 143, 387-397, doi:10.1242/dev.120576 (2016).

**46** Gittenberger-de Groot, A. C., Vrancken Peeters, M. P., Bergwerff, M., Mentink, M. M. & Poelmann, R. E. Epicardial outgrowth inhibition leads to compensatory mesothelial outflow tract collar and abnormal cardiac septation and coronary formation. Circ Res 87, 969-971 (2000).

**47** Goldstein, M. A. & Entman, M. L. Microtubules in mammalian heart muscle. J Cell Biol 80, 183-195 (1979).

**48** Gopal, D. M. & Sam, F. New and emerging biomarkers in left ventricular systolic dysfunction--insight into dilated cardiomyopathy. J Cardiovasc Transl Res 6, 516-527, doi:10.1007/s12265-013-9462-3 (2013).

**49** Kuo, P. L. et al. Myocyte shape regulates lateral registry of sarcomeres and contractility. Am J Pathol 181, 2030-2037, doi:10.1016/j.ajpath.2012.08.045 (2012).

**50** Hamdani, N. et al. Sarcomeric dysfunction in heart failure. Cardiovasc Res 77, 649-658, doi:10.1093/cvr/cvm079 (2008).

**51** Hamburger, V. & Hamilton, H. L. A series of normal stages in the development of the chick embryo. 1951. Dev Dyn 195, 231-272, doi:10.1002/aja.1001950404 (1992).

**52** Hein, S., Kostin, S., Heling, A., Maeno, Y. & Schaper, J. The role of the cytoskeleton in heart failure. Cardiovasc Res 45, 273-278 (2000).

**53** Henk & Granzier. The NH2 terminus of titin spans the Z-disc: its interaction with a novel 19-kD ligand (T-cap) is required for sarcomeric integrity. The Journal of cell biology 143 (4), 1013-1027, (1998). 298, 1998

**54** Herman, D. S. et al. Truncations of titin causing dilated cardiomyopathy. N Engl J Med 366, 619-628, doi:10.1056/NEJMoa1110186 (2012).

**55** Hirschy, A., Schatzmann, F., Ehler, E. & Perriard, J. C. Establishment of cardiac cytoarchitecture in the developing mouse heart. Dev Biol 289, 430-441, doi:10.1016/j.ydbio.2005.10.046 (2006).

**56** Ho, E. & Shimada, Y. Formation of the epicardium studied with the scanning electron microscope. Dev Biol 66, 579-585 (1978).

**57** Hwang, H. S. et al. Comparable calcium handling of human iPSC-derived cardiomyocytes generated by multiple laboratories. J Mol Cell Cardiol 85, 79-88, doi:10.1016/j.yjmcc.2015.05.003 (2015).

**58** Holt, S. V. et al. Silencing Cenp-F weakens centromeric cohesion, prevents chromosome alignment and activates the spindle checkpoint. J Cell Sci 118, 4889-4900, doi:10.1242/jcs.02614 (2005).

**59** Hussein, D. & Taylor, S. S. Farnesylation of Cenp-F is required for G2/M progression and degradation after mitosis. J Cell Sci 115, 3403-3414 (2002).

**60** Ishii, Y., Langberg, J. D., Hurtado, R., Lee, S. & Mikawa, T. Induction of proepicardial marker gene expression by the liver bud. Development 134, 3627-3637, doi:10.1242/dev.005280 (2007).

**61** Ishiwata, I., et al. Organogenesis of heart-vascular system derived from mouse 2 cell stage embryos and from early embryonic stem cells in vitro. Hum Cell 16(1): 15-22. (2003).

**62**

**63** Karsenti, E. Microtubule dynamics: severing microtubules in mitosis. Curr Biol 3, 208-210 (1993).

**64** Kavallaris, M. Microtubules and resistance to tubulin-binding agents. Nat Rev Cancer 10, 194-204, doi:10.1038/nrc2803 (2010).

**65** Kerr, J. P. et al. Detyrosinated microtubules modulate mechanotransduction in heart and skeletal muscle. Nat Commun 6, 8526, doi:10.1038/ncomms9526 (2015).

**66** Khairallah, R. J. et al. Microtubules underlie dysfunction in duchenne muscular dystrophy. Sci Signal 5, ra56, doi:10.1126/scisignal.2002829 (2012).

**67** Kohl, P., Camelliti, P., Burton, F. L. & Smith, G. L. Electrical coupling of fibroblasts and myocytes: relevance for cardiac propagation. J Electrocardiol 38, 45-50, doi:10.1016/j.jelectrocard.2005.06.096 (2005).

**68** Kostetskii, I. et al. Induced deletion of the N-cadherin gene in the heart leads to dissolution of the intercalated disc structure. Circ Res 96, 346-354, doi:10.1161/01.RES.0000156274.72390.2c (2005).

**69** Kovacic, J. C., Mercader, N., Torres, M., Boehm, M. & Fuster, V. Epithelial-to-mesenchymal and endothelial-to-mesenchymal transition: from cardiovascular development to disease. Circulation 125, 1795-1808, doi:10.1161/CIRCULATIONAHA.111.040352 (2012).

**70** Kruithof, B. P., van den Hoff, M. J., Wessels, A. & Moorman, A. F. Cardiac muscle cell formation after development of the linear heart tube. Dev Dyn 227, 1-13, doi:10.1002/dvdy.10269 (2003).

**71** Kuo, P. L. et al. Myocyte shape regulates lateral registry of sarcomeres and contractility. Am J Pathol 181, 2030-2037, doi:10.1016/j.ajpath.2012.08.045 (2012).

**72** Laugwitz, K. L., Moretti, A., Caron, L., Nakano, A. & Chien, K. R. Islet1 cardiovascular progenitors: a single source for heart lineages? Development 135, 193-205, doi:10.1242/dev.001883 (2008).

**73** Lengyel, E. Ovarian cancer development and metastasis. Am J Pathol 177, 1053-1064, doi:10.2353/ajpath.2010.100105 (2010).

**74** Li, P. et al. IGF signaling directs ventricular cardiomyocyte proliferation during embryonic heart development. Development 138, 1795-1805, doi:10.1242/dev.054338 (2011).

**75** Li, D., Wu, J., Bai, Y., Zhao, X. & Liu, L. Isolation and culture of adult mouse cardiomyocytes for cell signaling and in vitro cardiac hypertrophy. J Vis Exp, doi:10.3791/51357 (2014).

**76** Liao, H., Winkfein, R. J., Mack, G., Rattner, J. B. & Yen, T. J. CENP-F is a protein of the nuclear matrix that assembles onto kinetochores at late G2 and is rapidly degraded after mitosis. J Cell Biol 130, 507-518 (1995).

**77** Lim, C. C. et al. Anthracyclines induce calpain-dependent titin proteolysis and necrosis in cardiomyocytes. J Biol Chem 279, 8290-8299, doi:10.1074/jbc.M308033200 (2004).

**78** Loureiro, J. et al. Blocking TGF-beta1 protects the peritoneal membrane from dialysate-induced damage. J Am Soc Nephrol 22, 1682-1695, doi:10.1681/ASN.2010111197 (2011).

**79** Louch, W. E., Sheehan, K. A. & Wolska, B. M. Methods in cardiomyocyte isolation, culture, and gene transfer. J Mol Cell Cardiol 51, 288-298, doi:10.1016/j.yjmcc.2011.06.012 (2011).

**80** Machackova, J., Barta, J. & Dhalla, N. S. Myofibrillar remodeling in cardiac hypertrophy, heart failure and cardiomyopathies. Can J Cardiol 22, 953-968 (2006).

**81** Makarenko, I. et al. Passive stiffness changes caused by upregulation of compliant titin isoforms in human dilated cardiomyopathy hearts. Circ Res 95, 708-716, doi:10.1161/01.RES.0000143901.37063.2f (2004).

**82** Manasek, F. J. Embryonic development of the heart. II. Formation of the epicardium. J Embryol Exp Morphol 22, 333-348 (1969).

**83** Mandl-Weber, S., Cohen, C. D., Haslinger, B., Kretzler, M. & Sitter, T. Vascular endothelial growth factor production and regulation in human peritoneal mesothelial cells. Kidney Int 61, 570-578, doi:10.1046/j.1523-1755.2002.00143.x (2002).

**84** McKinley, K. L. & Cheeseman, I. M. The molecular basis for centromere identity and function. Nat Rev Mol Cell Biol 17, 16-29, doi:10.1038/nrm.2015.5 (2016).

**85** McNally, E. M., Golbus, J. R. & Puckelwartz, M. J. Genetic mutations and mechanisms in dilated cardiomyopathy. J Clin Invest 123, 19-26, doi:10.1172/JCI62862 (2013).

**86** Menna, P., Salvatorelli, E., Gianni, L. & Minotti, G. Anthracycline cardiotoxicity. Top Curr Chem 283, 21-44, doi:10.1007/128_2007_11 (2008).

**87** Menna, P., Salvatorelli, E. & Minotti, G. Cardiotoxicity of antitumor drugs. Chem Res Toxicol 21, 978-989, doi:10.1021/tx800002r (2008).

**88** Meunier, S. & Vernos, I. Microtubule assembly during mitosis - from distinct origins to distinct functions. J Cell Sci 125, 2805-2814, doi:10.1242/jcs.092429 (2012).

**89** Mi, Y. J. et al. Prognostic relevance and therapeutic implications of centromere protein F expression in patients with esophageal squamous cell carcinoma. Dis Esophagus 26, 636-643, doi:10.1111/dote.12002 (2013).

**90** Minotti, G., Salvatorelli, E. & Menna, P. Pharmacological foundations of cardio-oncology. J Pharmacol Exp Ther 334, 2-8, doi:10.1124/jpet.110.165860 (2010).

**91** Moghaddas, F., Joshua, F., Taylor, R., Fritzler, M. J. & Toh, B. H. Autoantibodies directed to centromere protein F in a patient with BRCA1 gene mutation. BMC Res Notes 9, 84, doi:10.1186/s13104-016-1908-7 (2016).

**92** Mohapatra, B. et al. Mutations in the muscle LIM protein and alpha-actinin-2 genes in dilated cardiomyopathy and endocardial fibroelastosis. Mol Genet Metab 80, 207-215 (2003).

**93** Moorman, A., Webb, S., Brown, N. A., Lamers, W. & Anderson, R. H. Development of the heart: (1) formation of the cardiac chambers and arterial trunks. Heart 89, 806-814 (2003).

**94** Moslehi, J., Amgalan, D. & Kitsis, R. N. Grounding Cardio-Oncology in Basic and Clinical Science. Circulation 136, 3-5, doi:10.1161/CIRCULATIONAHA.117.025393 (2017).

**95** Moynihan, K. L., Pooley, R., Miller, P. M., Kaverina, I. & Bader, D. M. Murine CENP-F regulates centrosomal microtubule nucleation and interacts with Hook2 at the centrosome. Mol Biol Cell 20, 4790-4803, doi:10.1091/mbc.E09-07-0560 (2009).

**96** Mutsaers, S. E. Mesothelial cells: their structure, function and role in serosal repair. Respirology 7, 171-191 (2002).

**97** Nagueh, S. F. et al. Altered titin expression, myocardial stiffness, and left ventricular function in patients with dilated cardiomyopathy. Circulation 110, 155-162, doi:10.1161/01.CIR.0000135591.37759.AF (2004).

**98** Nishimura, S. et al. Microtubules modulate the stiffness of cardiomyocytes against shear stress. Circ Res 98, 81-87, doi:10.1161/01.RES.0000197785.51819.e8 (2006).

**99** Neagoe, C. et al. Titin isoform switch in ischemic human heart disease. Circulation 106, 1333-1341 (2002).

**100** O'Brien, S. L. et al. CENP-F expression is associated with poor prognosis and chromosomal instability in patients with primary breast cancer. Int J Cancer 120, 1434-1443, doi:10.1002/ijc.22413 (2007).

**101** Oddoux, S. et al. Microtubules that form the stationary lattice of muscle fibers are dynamic and nucleated at Golgi elements. J Cell Biol 203, 205-213, doi:10.1083/jcb.201304063 (2013).

**102** Olivotto, I. et al. Defining phenotypes and disease progression in sarcomeric cardiomyopathies: contemporary role of clinical investigations. Cardiovasc Res 105, 409-423, doi:10.1093/cvr/cvv024 (2005).

**103** Olson, T. M. et al. Metavinculin mutations alter actin interaction in dilated cardiomyopathy. Circulation 105, 431-437 (2002).

**104** Osler, M. E. & Bader, D. M. Bves expression during avian embryogenesis. Dev Dyn 229, 658-667, doi:10.1002/dvdy.10490 (2004).

**105** Pantos, C. et al. Thyroid hormone changes cardiomyocyte shape and geometry via ERK signaling pathway: potential therapeutic implications in reversing cardiac remodeling? Mol Cell Biochem 297, 65-72, doi:10.1007/s11010-006-9323-3 (2007).

**106** Paradis, A. N., Gay, M. S. & Zhang, L. Binucleation of cardiomyocytes: the transition from a proliferative to a terminally differentiated state. Drug Discov Today 19, 602-609, doi:10.1016/j.drudis.2013.10.019 (2014).

**107** Pardanaud, L., Yassine, F. & Dieterlen-Lievre, F. Relationship between vasculogenesis, angiogenesis and haemopoiesis during avian ontogeny. Development 105, 473-485 (1989).

**108** Pfaltzgraff, E. R. et al. Loss of CENP-F results in distinct microtubule-related defects without chromosomal abnormalities. Mol Biol Cell 27, 1990-1999, doi:10.1091/mbc.E15-12-0848 (2016).

**109** Pinto, A. R., et al. Revisiting Cardiac Cellular Composition. Circ Res 118(3): 400-409. (2016).

**110** Pinz, I., Zhu, M., Mende, U. & Ingwall, J. S. An improved isolation procedure for adult mouse cardiomyocytes. Cell Biochem Biophys 61, 93-101, doi:10.1007/s12013-011-9165-9 (2011).

**111** Planavila, A. et al. Dilated cardiomyopathy and mitochondrial dysfunction in Sirt1-deficient mice: a role for Sirt1-Mef2 in adult heart. J Mol Cell Cardiol 53, 521-531, doi:10.1016/j.yjmcc.2012.07.019 (2012).

**112** Pollack, G. H., Ishiwata, S. & Sugi, H. Molecular and cellular aspects of muscle contraction. General discussion part I. Adv Exp Med Biol 538, 647-654, 687-648 (2003).

**113** Pooley, R. D. et al. Murine CENPF interacts with syntaxin 4 in the regulation of vesicular transport. J Cell Sci 121, 3413-3421, doi:10.1242/jcs.032847 (2008).

**114** Poulain, F. E. & Sobel, A. The microtubule network and neuronal morphogenesis: Dynamic and coordinated orchestration through multiple players. Mol Cell Neurosci 43, 15-32, doi:10.1016/j.mcn.2009.07.012 (2010).

**115** Prathipati, P., Metreveli, N., Nandi, S. S., Tyagi, S. C. & Mishra, P. K. Ablation of Matrix Metalloproteinase-9 Prevents Cardiomyocytes Contractile Dysfunction in Diabetics. Front Physiol 7, 93, doi:10.3389/fphys.2016.00093 (2016).

**116** Que, J. et al. Mesothelium contributes to vascular smooth muscle and mesenchyme during lung development. Proc Natl Acad Sci U S A 105, 16626-16630, doi:10.1073/pnas.0808649105 (2008).

**117** Ribeiro, A. J. et al. Contractility of single cardiomyocytes differentiated from pluripotent stem cells depends on physiological shape and substrate stiffness. Proc Natl Acad Sci U S A 112, 12705-12710, doi:10.1073/pnas.1508073112 (2015).

**118** Robison, P. et al. Detyrosinated microtubules buckle and bear load in contracting cardiomyocytes. Science 352, aaf0659, doi:10.1126/science.aaf0659 (2016).

**119** Roden, D. M. et al. Development of a large-scale de-identified DNA biobank to enable personalized medicine. Clin Pharmacol Ther 84, 362-369, doi:10.1038/clpt.2008.89 (2008).

**120** Roostalu, J. & Surrey, T. Microtubule nucleation: beyond the template. Nat Rev Mol Cell Biol 18, 702-710, doi:10.1038/nrm.2017.75 (2017).

**121** Roth, G. M., Bader, D. M. & Pfaltzgraff, E. R. Isolation and physiological analysis of mouse cardiomyocytes. J Vis Exp, e51109, doi:10.3791/51109 (2014).

**122** Rowinsky, E. K. The development and clinical utility of the taxane class of antimicrotubule chemotherapy agents. Annu Rev Med 48, 353-374, doi:10.1146/annurev.med.48.1.353 (1997).

**123** Sato, Y. et al. Dynamic analysis of vascular morphogenesis using transgenic quail embryos. PLoS One 5, e12674, doi:10.1371/journal.pone.0012674 (2010).

**124** Savolainen, S. M., Foley, J. F. & Elmore, S. A. Histology atlas of the developing mouse heart with emphasis on E11.5 to E18.5. Toxicol Pathol 37, 395-414, doi:10.1177/0192623309335060 (2009).

**125** Senyo, S. E., Lee, R. T. & Kuhn, B. Cardiac regeneration based on mechanisms of cardiomyocyte proliferation and differentiation. Stem Cell Res 13, 532-541, doi:10.1016/j.scr.2014.09.003 (2014).

**126** Sequeira, V., Nijenkamp, L. L., Regan, J. A. & van der Velden, J. The physiological role of cardiac cytoskeleton and its alterations in heart failure. Biochim Biophys Acta 1838, 700-722, doi:10.1016/j.bbamem.2013.07.011 (2014).

**127** Souders, C. A., Bowers, S. L. & Baudino, T. A. Cardiac fibroblast: the renaissance cell. Circ Res 105, 1164-1176, doi:10.1161/CIRCRESAHA.109.209809 (2009).

**128** Spater, D., Hansson, E. M., Zangi, L. & Chien, K. R. How to make a cardiomyocyte. Development 141, 4418-4431, doi:10.1242/dev.091538 (2014).

**129** Sylva, M., van den Hoff, M. J. & Moorman, A. F. Development of the human heart. Am J Med Genet A 164A, 1347-1371, doi:10.1002/ajmg.a.35896 (2014).

**130** Tagawa, H. et al. Cytoskeletal role in the transition from compensated to decompensated hypertrophy during adult canine left ventricular pressure overloading. Circ Res 82, 751-761 (1998).

**131** Takahashi, M. et al. Role of microtubules in the contractile dysfunction of myocytes from tachycardia-induced dilated cardiomyopathy. J Mol Cell Cardiol 30, 1047-1057, doi:10.1006/jmcc.1998.0674 (1998).

**132** Tassin, A. M., Maro, B. & Bornens, M. Fate of microtubule-organizing centers during myogenesis in vitro. J Cell Biol 100, 35-46 (1985).

**133** ter Keurs, H. E. Microtubules in cardiac hypertrophy: a mechanical role in decompensation? Circ Res 82, 828-831 (1998).

**134** Thomason, R. T., et al. Comprehensive timeline of mesodermal development in the quail small intestine. Dev Dyn 241(11): 1678-1694. (2012).

**135** Tietze, L. et al. Modulation of pro- and antifibrinolytic properties of human peritoneal mesothelial cells by transforming growth factor beta1 (TGF-beta1), tumor necrosis factor alpha (TNF-alpha) and interleukin 1beta (IL-1beta). Thromb Haemost 79, 362-370 (1998).

**136** Tsutsui, H., et al. Cytoskeletal role in the contractile dysfunction of hypertrophied myocardium. Science 260(5108): 682-687. (1993).

**137** van Eldik, W. & Passier, R. Signalling in sarcomeres in development and disease. Neth Heart J 21, 367-371, doi:10.1007/s12471-013-0435-6 (2013).

**138** Vergnolle, M. A. & Taylor, S. S. Cenp-F links kinetochores to Ndel1/Nde1/Lis1/dynein microtubule motor complexes. Curr Biol 17, 1173-1179, doi:10.1016/j.cub.2007.05.077 (2007).

**139** Vincent, A. E. et al. Mitochondrial dysfunction in myofibrillar myopathy. Neuromuscul Disord 26, 691-701, doi:10.1016/j.nmd.2016.08.004 (2016).

**140** Viragh, S., Gittenberger-de Groot, A. C., Poelmann, R. E. & Kalman, F. Early development of quail heart epicardium and associated vascular and glandular structures. Anat Embryol (Berl) 188, 381-393 (1993).

**141** Volkov, V. A. et al. Centromere protein F includes two sites that couple efficiently to depolymerizing microtubules. J Cell Biol 209, 813-828, doi:10.1083/jcb.201408083 (2015).

**142** von Gise, A. & Pu, W. T. Endocardial and epicardial epithelial to mesenchymal transitions in heart development and disease. Circ Res 110, 1628-1645, doi:10.1161/CIRCRESAHA.111.259960 (2012).

**143** Wang, K. et al. Cardiac tissue slices: preparation, handling, and successful optical mapping. Am J Physiol Heart Circ Physiol 308, H1112-1125, doi:10.1152/ajpheart.00556.2014 (2015).

**144** Waters, A. M. et al. The kinetochore protein, CENPF, is mutated in human ciliopathy and microcephaly phenotypes. J Med Genet 52, 147-156, doi:10.1136/jmedgenet-2014-102691 (2015).

**145** Webster, D. R. Regulation of post-translationally modified microtubule populations during neonatal cardiac development. J Mol Cell Cardiol 29, 1747-1761, doi:10.1006/jmcc.1997.0421 (1997).

**146** Webster, D. R. Microtubules in cardiac toxicity and disease. Cardiovasc Toxicol 2, 75-89 (2002).

**147** Welner, S. et al. Correlation between centromere protein-F autoantibodies and cancer analyzed by enzyme-linked immunosorbent assay. Mol Cancer 12, 95, doi:10.1186/1476-4598-12-95 (2013).

**148** Westermann, D. et al. Role of left ventricular stiffness in heart failure with normal ejection fraction. Circulation 117, 2051-2060, doi:10.1161/CIRCULATIONAHA.107.716886 (2008).

**149** Wilm, B., Ipenberg, A., Hastie, N. D., Burch, J. B. & Bader, D. M. The serosal mesothelium is a major source of smooth muscle cells of the gut vasculature. Development 132, 5317-5328, doi:10.1242/dev.02141 (2005).

**150** Wilsbacher, L. D. & Coughlin, S. R. Analysis of cardiomyocyte development using immunofluorescence in embryonic mouse heart. J Vis Exp, doi:10.3791/52644 (2015).

**151** Winters, N. I., Thomason, R. T. & Bader, D. M. Identification of a novel developmental mechanism in the generation of mesothelia. Development 139, 2926-2934, doi:10.1242/dev.082396 (2012).

**152** Xin, M., Olson, E. N. & Bassel-Duby, R. Mending broken hearts: cardiac development as a basis for adult heart regeneration and repair. Nat Rev Mol Cell Biol 14, 529-541, doi:10.1038/nrm3619 (2013).

**153** Yancey, D. M. et al. Cardiomyocyte mitochondrial oxidative stress and cytoskeletal breakdown in the heart with a primary volume overload. Am J Physiol Heart Circ Physiol 308, H651-663, doi:10.1152/ajpheart.00638.2014 (2015).

**154** Yanez-Mo, M. et al. Peritoneal dialysis and epithelial-to-mesenchymal transition of mesothelial cells. N Engl J Med 348, 403-413, doi:10.1056/NEJMoa020809 (2003).

**155** Yang, Z. et al. Silencing mitosin induces misaligned chromosomes, premature chromosome decondensation before anaphase onset, and mitotic cell death. Mol Cell Biol 25, 4062-4074, doi:10.1128/MCB.25.10.4062-4074.2005 (2005).

**156** Yang, Z. Y. et al. Mitosin/CENP-F is a conserved kinetochore protein subjected to cytoplasmic dynein-mediated poleward transport. Cell Res 13, 275-283, doi:10.1038/sj.cr.7290172 (2003).

**157** Yassine, F., Fedecka-Bruner, B. & Dieterlen-Lievre, F. Ontogeny of the chick embryo spleen--a cytological study. Cell Differ Dev 27, 29-45 (1989).

**158** Yin, Y., Wang, F. & Ornitz, D. M. Mesothelial- and epithelial-derived FGF9 have distinct functions in the regulation of lung development. Development 138, 3169-3177, doi:10.1242/dev.065110 (2011).

**159** Yvon, A. M., Wadsworth, P. & Jordan, M. A. Taxol suppresses dynamics of individual microtubules in living human tumor cells. Mol Biol Cell 10, 947-959 (1999).

**160** Zhou, J. and P. Giannakakou. Targeting microtubules for cancer chemotherapy. Curr Med Chem Anticancer Agents 5(1): 65-71. (2005)

**161** Zile, M. R., Baicu, C. F. & Gaasch, W. H. Diastolic heart failure--abnormalities in active relaxation and passive stiffness of the left ventricle. N Engl J Med 350, 1953-1959, doi:10.1056/NEJMoa032566 (2004).